2011

The Synthesis and Host-Guest Applications of Synthetic Receptor Molecules

Zachary Richard Osner
Loyola University Chicago

THE SYNTHESIS AND HOST-GUEST APPLICATIONS OF SYNTHETIC RECEPTOR MOLECULES

A DISSERTATION SUBMITTED TO

THE FACULUTY OF THE GRADUATE SCHOOL

IN THE CANDIDACY FOR THE DEGREE OF

DOCTOR OF PHILOSOPHY

PROGRAM IN CHEMISTRY

BY

ZACHARY R. OSNER

CHICAGO, IL

MAY 2012

ACKNOWLEDGEMENTS

I would like to thank my advisor Richard Holz, PhD for taking me into his group, for affording me the opportunities to learn more about chemistry and myself than I knew possible, and especially for pushing me to finish what I started. I would like to extend a special thank you to my co-advisor, Daniel P. Becker, PhD. I would not have become the chemist or the person that I am without your support and guidance.

I would also like to thank my family and friends, especially my lovely wife Megan. It truly was your encouragement and support that carried me through this, especially when I wanted to give up. Thank you.

To Megan and Sophie
This wouldn't have been possible without you.

TABLE OF CONTENTS

LIST OF SCHEMES

LIST OF FIGURES

LIST OF TABLES

LIST OF ABBREVIATIONS

CTV	cyclotriveratrylene
$^{99}TcO_4^-$	pertechnetate
$Ag[CF_3SO_3]$	silver trifluoromethanesulfonic anhydride
CF_3CO_2H	trifluoroacetic acid
$CF_3SO_3^-$	trifluoromethanesulfonic anion
ReO_4^-	perrhenate
Ru(II)	ruthenium ion
Ir(III)	iridium ion
DMF	N,N-dimethylformamide
$CuCl_2$	copper (II) chloride
CDC	Center for Disease Control
Gal	galactose
K_D	dissociation constant
nm	nanometer
SAMs	self-assembled monolayers
O_2	oxygen
STP	standard temperature and pressure
UHV	ultra-high vacuum

kcal	kilocalorie
mol	mole
Au	elemental gold
MEMS	microelectromechanical systems
DNA	deoxyribonucleic acid
AuNPs	gold nanoparticles
B.C.	before Christ
$HAuCl_4$	chloroauric acid
et al.	et alii
$NaBH_4$	sodium borohydride
S	elemental sulfur
$AuCl(PPh_3)$	chloro(triphenylphosphine) gold (I)
Hg^{2+}	mercuric ion
PC	phthalocyanine photosensitizer
RNA	ribonucleic acid
MMPCs	mixed monolayer protected clusters
GSH	glutathione
PDMS	polydimethylsiloxane
μCP	microcontact printing
MHA	16-thiohexadecanoic acid
PLL	poly-L-lysine
PEG-SH	11-thioundecyl-penta(ethylene glycol)
MOU	11-mercapto-1-undecanol

E. coli	*Escherichia coli*
AFM	atomic force microscope
mV	millivolt
LPS	lipopolysaccharide
EDTA	ethylenediaminetetraacetic acid
DPN	dip-pen nanolithography
TEM	transmission electron microscope
TMV	tobacco mosaic virus
Zn^{2+}	zinc ion
P. aeruginosa	*Pseudomoas aeruginosa*
TMAFM	tapping-mode atomic force microscopy
μm	micrometer
SiO_2	silicon dioxide
Si	silicon
C_{60}	fullerene-60
SAMDI-TOF MS	matrix assisted laser desorption-ionization time-of-flight mass spectrometry
Ac_2O	acetic anhydride
H_2SO_4·	sulfuric acid
$TiCl_4$	titanium (IV) chloride
CH_2Cl_2	dichloromethane
$HO(CH_2)_{11}SAc$	11-(hydroxyundecyl) ethanethioate
$Hg(CN)_2$	mercury (II) cyanide

K_2CO_3	potassium carbonate
MeOH	methanol
$SnCl_4$	tin (IV) chloride
$HClO_4$	perchloric acid
$ZnCl_2$	zinc (II) chloride
TMSCl	trimethylsilyl chloride
$FeCl_3$	iron (III) chloride
$Cu(OTf)_2$	copper triflate
^1H NMR	proton nuclear magnetic resonance
$HgBr_2$	mercury (II) bromide
Ag_2CO_3	silver carbonate
$AgClO_4$	silver perchlorate
AgOTf	silver trifluoromethanesulfonate
$HO(CH_2)_{11}Br$	11-bromoundecanol
KSAc	potassium thioacetate
TLC	thin layer chromatography
AcOEt	ethyl acetate
PE	petroleum ether
H_2O	water
Na^+	sodium ion
K^+	potassium ion
Rb^+	rubidium ion
Cs^+	cesium ion

SPR	surface plasmon resonance
DCC	N, N'-dicyclohexylcarbodiimide
HOBT	hydroxybenzotriazole
THF	tetrahydrofuran
MeCN	acetonitrile
Cu^{2+}	copper (II) ion
Pb^{2+}	lead (II) ion
Hg^{2+}	mercury (II) ion
Zn^{2+}	zinc (II) ion
Cd^{2+}	cadmium (II) ion
μM	micromolar
μL	microliter
M^{+}	metal ion
P	number of binding sites
R	binding function
PET	photoinduced electron transfer
NEMS	nanoelectromechanical systems
LFM	lateral force microscopy
TMS	trimethylsilane
$NaHCO_3$	sodium bicarbonate
Na_2SO_4	sodium sulfate
CH_2Cl_2	dichloromethane
H_2O_2	hydrogen peroxide

LB	Luria-Bertani
OD	optical density
HCl	hydrochloric acid
HNO_3	nitric acid
N_2	nitrogen

CHAPTER ONE

AN INTRODUCTION TO HOST-GUEST AND SUPRAMOLECULAR CHEMISTRY WITH THEIR APPLICATIONS IN NANOTECHNOLOGY

Host-Guest Supramolecular Chemistry

Host-guest chemistry involves complementary binding between two molecules. These binding interactions can involve electrostatics, hydrogen bonding, π-π stacking interactions, dispersion and inductive forces, and hydrophobic or solvatophobic effects. Organic host molecules have been synthesized to bind anions, cations, and neutral molecules such as proteins and enzymes, and have been used as optical sensors, electrochemical sensors, supramolecular catalysts, and in the pharmaceutical industry as anti-cancer agents.[1]

Calixarenes are macrocylic molecules that have been shown to act as host molecules for small guests including solvent molecules, anions, and cations. Cyclotriveratrylene (CTV) is a calixarene and a common supramolecular scaffold that has been extensively employed in guest-host chemistry.[2] CTV was first synthesized *via* the acid catalyzed condensation of veratryl alcohol by G. M. Robinson in 1915 (Scheme 1), and involves the cyclic trimerization of veratryl alcohol *via* the veratryl cation.[3]

Scheme 1. Direct trimerization of veratryl alcohol to afford CTV

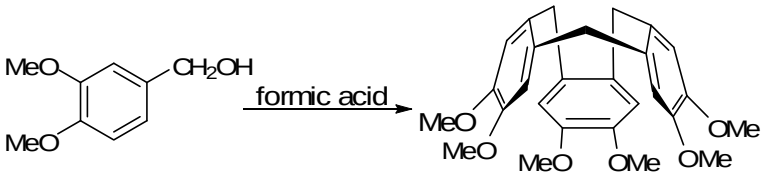

In 1995 Atwood *et al*.[4] synthesized a CTV-ruthenium organometallic sandwich species that acts as a host molecule for the removal of nitrates, phosphates, and nuclear waste by-products such as $^{99}TcO_4^-$ from waste water. This ruthenium organometallic-CTV host ligand was synthesized in situ by mixing [{Ru(η^6-*p*-MeC_6H_4-$CHMe_2$)Cl(μ-Cl)}$_2$] with Ag[CF_3SO_3] in acetone, and then refluxing with CTV in neat CF_3CO_2H. The X-ray structure revealed that the ruthenium metal complexes are sandwiched between the aromatic rings of the CTV, and are involved in π-π interactions with the MeC_6H_4-$CHMe_2$ aromatic ring from the organo-ruthenium complex. The $CF_3SO_3^-$ counter anion was found to be captured in the intercavity of the CTV bowl. In order to determine the host-guest potential of the CTV-organometallo complex, the anion binding properties were tested by exposure to [NBu_4][ReO_4] in nitromethane. Here, Atwood *et al*.[4] showed that the ReO_4^- anion had replaced the $CF_3SO_3^-$ anion within the CTV cavity.

CTV has also been shown to be a good host molecule with other organometallic guests, including Ru(II) and Ir(III) complexes. In 1996, Steed *et al*.[5] determined that due to the electron donation from the methoxy groups into the arene rings, the aromatic rings were electron rich, making these rings excellent ligand sites forming stable arene complexes with transition metals. Derivatized CTV chelating ligands have also been shown to form metallo-gels when in the presence of dimethylformamide (DMF) and 3 equivalents of $CuCl_2$.[6]

In nature, host-guest chemistry is involved in interactions between bacteria and oligosaccharides for adhesion. Cell surface carbohydrates (*e.g*. glycoproteins and glycolipids) play a critical role in cell-cell recognition, adhesion, and signaling.[7, 8] For example, pathogenic bacteria utilize carbohydrates on the surface of human cells for host recognition and attachment.[9] Interactions between pathogenic bacteria and carbohydrates can be highly specific, and carbohydrate-binding specificities are known for a wide variety of microbes (Table 1).[10, 11] For example, D-mannose binding is involved in *Escherichia coli* attachment in urinary tract infections [12] and adhesion lectins from *Pseudomonas aeruginosa* have been structurally characterized and shown to tightly bind monosaccharides.[13] Therefore, carbohydrates are the biomolecule of choice for the recognition and capture of pathogenic bacteria. One challenge is the relatively low affinity between glycan-binding proteins and carbohydrates. Typically the monomeric K_d values are in the micromolar to millimolar range. In biological systems this low affinity is overcome through multivalent interactions.[14]

As with most bacterial species, pathogenic bacteria exhibit significant variation between strains, including variations in the presence of genes encoding virulence factors, toxins, and antibiotic resistance.[15] Understanding the specific characteristics of an individual pathogenic strain (*e.g*. antibiotic resistance traits) can play a significant role in diagnosis and treatment of bacterial infections. However, determining these characteristics requires analyses that go beyond simple detection of a pathogenic bacterial species. In addition, genomic analysis of a pathogenic organism (which also requires significant analysis beyond simple detection) enables researchers to identify the source of

a pathogen and track its spread, which can facilitate more effective prevention.[16] Interaction of microbial proteins and host cell-surface carbohydrates is considered essential for successful infection, and the degree to which bacterial pathogens bind to cell-surface carbohydrates has been shown to correlate with virulence.[17, 18]

This important host-guest interaction allows bacterial cells to target host cells for infection as well as cell-cell signaling. Nosocomial infections are a significant cause of morbidity and mortality in the United States. In 2002, the estimated number of nosocomial infections in U.S. hospitals was 1.7 million, which represents approximately 5% of hospital admissions, and the estimated deaths associated with these infections were greater than 98,000.[19] Three of the most common organisms causing nosocomial infections are *Escherichia coli*, *Staphylococcus aureus*, and *Pseudomonas aeruginosa*. The Centers for Disease Control (CDC) estimates that more than 76 million cases of food-borne illness occur each year in the US resulting in >300,000 hospitalizations and more than 5,000 deaths (www.cdc.gov). Two of the most common causes of food borne infections are *Escherichia coli* and *Salmonella enterica*. Therefore, there is a need for rapid pathogen detection in industrial and hospital settings, and any detection and capture format based on carbohydrates must enable polyvalent interactions in order to be effective.[10]

Table 1. Carbohydrate specificity of selected bacterial strains.

Bacteria	Carbohydrate Specificity
Pseudomonas aeruginosa	D-galactose, L-fucose, L-rhamnose
Streptococcus aureus	6'SLn, 3'SL[2], Galβ1-4GlcNAc
Escherichia coli	D-mannose
Salmonella enterica	Galβ1-4(Fuc α(1-3))GlcNAc
Candida albicans	L-fucose
Heliobacter pylori	Neu5Ac(α2,3)Gal
Streptococcus suis	Gal(α1,4)Gal

The overall goal of this research is to fabricate pre-designed, spatially controlled arrays of supramolecular and biological molecules utilizing both bottom-up and top-down approaches. The data described in this thesis utilizes host-guest interactions between biologically active molecules as well as supramolecular scaffolds. These explorations of host-guest interactions will advance the field of nanotechnology in the development and fabrication of biological nanoarrays, explore the interactions between metal binding ligands and transition metal ions in solution, as well as designing a new fabrication method for the development of nanoelectronic devices through host – guest interactions.

Nanotechnology

Nanoscience is the study of molecular structures in the 1 – 100 nm range.[20] At the nanoscale level, molecular structures exhibit different properties than their corresponding bulk materials based on quantum and subdomain phenomena.[21-23] Nanoscale structures exist in nature that have the capability to act as photonic devices, motors, and power generators in the forms of photosynthetic apparatuses, isomerases and helicases, and mitochondria and chloroplasts.[24] One of the goals of nanotechnology is to

be able to mimic these processes through the development of nanoelectronic and nano-optical devices, drug delivery systems, and magnetic storage media.

One commonly used nanofabrication method for the development of nanoelectronic and nano-optical devices is bottom-up, layer-by-layer assembly on a solid surface.[25] Bottom-up, layer-by-layer assembly on surface substrates is achieved through the formation of molecules into self-assembled monolayers (SAMs) onto the surface. The standard and most studied substrate used is a gold surface. Thin-film gold surfaces are prepared by physical vapor deposition, sputtering, or electrodeposition; and gold can also be easily patterned onto surfaces by a combination of micromachining, photolithography, or chemical etchants. In addition gold is a relatively inert metal that does not react with atmospheric O_2, nor is it easily oxidized at temperatures below its melting point.[20] The combination of these properties allows the formation of SAMs to occur at standard temperature and pressure (STP) and obviates the need for an ultra-high vacuum (UHV) and clean room environment. SAMs have been shown to form easily on gold surfaces because gold has a high affinity for sulfur atoms thus quickly forming a strong gold-sulfur bond.[26] The stability of the gold-sulfur bond that is formed is most likely due to a charge transfer from gold to the sulfur with an activation barrier around 30 kcal/mol on an Au(111) surface.[27, 28]

A growing priority in the field of nanoscience utilizes the gold-sulfur bond on surfaces for the building of new hybrid nanoelectronic and biological devices (*e.g.* bioarrays, biochips, biosensors, or microelectromechanical systems (MEMS)), and to understand the attachment chemistry, adhesion forces, and material compatibility of the

building blocks of these devices. Significant efforts have been made to search for specific biological linkers [29-33] and resists [32-37] to provide selective and efficient binding of biomolecules, including living cells, to functionalized surfaces. The mechanisms responsible for the adhesion chemistry of molecules to surfaces may include electrostatic interactions,[34, 38, 39] hydrophobic interactions,[33] or specific recognition.[29-31, 40] Therefore, developing methods to pattern and immobilize supramolecular and biological molecules with micro- to nanometer spatial control will result in a broad range of new technological advancements not only in basic research but also in diagnostics and drug discovery.[41-44] Some of the most interesting and useful advancements have come in the areas of biochip array development that utilize DNA, proteins, or carbohydrates as linker molecules.[7, 45] Biochip development is particularly important given the explosion of proteomic and genomic studies requiring oligonucleotides or peptides bound to glass surfaces. Patterned substrates have also been used as scaffolds for biomolecule binding and cell adhesion in tissue engineering studies, as well as components for microfluidic bioanalysis.[8, 46, 47] However, many challenges remain, particularly the development of patterning methods that combine micro- to nanoscale surface features with adhesion chemistries that not only provide selectivity in biomolecule binding and positioning but also preserve biological activities. Importantly, unpatterned areas of the surface must resist non-specific biomolecule binding for the effective development of most biological and commercial applications.

A specific area that has not been extensively examined is the selective and directed binding of biological molecules and bacterial cells to *pre-designed*, *spatially*

controlled nano- or micron scale arrays in *directed* orientations so that the biologically active center is accessible to substrates, or in the case of DNA or carbohydrates, complementary strands or receptor sites. Moreover, the principles of molecular recognition such as hydrogen bonding, hydrophobic forces, van der Waals forces, π -π interactions, and electrostatic effects have not been fully explored for biological surface sensing and/or detection. In order to selectively bind biologically active molecules such as proteins, oligonuclotides, carbohydrates, or linkers to surfaces in a controlled and directed fashion, control over both productive and nonproductive orientations is required. Overcoming these issues will open the door to fundamental studies involving enzymatic function as well as basic cellular function.[8] Such spatially-controlled, directed biomolecule binding can also be utilized to fabricate artificial surface receptors, which will allow biological signaling processes to be studied and may prove useful in the design and development of detection systems or laboratories-on-a-chip.[48]

Surface Patterning Methods

Microcontact Printing

A common method for transferring molecules to surfaces is through the patterning method of microcontact printing (μCP) which uses an elastic stamp made of polydimethylsiloxane (PDMS). Deposition of molecules via μCP occurs when a PDMS stamp is "inked" with an organosulfur compound and the PDMS stamp comes into contact with a gold surface, allowing the molecules to be deposited onto the surface and a thiolate bond to form. For example, in a study by Mrksich *et al*.[49] PDMS stamps were

used to pattern organosulfur SAMs that terminated in hydrophobic methyl groups for the adsorption of proteins onto the surface.

Recent research on the immobilization of bacteria cells on surfaces in order to explore bacterial cell adhesion chemistries as well as methods for the fabrication of microarrays capable of binding motile bacterial cells in specific positions and alignments (Figure 6) utilized μCP.[50] For example, micro-contact printing was used to prepare pre-designed microarrays of 16-thiohexadecanoic acid (MHA), which were then covalently functionalized with *Escherichia coli* antibodies or poly-L-lysine (PLL). The bare gold surfaces were passivated with 11-mercaptoundecyl-penta(ethylene glycol) (PEG-SH) or 11-mercapto-1-undecanol (MOU) (Figure 1).[50]

Figure 1. Schematic for the preparation of pre-designed microarrays for the attachment of motile bacterial cells to surfaces.[51]

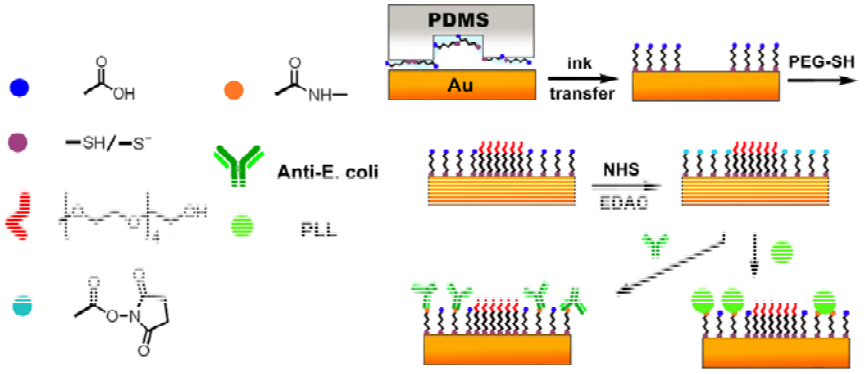

Once these pre-designed microarrays were prepared, *E. coli* K-12 cells were attached with little or no non-specific binding (Figure 2). These data indicate that motile *E. coli* cells can be attached to pre-designed line or dot features and binding occurs *via* the cell body or the bacterium's flagellum. Interestingly, bacterial cells exhibit selective

adsorption to substrates patterned with poly-L-lysine and anti-lipopolysaccharide. Moreover, *E. coli* K-12 cells are alive and motile after adhesion to patterned surface features for more than four hours, based on direct optical monitoring utilizing a two color fluorescence viability assay.[50] In addition, individual motile bacterial cells were shown to require a minimum pre-designed surface feature of at least 1.3 μm in diameter for reasonable attachment efficiencies to be obtained.[50] High-resolution AFM images of bacterial cells, flagella and pilli, immobilized on MHA-PLL modified gold surfaces were presented. The importance of controlling the adhesion of a single bacterial cell to a surface was discussed and one obstacle in the preparation of a biomotor powered by motile bacterial cells was overcome, *i.e.* increasing the percent attachment of motile bacterial cells to a surface with the formation of site-specific, uniform, microarrays of bacterial cells.[31, 36, 52-55]

Figure 2. Attachment of *E. coli* cells to pre-fabricated poly-L-lysine patterned surfaces.[51]

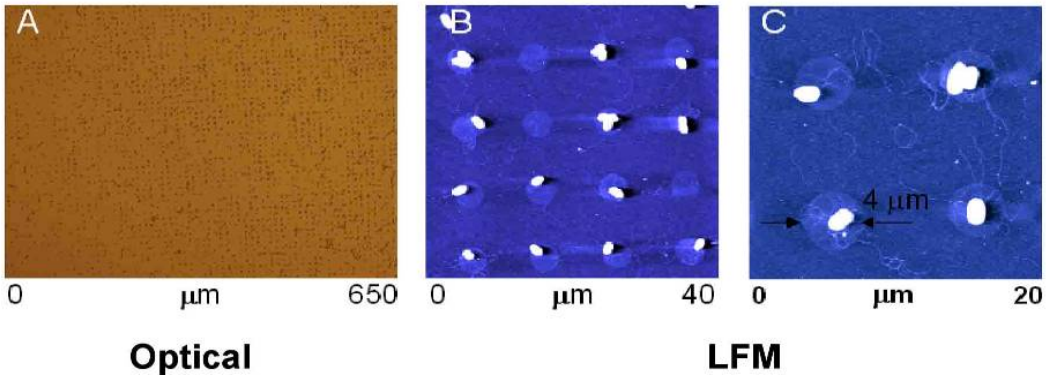

The attachment of *E. coli* K-12 cells to MHA-PLL surfaces was hypothesized to be due to electrostatic interactions between negatively charged groups on the cell surface of *E. coli* K-12 cells and the positively charged PLL molecule.[50] In order to test this

hypothesis, the effect of electrochemical potential on *E. coli* K-12 bacterial cell adhesion to bare gold surfaces was examined.[56] The attachment of *E. coli* K-12 bacterial cells to bare gold surfaces was performed under ambient conditions using a BAS 100 electrochemical apparatus. Optical images of *E. coli* K-12 cells bound to bare gold surfaces at +1000, 0, and –1000 mV indicate that negatively charged surfaces repel *E. coli* K-12 cells while positively charged surfaces attract them and cause cell surface attachment. These data are consistent with the proposal that *E. coli* cell surfaces are negatively charged due to surface phosphate and carboxylate groups, composing the core region of lipopollysaccharide (LPS) molecules.[57] Applying a negative potential (-1,000 mV) to electrochemically attached *E. coli* K-12 cells removes ~60% of the bacteria from the gold electrode surface. These data indicate that the electrochemical attachment process is only partially reversible. Based on the data, *E. coli* K-12 cells are only attracted to the gold electrode surface when a potential of at least +750 mV is applied. These data provide evidence that the negatively charged *E. coli* K-12 cells bind to positively charged PLL. In addition, treatment of *E. coli* K-12 cells with ethylenediaminetetraacetic acid (EDTA) disrupted surface LPS molecules, which resulted in a loss of the negative charge on the cell surface. Therefore, LPS is likely the main negatively charged species on the cell surface and, therefore, accounts for most of the electrostatic interaction with PLL. These data also indicate that applying an electrical potential allows the direct, real time detection of live, dead, or damaged bacterial cells.

The results presented in Chapter 2 shows the development and synthesis of carbohydrate derivatives with alkanethiol linkages that are capable of being patterned

onto gold surfaces for the development of carbohydrate nano- or micron sized arrays. These arrays consist of pathogen-specific carbohydrates immobilized on a solid support, which were used to specifically capture whole, live bacterial cells in parallel. Carbohydrate-based arrays have the potential to meet the challenge of rapid and accurate bacterial pathogen detection while simultaneously capturing whole, viable bacterial cells that can be utilized for post-capture analysis (Figure 3).

Figure 3. Schematic of a carbohydrate microarray made up of six different carbohydrate inks. Upon addition of a pathogenic bacterial cell with binding specificity to one of the carbohydrates used (red), cellular recognition and capture occurs allowing rapid detection of the pathogenic bacterium.

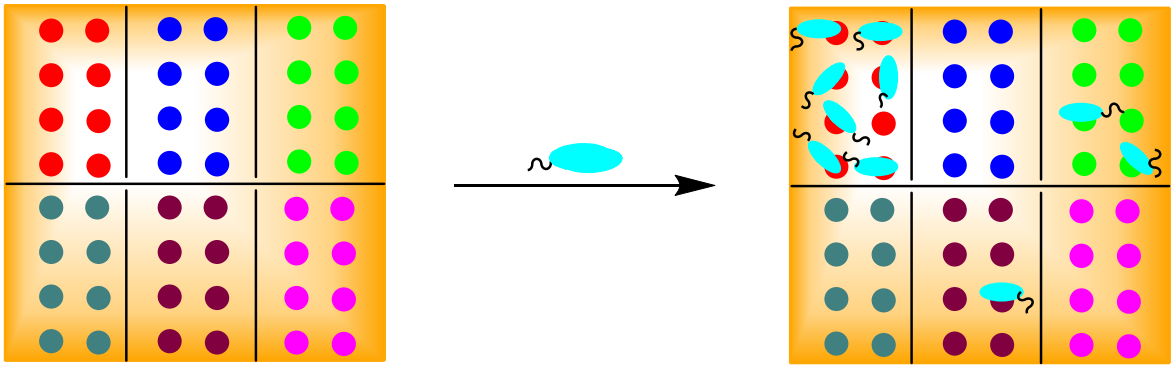

Dip-Pen Nanolithography

In 1999, Mirkin *et al.*[58], showed that thiolated molecules could be directly deposited onto a gold surface with an atomic force microscope (AFM) tip. This deposition method was termed Dip-Pen Nanolithography (DPN), and this lithographic method affords the user the ability to transport an "ink" through the diffusion of the molecule through the water meniscus that is formed between the tip of a coated AFM cantilever and the gold surface.[39] The DPN process of patterning can be broken into two

separate steps: 1) molecular transport of the ink from the tip to the surface through dissolution of the "ink" into the meniscus that form between the cantilever's tip and the surface, and 2) adsorption of the "ink" onto the surface and the subsequent formation of the gold-sulfur bond.[39] DPN is a particularly important nanolithography method for the patterning of biomolecules, since DPN is capable of positioning molecules on a substrate with 10 nm resolution.[59] DPN has been used to prepare surface patterns of tailored inks, leading to nanoscale positioning of active proteins, virus particles, and cells. In an innovative study by Maspoch *et al*., ferritin proteins, which can be visualized by a Transmission Electron Microscope (TEM), were patterned into dot patterns onto TEM slides to determine what controls the number of molecules deposited with DPN. This study concluded that the factors that determine the amount of particle deposition onto the surface is controlled by the contact angle between the ink solution and the substrate, the initial concentration of the ink, and the size of the dot patterned onto the substrate.[60]

DPN technology has been employed to create biological sensing devices, nanocircuitry for electronic devices, and hybrid nanodevices.[59] Many of these patterned devices require the use of host-guest interactions to develop bottom-up, layer-by-layer assemblies. For example, Mirkin *et al*.[61] were able to create predefined virus nanoarrays with the guest tobacco mosaic virus (TMV) through the patterning of the host MHA onto gold substrates. The surface was passivated with a monolayer of 11-thioundecyl-penta(ethylene glycol) (PEG-SH) and Zn^{2+} was used to coordinate between the carboxylic acid groups of the MHA layer and the carboxylate-rich TMV surface.[61] In a separate study, Mirkin *et al*.[62] successfully utilized DPN to pattern oligonucleotides to a

silicon surface. However, in this case as well the entire surface was modified with MPTMS prior to the attachment of acrylamide-terminated oligonucleotides.

In an effort to explore bacterial cell adhesion chemistries as well as methods for the fabrication of arrays capable of binding motile bacterial cells in specific positions and alignments,[63] submicron DPN-generated MHA line patterns that were covalently functionalized with PLL.[50] "Blocks" were prepared in order to increase the surface area available for the electrostatic interaction with PLL. An approximately 2 μm feature was prepared, which was made up of multiple closely spaced lines allowing PLL to span these surface features. "Blocks" with 100 nm spacing between MHA lines were prepared using DPN and used for the attachment of motile *Pseudomonas aeruginosa* cells. Motile *P. aeruginosa* cells were observed to bind to DPN generated MHA/PLL line patterns, "Blocks" made up of eight lines with 100 nm spacing, with ~80% occupancy (Figure 4). Cellular binding to these "Block" surface structures occurred *via* an electrostatic interaction between negatively charged groups on the bacterial cell surface with positively charged PLL assemblies. It should be noted that the attached *P. aeruginosa* cells survived for >6 hours in an aqueous environment based on direct optical monitoring. Motile *P. aeruginosa* cells mostly attached through their body rather than their single flagellum suggesting an electrostatic interaction between the cell body and the MHA/PLL microarray is the predominant immobilization process. Cellular attachment to pre-designed DPN generated microarrays was found to be dependent on the shape and size of the surface feature. While this observation is likely due in part to dense, well formed MHA monolayers generated *via* DPN, it may also simply be due to the physical shape of

the surface structure. These data indicate that these DPN generated "block" surface structures provide a promising footprint for the attachment of motile bacterial cells that may find utility in cell based biosensors or single cell studies.

Figure 4. TMAFM phase images of the *P. aeruginosa* cells attached to the DPN generated templates. Scan sizes are a) 18 x 18 μm^2 and b) 6 x 6 μm^2. The attachment of the bacterial cells is directed by the pre-programmed templates which are lines spaced by 100 nm.

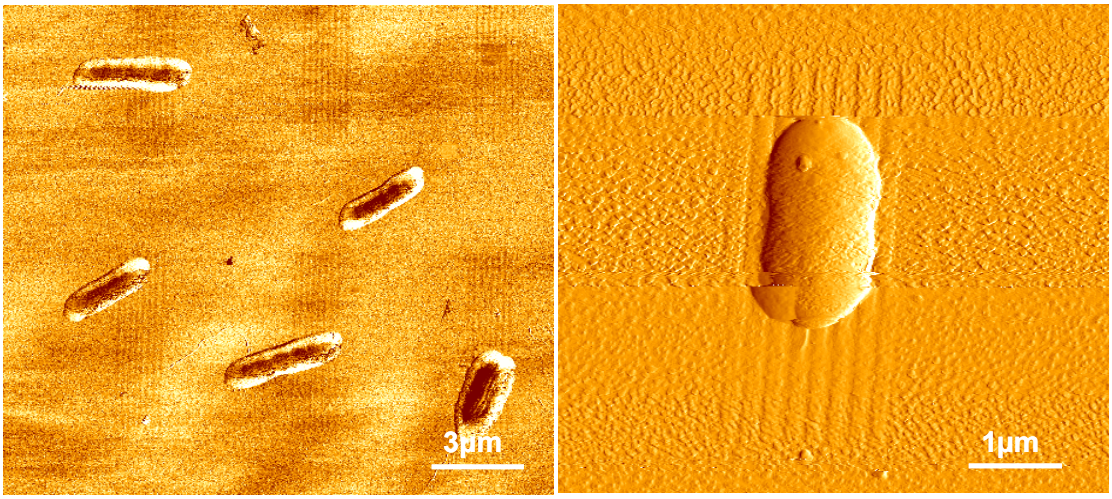

DPN has also been utilized for the development of novel nanoelectrical systems. In an impressive study by Bao *et al.*,[64] DPN was used to create gold electrodes on graphene sheets on SiO_2/Si substrates. This innovative process involved the deposition of a 10 nm optically transparent film onto a graphene sheet. MHA was then written onto the gold surface as a mask. The deposited gold layer was then removed by wet etching with a ferric nitrate/thiourea solution, and the exposed graphene surface was then O_2 plasma etched to reveal the graphene layer that was deposited with gold and masked by the MHA.[65] The substrate was wet etched again to remove the MHA mask and gold layer, leaving only the graphene on the substrate. In order to complete the gold contacts

to the graphene, a 10 nm thin film was again deposited onto the substrate. From there, DPN was used to selectively deposit another MHA resist to define the gold contacts to the graphene. Again, the substrate was wet etched to reveal the graphene with the two gold contacts.

In an effort to advance the field of fabrication of nanoelectronic devices, the research described in Chapter 3 utilizes host – guest interactions for a novel apex-modified CTV derivative with an attached thiolane-containing lipoic acid linker that was directly patterned onto gold substrates via DPN. The addition of a dithiolane-containing linker to the apex of CTV provides a molecule that can adhere to a gold surface with its bowl shaped cavity directed *away* from the surface thereby providing a surface-bound CTV host that can be used for the directed assembly of guest molecules. Subsequent exposure of these CTV microarrays to C_{60} in toluene resulted in the directed assembly of predesigned, spatially controlled, high-density microarrays of C_{60}. The molecular recognition capabilities of this CTV-template toward C_{60} provides proof-of-concept that supramolecular CTV scaffolds can be directly patterned onto surfaces providing a foundation for the development of organic electronic and optoelectronic materials.

Nanoparticles

The first known historical use of gold nanoparticles (AuNPs), also known as colloidal gold or "soluble" gold, dates back to the 4th or 5th century B.C., where the Chinese and Egyptians were known to have used the "soluble" gold for both curative and artistic purposes. In the Middle Ages, it was believed that colloidal gold could be used to cure dysentery, epilepsy, tumors, as well as heart and venereal complications. In the last

two decades, there has been an explosion of interest in the use of AuNPs for therapeutics, detection, and new pharmaceuticals.

There are three conventional methods for the synthesis of AuNPs from the reduction of Au(III) salts (Table 2). The classical method for the synthesis of AuNPs was introduced by Turkevitch *et al.* in 1951.[66] This synthesis involves the reduction of $HAuCl_4$ in water by sodium citrate and leads to AuNPs that are approximately 20 nm in diameter. In 1973, Frens[67] found that nucleation of the AuNP from 16 – 147 nm could be controlled by reducing the Au(III) salt in the presence of an *n*-alkane thiol stabilizing agent (Scheme 2). The modern method for the synthesis of AuNPs is the Brust-Schiffrin two-phase method that was developed in 1994.[68] This method advanced the field of nanoparticle synthesis by offering a synthetic method that produces AuNPs that are in the 1.5 – 5.2 nm range, that are easily functionalized, repeatedly isolated, and can be redissolved in organic solvents without decomposition or aggregation. In this synthetic method, $AuCl_4^-$ is transferred from the aqueous phase to an organic phase (toluene) using tetraoctylammonium bromide as the phase-transfer agent. $AuCl_4^-$ is reduced with $NaBH_4$, and due to the soft character of both S and Au, a simple alkanethiol caps and stabilizes the AuNP.[69]

Table 2. Synthetic methods and capping agents for AuNPs of varying size.[70]

Core size (d)	Synthetic methods	Capping Agents
1 – 2 nm	Reduction of $AuCl(PPh_3)$ with diborane or sodium borohydride	Phosphine
1.5 – 5 nm	Biphasic reduction of $HAuCl_4$ by sodium borohydride in the presence of thiol capping agents	Alkanethiol
10 – 150 nm	Reduction of $HAuCl_4$ with sodium citrate in water	Citrate

Scheme 2. Synthesis of AuNPs by reduction with sodium citrate and subsequent stabilization with *n*-alkanethiol.

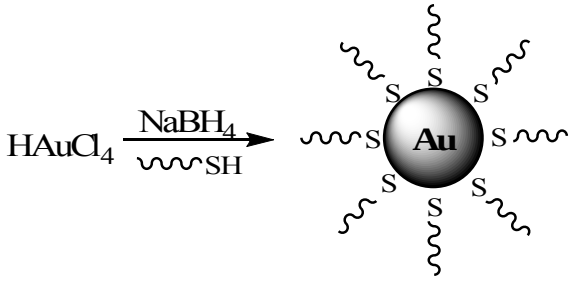

Due to their unique distance-dependent optical properties, and large extinction coefficients, AuNPs have been functionalized to be highly selective and sensitive colorimetric detection systems for oligonucleotides, proteins, and metal ions. In 2007, Mirkin *et al*.[71] devised a selective and highly sensitive mercuric ion (Hg^{2+}) colorimetric detection system that exploited thymidine-Hg^{2+}-thymidine coordination chemistry (Figure 5). In this colorimetric Hg^{2+} detection system, two different types of AuNPs were functionalized with complementary thiolated-DNA sequences with the exception of a single thymidine-thymidine mismatch. In the presence of an aqueous solution of Hg^{2+}, the complementary thymidine-thymidine mismatched DNA strands selectively coordinated with the mercuric ion, forming stable aggregates. The formation of the DNA-AuNP aggregates turned the solution from a bright red in color to purple. This selective colorimetric Hg^{2+} sensor was capable of measuring Hg^{2+} concentrations in the low micromolar range.

Figure 5. DNA-functionalized AuNPs used for the colorimetric detection of mercuric ions (Hg^{2+}).[71]

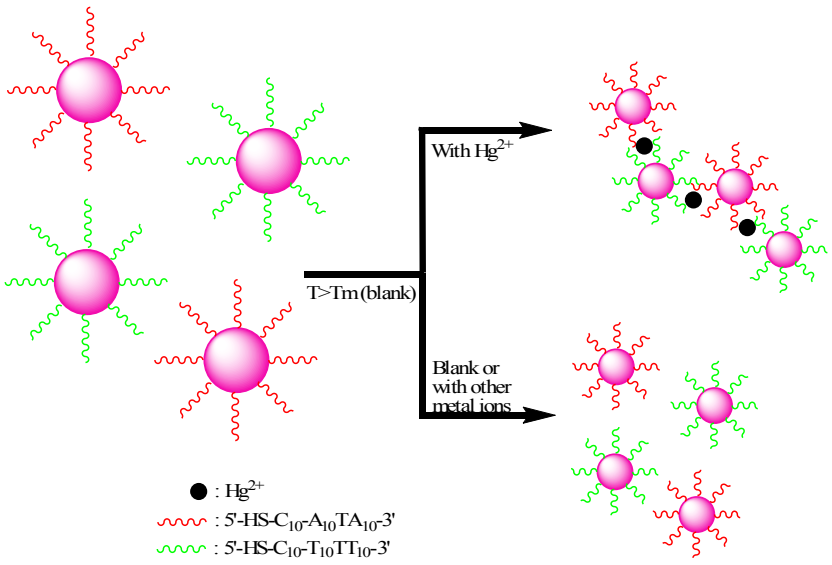

A growing field in the area of nanoscience is the use of AuNPs as nanocarriers for target-specific delivery of therapeutic agents to treat human diseases.[70] An advantage that AuNPs have in the delivery of drugs over traditional delivery systems is the improved solubility, *in vivo* stability, biodistribution, and large pharmaceutical loading ability of AuNPs.[70] For example, Zubarev *et al.*[72] was able to couple the chemotherapeutic drug, paclitaxel, in a ratio of ~ 70 molecules per 2 nm AuNP.

AuNPs have also been utilized for the delivery and release of diatomic therapeutic agents like nitric oxide and singlet oxygen. In 2002, Russell *et al.*[73] functionalized 2 – 4 nm AuNPs with a phthalocyanine (PC) photosensitizer that were soluble in polar solvents to be used in photodynamic therapy. These PC functionalized AuNPs were shown to have a 50 % increase in the production of singlet oxygen when compared to free PC in solution. Due to their high surface-to-volume ratio and large loading capabilities, AuNPs also offer the delivery of DNA and RNA for gene therapy.[70] Recently, it has been shown

that positively charged triethylammonium-functionalized mixed monolayer protected clusters (MMPCs) are capable of binding to DNA through complementary electrostatic interactions.[74] These MMPC-DNA complexes were shown to completely inhibit the transcription of T7 RNA polymerase. Intracellular concentrations of glutathione (GSH) were shown to release the DNA from the nanoparticle and recover DNA transcription.

The results described in Chapter 4 describes the synthesis of an apex-modified CTV derivative with an attached thiol linker that was used to functionalize AuNPs. Previous X-ray crystallographic studies revealed that native CTV can form host-guest polymer aggregates with group 1 and lanthanide metal cations.[75] Since the aggregation of AuNPs results in colorimetric changes, these CTV-functionalized AuNPs were used to develop a spectrophometric method to study the binding affinity between the CTV scaffold with transition metal ions in solution.

Conclusion

The research described in this dissertation focuses on a bottom-up, layer-by-layer approach to fabricate supramolecular scaffolds for biological and inorganic detection or sensing. The research focuses on the design and synthesis of biologically relevant linker molecules and supramolecular scaffolds that can be attached to gold surfaces. These molecules were patterned into pre-designed arrays using both parallel lithiographic methods such as μCP and serial methods such as DPN. Once patterned, the biological activity of the newly generated arrays was examined to provide "proof-of-concept" that the newly synthesized linker molecules retained their desired activity. This work has also provided insight into the adhesion chemistries of both supramolecular scaffolds and

biologically relevant molecules. The importance of this project is underscored by the growing demand for pre-designed arrays of immobilized supramolecular and biological molecules with micro- to nanometer scale control, given the explosion in studies related to nanoelectrical, MEMs, proteomic and genetic screening as well as detection and sensing of biological molecules and microorganisms.

CHAPTER TWO

DIRECT PATTERNING OF CARBOHYDRATE MICROARRAYS WITH AFFINITY FOR INDIVIDUAL BACTERIAL CELLS

Introduction

Cell surface carbohydrates (*e.g.* glycoproteins and glycolipids) play a critical role in cell-cell recognition, adhesion, and signaling, and lectins are glycan-binding proteins of bacterial pathogens that are located on the outer membrane and are believed to be responsible for cell-cell interactions and the formation of biofilms.[7, 8] For example, all pathogenic bacteria utilize carbohydrates on the surface of human cells for host recognition and attachment.[9] Attachment of microbial proteins to host cell-surface carbohydrates is considered essential for successful infection, and the degree to which bacterial pathogens bind to cell-surface carbohydrates has been shown to correlate with virulence.[17, 18] Interactions between pathogenic bacteria and carbohydrates can be highly specific, and carbohydrate-binding specificities are known for a wide variety of microbes.[10, 76] For example, Gal(α-l,4)Gal binding is involved in *Escherichia coli* attachment in urinary tract infections and adhesion lectins from *Pseudomonas aeruginosa* have been structurally characterized and shown to bind tightly to monosaccharides.[77, 78] Therefore, carbohydrates are the biomolecule of choice for the recognition and capture of pathogenic bacteria. One challenge is the relatively low affinity between glycan-binding

proteins and carbohydrates. Typically the monomeric K_d values are in the micromolar to millimolar range. In biological systems this low affinity is overcome through multivalent interactions suggesting that multivalent interactions should be essential for experimental detection and capture as well.[79]

Microarrays are widely used in the biological sciences as tools for monitoring gene expression.[80] These gene expression microarrays generally consist of nucleic acids arrayed and bound to a solid surface, and they enable massively parallel hybridization reactions to be conducted within a small surface area. More recently the microarray approach has been applied to carbohydrates. In general, carbohydrate microarrays have been based on carbohydrate libraries from natural sources or chemical synthesis and the attachment of carbohydrates to a solid surface *via* covalent or noncovalent binding.[81] Carbohydrate microarrays have been used primarily for the study of carbohydrate–protein interactions.[14] However, carbohydrate microarrays have also been used recently to investigate the carbohydrate-binding specificity of intact bacterial cells.[82] For example, Walz *et al.* [83] used a glycoconjugate array to characterize the adhesion specificities of *Helicobacter pylori*. Microarrays are also an ideal format for studying the interactions between bacterial cells and carbohydrates since microarrays allow for polyvalent interactions between whole cells and carbohydrate monomers bound to the microarray.[10, 14] Therefore, mimicking the selective extracellular matrix on an artificial surface will allow for the immobilization and study of single cell binding interactions, potentially leading to the next generation of biological detection systems.[64, 84-87]

Previous uses of carbohydrate arrays have been limited by the large size of the arrays.[72] Traditionally carbohydrate microarrays have not been built by directed self-assembly on the nanoscale, but rather these microarrays are functionalized regions of bound carbohydrates in the ~100 μm – 1 mm diameter range that have been prepared on functionalized glass or gold slides in no pre-defined patterns.[73, 74, 88-91] For example, Disney *et al*.[92] generated carbohydrate arrays to detect pathogenic bacteria, where the average carbohydrate spot size was ~250 μm and the carbohydrate was not directly patterned onto the surface. The functionalized carbohydrates employed by Disney were terminated with an amine and the substrate was pre-coated with an amine-reactive homobifunctional disuccinimidyl carbonate linker. In 2008, Mrksich *et al*.[93] developed a new methodology for generating oligosaccharide biochips where the synthesis and growth of the oligosaccharide on the surface occurred in situ. Matrix-assisted laser desorption-ionization time-of-flight mass spectrometry (SAMDI-TOF MS) was used to monitor the reaction intermediates on the surface during the growth of the oligosaccharide. However, none of these methods offer a directed, bottom-up, layer-by-layer approach to assembling carbohydrates into pre-defined patterns on a surface for formation of carbohydrate microarrays.

Carbohydrates have also been derivatized and attached to gold nanoparticles and magnetic beads for the colorimetric detection of bacteria and their corresponding lectin binding proteins.[94, 95] For example, Chen *et al*.[96] encapsulated 4 nm gold nanoparticles with D-galactose for the selective detection of the PA-1L lectin binding protein in solution. These D-galactose derivatives were terminated with a thio-ethylene glycol

chain. Incubation of these galactose coated AuNPs with PA-1L showed that these galactose-AuNPs had a detection limit of 78 fmol of PA-1L. The binding between the galactose modified AuNPs and the PA-1L binding lectins were confirmed *via* MALDI-TOF MS and TEM.

Herein, is described a reproducible method to generate spatially controlled, bottom-up, layer-by-layer L-rhamnose microarrays in directed orientations, so that the biologically relevant carbohydrate moiety is directed *away* from the surface and is accessible for the binding of biological molecules and bacterial cells. Two L-rhamnose derivatives that are terminated with an alkyl-thiol linker providing a surface-bound carbohydrate where the monosaccharide head group is directed *away* from the surface were designed and synthesized making the L-rhamnose available for interacting with bacterial lectins. The use of the soft lithographic technique of micro-contact printing (μCP) to pattern the carbohydrates provided a method to pre-position the carbohydrate patterns down to ~0.3 μm resolution.[11] The observed binding of *P. aeruginosa* to L-rhamnose microarrays to provides proof-of-concept that carbohydrate scaffolds retain their biologically-relevant function after being patterned onto gold surfaces. These studies provide a foundation for the development of the next generation of nanoscale biological detection and diagnostic systems.

Experimental Section

All solvents and reagents were used without further purification unless otherwise noted. All solvents were distilled prior to use. All reactions were conducted under a nitrogen atmosphere. Sorbent Technologies silica gel 60 Å, 40 – 75 μm (200 x 400

mesh) was used for column chromatography unless otherwise noted. Sorbent Technologies aluminum-backed silica gel 200 μm plates were used for thin layer chromatography (TLC). ^{1}H NMR spectra were obtained utilizing either a Varian INOVA 300 or Varian GEMINI 2000 300 MHz spectrometer with trimethylsilane (TMS) as the internal standard. CEM Discover ® Microwave (MW) Model # 908005 was used in all MW reactions.

*L-Rhamnopyranose tetraacetate (**2a**)*

To a mixture of L-rhamnose **1a** (1.00g, 5.48 mmol) and acetic anhydride (20 mL) cooled to 0ºC was added 4 drops of H_2SO_4. The reaction was allowed to stir for 20 h. The reaction was quenched with aqueous $NaHCO_3$ (100 mL) and AcOEt (25 mL) and allowed to stir until all unreacted acetic anhydride was removed. The two phases were separated and the organic phase was washed 3 × 5 mL aqueous $NaHCO_3$ and 5 mL H_2O. The organic phase was dried over sodium sulfate and the solvent was removed under reduced pressure to afford rhamonose tetraacetate **2a** as a yellow oil (1.42 g, 88 %). ^{1}H NMR (300 MHz, $CDCl_3$) δ 6.02 (s, 1H), 5.29 (d, 1H), 5.25 (d, 1H), 5.10 (t, 1H), 3.94 (p, 1H), 2.17 (s, 3H), 2.16 (s, 3H), 2.07 (s, 3H), 2.01 (s, 3H), 1.23 (d, 3H).

*2,3,4-tri-O-acetyl-β-L-rhamnopyranose chloride (**3**)*

Rhamnose tetraacetate derivative, **2a** (838 mg, 2.60 mmol) was mixed with $SnCl_4$ (0.30 mL, 2.68 mmol) in 5.2 mL of CH_2Cl_2 in a microwave tube according to the general procedure of Steinmann *et al.*[99] The reaction mixture was heated to 70º C for 30 minutes and monitored via TLC using AcOEt/hexane (3/7) as the eluent. Upon consumption of the starting material, the reaction was quenched with 40 mL of an

ice/H_2O mixture. The two phases were separated, and the aqueous phase was extracted with 4 × 10 mL of CH_2Cl_2. The organic extracts were collected and washed with 2 × 10 mL of H_2O. The organic phase was dried over Na_2SO_4. The solvent was removed under reduced pressure to afford the chloro derivative **3** as a brown oil (630 mg, 78%). ^1H NMR (300 MHz, $CDCl_3$) δ 5.94 (d, 1H), 5.54 (dd, 1H), 5.39 (d, 1H), 5.14 (t, 1H), 5.18 (m, 1H), 2.17 (s, 3H), 2.07 (s, 3H), 2.01 (s, 3H), 1.26 (d, 3H).

*11-Bromoundecyl 2,3,4-tri-O-acetyl-β-L-rhamnopyranoside (**4a**)*

To a mixture of rhamnose tetraacetate derivative **2a** was added 1.3 equivalents of 11-bromo-undecanol and 0.13 M CH_2Cl_2. The reaction was cooled to 0ºC and stirred for 20 min, then 1.5 equivalents of $SnCl_4$ (1.0 M heptane) was added dropwise and allowed to stir for 20 h warming to room temperature. The reaction was monitored *via* TLC using 1/2 AcOEt/petroleum ether. The reaction was quenched with AcOEt (200 mL) and aqueous $NaHCO_3$ (200 mL) and allowed to stir for 2 h then filtered over celite. The filtrate was washed with 3 × 50 mL of AcOEt. The organic phase was washed with 3 × 25 mL of H_2O and 25 mL of brine. The aqueous fractions were combined and then extracted with 3 × 25 mL of AcOEt. The organic fractions were collected and filtered over sodium sulfate, then concentrated under vacuum. The crude reaction was purified by column chromatography on silica gel eluting with a gradient of AcOEt/petroleum ether (1/3 to1.5/3) providing **4a** as a viscous orange oil (mg, 48%). ^1H NMR ($CDCl_3$): δ 5.29 (dd, 1H), 5.22 (dd, 1H), 5.04 (t, 1H), 4.71 (d, 1H), 3.82 (q, 1H), 3.64 (m, 2H), 3.40 (t, 2H), 2.15 (s, 3H), 2.05 (s, 3H), 1.99 (s, 3H), 1.84 (m ,3H), 1.57 (m, 3H), 1.41 (m, 3H), 1.29 (m, 11H), 1.22 (d, 3H).

*11-Acetylthioundecyl 2,3,4-tri-O-acetyl-β-L-rhamnopyranoside (**5a**)*

For the synthesis of the β-alkyl acetyl thio-rhamnose derivative according to the general procedure of Lin *et al*.,[95] **3** (610 mg, 2.0 mmol) was diluted with 6 mL of toluene in a flame dried round bottom flask. The solvent was removed under reduced pressure to azeotrope any remaining H_2O from the round bottom flask. $Hg(CN)_2$ (303 mg, 2.4 mmol), drierite (950 mg), toluene (1.25 mL) and MeCN (1.25 mL) were then added to the reaction flask. The reaction was allowed to stir for 10 minutes before a solution of $HO(CH_2)_{11}SAc$ in toluene (1.25 mL) and MeCN (1.25 mL) was added to the reaction dropwise. The reaction was allowed to stir for 24 h and was monitored via TLC using AcOEt/hexane (1/2) as the eluent. Upon consumption of the starting material, the reaction was filtered and rinsed with 10 mL of CH_2Cl_2. The solvent was then removed under reduced pressure and the crude reaction mixture was diluted with 50 mL of CH_2Cl_2. The organic phase was washed 3 × 10 mL of H_2O, 1 × 10 mL of brine, and then dried over Na_2SO_4. The solvent was removed under reduced pressure, and the crude mixture was purified using column chromatography with a 75× loading ratio and an eluent of AcOEt/hexane (1/3) to afford β-alkyl acetyl thio-rhamnose **5a** as a yellow-tinted solid (238 mg, yield: 23%). ^{1}H NMR (300 MHz, $CDCl_3$) δ 5.29 (dd, 1H), 5.22 (dd, 1H), 5.06 (t, 1H), 4.71 (d, 1H), 3.87 (m, 1H), 3.64 (dt, 1H), 3.43 (dt, 1H), 2.83 (t, 2H), 2.32 (s, 3H), 2.15, (s, 3H), 2.05 (s, 3H), 1.99 (s, 3H), 1.56 (m, 4H), 1.27 (m, 14H), 1.23 (d, 3H).

*11-Mercaptoundecyl β-L-rhamnopyranoside (**6a**)*

For the synthesis of the alkyl-thiol terminated rhamnose derivative according to Robinson *et al.*,[97] 11-acetylthioundecyl 2,3,4-tri-O-acetyl-β-L-rhamnopyranoside **5a** (215 mg, 0.4 mmol), K_2CO_3 (20 mg), and 4.2 mL of methanol were mixed in a round bottom flask. The reaction was allowed to stir at room temperature for 24 h and was monitored via TLC using MeOH/CH_2Cl_2 (1/9) as the eluent. Upon consumption of the starting material, the reaction was filtered and rinsed with 3 × 5 mL MeOH. The solvent was removed under reduced pressure. The crude mixture was purified using column chromatography with a 75 × loading ratio and eluting with MeOH/CH_2Cl_2 (1/8) affording the alkyl-thiol terminated rhamnose derivative **6a** as a white solid (29 mg, yield: 20%). ^{1}H NMR (300 MHz, $CDCl_3$) δ 4.75 (s, 1H), 3.92 (s, 1H), 3.75 (d, 1H), 3.61 (m, 2H), 3.49 (d, 2H), 3.39 (m, 2H), 2.51 (q, 2H), 1.56 (m, 4H), 1.31 (m, 19H).

*L-Fucopyranose tetraacetate (**2b**)*

To a mixture of L-fucose **1b** (1.00g, 6.09 mmol) and acetic anhydride (20 mL) cooled to 0ºC was added 4 drops of H_2SO_4. The reaction was allowed to stir for 20 h and allowed to warm to room temperature. The reaction was quenched with aqueous $NaHCO_3$ (100 mL) and AcOEt (25 mL) and allowed to stir until all unreacted acetic anhydride was removed. The two phases were separated and the organic phase was washed with 3 × 5 mL aq $NaHCO_3$ and 5 mL H_2O. The organic phase was filtered over sodium sulfate and concentrated under vacuum to afford **2b** as a white solid (1.02 g, 63%). ^{1}H NMR ($CDCl_3$): δ 6.34 (d, 1H), 5.33 (m, 3H), 4.31 (p, 1H), 2.18 (s, 3H), 2.15 (s, 3H), 2.02 (s, 3H), 2.01 (s, 3H), 1.53 (d, 3H).

*11-Bromoundecyl 2,3,4-tri-O-acetyl-β-L-fucopyranoside (**4b**)*

To a solution of L-fucopyranose tetraacetate **2b** (1.23 g, 3.82 mmol) in 38.2 mL of CH_2Cl_2, was added 11-bromo-undecanol (1.25 g, 4.97 mmol). The reaction was cooled to 0ºC and stirred for 20 min. A solution of $SnCl_4$ (7.64 mL, of 1.0 M in heptane) was added dropwise and the reaction allowed to stir for 20 h and allowed to warm to room temperature. The reaction was monitored *via* TLC using AcOEt/petroleum ether (1/2). The reaction was quenched with aqueous $NaHCO_3$ (200 mL) and AcOEt (200 mL) and allowed to stir for 2 h then filtered over celite. The filtrate was washed with 3 × 50 mL of AcOEt and the two phases were separated. The organic phase was washed with 3 × 25 mL of H_2O and 25 mL of brine. The aqueous fractions were combined and then extracted with 3 × 25 mL of AcOEt. The organic fractions were collected and dried over Na_2SO_4, then concentrated under vacuum. The crude reaction was purified by column chromatography on silica gel eluting with a gradient of AcOEt/petroleum ether (1/3 to 1.5/3). The solvent was removed under vacuum pressure to afford an orange oil (836 mg, 42 %). ^{1}H NMR ($CDCl_3$) δ 5.33 (dd, 1H), 5.29 (dd, 1H), 5.08 (dd, 1H), 5.04 (d, 1H), 4.14 (p, 1H), 3.65 (m, 2H), 3.39 (t, 2H), 2.16 (s, 3H), 2.05 (s, 3H), 1.99 (s, 3H), 1.81 (p, 3H), 1.55 (m, 3H), 1.28 (m, 14H), 1.13 (d, 3H).

*11-Acetylthioundecyl 2,3,4-tri-O-acetyl-β-L-fucopyranoside (**5b**)*

For the addition of the thio-acetyl group to the alkyl linked fucopyranoside, 11-bromoundecyl 2,3,4-tri-O-acetyl-β-L-fucopyranoside **4b** (84 mg, 0.161 mmol) and potassium thioacetate (55 mg, 0.483) were mixed in a round bottom flask with 1.25 mL of DMF. The reaction was stirred for 20 h and monitored *via* TLC with a mixture of

AcOEt/petroleum ether (1/3) as the eluent. Upon consumption of the starting material, the reaction was quenched with 20 mL of H_2O and 20 mL of AcOEt/petroleum ether (1/1). The two phases were separated and the aqueous phase was extracted 3 × 6 mL AcOEt/petroleum-ether (1/1). The organic fractions were combined and washed with 3 × 6 mL of H_2O. The reaction was dried over Na_2SO_4 and concentrated under vacuum providing **5b** as a brown oil (66 mg, 79 %). ^{1}H NMR ($CDCl_3$) δ 5.33 (dd, 1H), 5.29 (dd, 1H), 5.08 (dd, 1H), 5.04 (d, 1H), 4.14 (p, 1H), 3.64 (m, 1H), 3.38 (m, 1H), 2.84 (t, 2H), 2.32 (s, 3H), 2.16 (s, 3H), 2.07 (s, 3H), 1.99 (s, 3H), 1.54 (p, 6H), 1.23 (m, 15H), 1.13 (d, 3H).

*11-Mercaptoundecyl β-L-fucopyranoside (**6b**)*

For the synthesis of the alkyl-thiol terminated rhamnose derivative, 11-acetylthioundecyl 2,3,4-tri-O-acetyl-β-L-fucopyranoside **5b** (66 mg, 0.127 mmol) K_2CO_3 (5.0 mg), and 0.7 mL of methanol were mixed in a round bottom flask. The reaction was allowed to stir at room temperature for ~24 hours and monitored via TLC using MeOH/CH_2Cl_2 (1/9) as the eluent. Upon consumption of the starting material, the reaction was filtered and rinsed with 3 × 5 mL of MeOH. The solvent was removed under reduced pressure. The crude mixture was purified using column chromatography with a 75 × loading ratio and an eluent of MeOH/CH_2Cl_2 (1/8). The alkyl-thiol terminated fucose derivative (**6b**) fractions were combined and removal of solvent to provide **6b** as a white solid (10 mg, 23%). ^{1}H NMR ($CDCl_3$): δ 4.77 (s, 1H), 3.93 (s, 1H), 3.79 (d, 1H), 3.62 (m, 2H), 3.37 (m, 4H), 2.49 (p, 2H), 1.52 (m, 4H), 1.28 (m, 19H).

*D-Glucopyranose pentaacetate (**2c**)*

A mixture of D-glucose **1c** (1.00 g, 5.55 mmol) and 20 mL acetic anhydride was placed into a round bottom flask and cooled to 0ºC. Four drops of H_2SO_4 were then added to the reaction mixture. The reaction was allowed to stir for 20 h and allowed to warm to room temperature. The reaction was quenched with 100 mL aqueous $NaHCO_3$ and 25 mL AcOEt and allowed to stir until all unreacted acetic anhydride was removed. The two phases were separated and the organic phase was washed with 3 × 5 mL aqueous $NaHCO_3$ and 5 mL H_2O. The organic phase was dried over Na_2SO_4 and concentrated under vacuum provided **2c** as a white solid (1.63 g, 75 %). ^{1}H NMR ($CDCl_3$): δ 6.33 (d, 1H), 5.45 (t, 1H), 5.13 (m, 2H), 4.25 (m, 1H), 2.19 (s, 3H), 2.10 (s, 3H), 2.03 (s, 3H), 2.02 (s, 3H), 1.24 (t, 2H).

*11-Bromoundecyl 2,3,4,6-tetra-O-acetyl-β-D-glucopyranoside (**4c**)*

To a solution of D-glucopyranose pentaacetate **2c** (1.63 g, 4.18 mmol) in 42 mL of CH_2Cl_2, was added 11-bromo-undecanol (1.36 g, 5.43 mmol). The reaction was cooled to 0ºC and stirred for 20 min. A solution of $SnCl_4$ (6.27 mL, 1.0 M in heptane) was added dropwise and the reaction was allowed to stir for 20 h and allowed to warm to room temperature. The reaction was monitored *via* TLC eluting with AcOEt/petroleum ether (1.5/3). The reaction was quenched with 200 mL AcOEt and 200 mL aqueous $NaHCO_3$ and allowed to stir for 2 h then filtered through celite. The filtrate was extracted with 3 × 50 mL of AcOEt. The organic phase was washed with 3 × 25 mL of H_2O and 25 mL of brine. The aqueous fractions were combined and then extracted with 3 × 25 mL of AcOEt. The organic fractions were collected and dried over Na_2SO_4, then

concentrated under vacuum. The crude reaction was purified by column chromatography eluting with a gradient eluent of AcOEt/petroleum ether (1/3 to 1.5/3). The solvent was removed under vacuum to provide glucopyranoside **4c** as an orange oil (419 mg, 17 %). ^{1}H NMR ($CDCl_3$): δ 5.48 (t, 1H), 5.06 (m, 2H), 4.85 (dd, 1H), 4.25 (dd, 1H), 4.01 (m, 1H), 4.00 (m, 1H), 3.68 (dt, 1H), 3.42 (m, 3H), 2.09 (s, 3H), 2.06 (s, 3H), 2.03 (s, 3H), 2.01 (s, 3H), 1.86 (q, 2H), 1.59 (p, 2H), 1.43 (p, 2H), 1.29 (m, 12H).

*11-Acetylthioundecyl 2,3,4,6-tetra-O-acetyl-β-D-glucopyranoside (**5c**)*

For the addition of the thio-acetyl group to the alkyl linked glucopyranoside, 11-bromoundecyl 2,3,4-tri-O-acetyl-β-D-glucopyranoside **4c** (84 mg, 0.161 mmol) and potassium thioacetate (55 mg, 0.483) were mixed in a round bottom flask with 1.2 mL of DMF. The reaction stirred for 20 h and was monitored *via* TLC using a mixture of AcOEt/petroleum ether (1/3) as the eluent. Upon consumption of the starting material, the reaction was quenched with 20 mL of AcOEt/petroleum ether (1/1) and 20 mL of H_2O. The aqueous phase was extracted with 3 × 6 mL AcOEt/petroleum ether (1/1). The organic fractions were combined and washed with 3 × 6 mL of H_2O. The reaction was dried over Na_2SO_4 and concentrated under vacuum providing **5c** as a brown oil (66 mg, yield: 79 %). ^{1}H NMR ($CDCl_3$) δ 5.46 (t, 1H), 5.05 (dd, 2H), 4.84 (dd, 1H), 4.24 (m, 1H), 4.08 (dd, 1H), 3.99 (m, 1H), 3.65 (m, 1H), 3.39 (m, 1H), 2.85 (t, 2H), 2.32 (s, 3H), 2.09 (s, 3H), 2.06 (s, 3H), 2.03 (s, 3H), 2.01 (s, 3H), 1.56 (m, 7H), 1.27 (bm, 11 H).

*D-Galactopyranose pentaacetate (**2d**)*

To a mixture of D-galactose **1d** (1.00g, 5.55 mmol) and acetic anhydride (20 mL) cooled to 0ºC, was added 4 drops of H_2SO_4. The reaction was allowed to stir for 20 h

warming up to room temperature. The reaction was quenched with 100 mL aqueous $NaHCO_3$ and 25 mL AcOEt and allowed to stir until all unreacted acetic anhydride was consumed. The organic phase was washed with 3 × 5 mL aqueous $NaHCO_3$ and 5 mL H_2O, dried over sodium sulfate, and concentrated under vacuum providing the desired acetylated pentaacetate **2d** as a white solid (1.50 g, 69 %). ^{1}H NMR ($CDCl_3$): δ 6.38 (d, 1H), 5.51 (d, 1H), 5.34 (d, 2H), 4.33 (t, 1H), 4.09 (m, 3H), 2.17 (s, 6H), 2.05 (s, 3H), 2.03 (s, 3H), 2.01 (s, 3H).

*11-Bromoundecyl 2,3,4,6-tetra-O-acetyl-β-D-galactopyranoside (**4d**)*

To a solution of D-galactopyranose pentaacetate **2d** (1.12 g, 2.88 mmol) was added 11-bromo-undecanol (943 mg, 3.75 mmol) in 29 mL CH_2Cl_2. The reaction was cooled to 0ºC and stirred for 20 min. A solution of $SnCl_4$ (4.30 mL 1.0 M in heptane) was added dropwise and allowed to stir for 20 h warming to room temperature. The reaction was monitored *via* TLC eluting with AcOEt/petroleum ether (1.5/3). The reaction was quenched with 250 mL aqueous $NaHCO_3$ and 250 mL AcOEt and allowed to stir for 2 h then filtered over celite. The filtrate was extracted with 3 × 50 mL of AcOEt. The organic phase was washed 3 × 25 mL of H_2O and 25 mL of brine. The organic fractions were collected and dried over Na_2SO_4, then concentrated under vacuum. The crude reaction was purified by column chromatography with a gradient eluent of AcOEt-petroleum ether (1/3 to 1.5/3), to provide galactopyranoside **4d** a viscous orange oil (586 mg, 35 %). ^{1}H NMR ($CDCl_3$): δ 5.45 (dd, 1H), 5.34 (m, 1H), 5.10 (m, 2H), 4.22 (t, 1H), 4.11 (m, 2H), 3.66 (dt, 1H), 3.41 (m, 3H), 2.14 (s, 3H), 2.07 (s, 3H), 2.05 (s, 3H), 1.99 (s, 3H), 1.86 (p, 2H), 1.59 (m, 2H), 1.28 (m, 14H).

*11-Acetylthioundecyl 2,3,4,6-tetra-O-acetyl-β-D-galactopyranoside (**5d**)*

For the addition of the thio-acetyl group to the alkyl linked galactopyranoside, 11-bromoundecyl 2,3,4,6-tetra-O-acetyl-β-D-galactopyranoside **4d** (586 mg, 1.01 mmol) and potassium thioacetate (346 mg, 3.03 mmol) were mixed in a round bottom flask with 8 mL of DMF. The reaction stirred for 20 h and was monitored *via* TLC eluting with AcOEt/petroleum ether (1/3) as the eluent. Upon consumption of the starting material, the reaction was quenched with 20 mL of H_2O and 20 mL of AcOEt/petroleum ether (1/1). The aqueous phase was extracted with 3 × 6 mL AcOEt/petroleum ether (1/1). The organic fractions were combined and washed with 3 × 6 mL of H_2O. The reaction was dried over Na_2SO_4 and concentrated under vacuum to provide thioacetate **5d** as a brown oil (482 mg, 83 %). ^{1}H NMR ($CDCl_3$): δ 5.45 (dd, 1H), 5.33 (m, 1H), 5.09 (m, 2H), 4.19 (t, 1H), 4.11 (s, 1H), 4.08 (d, 1H), 3.64 (m, 1H), 3.38 (m, 1H), 2.84 (t, 2H), 2.32 (s, 3H), 2.14 (s, 3H), 2.08 (s, 3H), 2.05 (s, 3H), 1.99 (s, 3H), 1.54 (m 5H), 1.27 (m, 15 H).

*11-Mercaptoundecyl β-D-galactopyranoside (**6d**)*

For the synthesis of the alkyl-thiol terminated rhamnose derivative, according to Lin *et al.*,[97] 11-acetylthioundecyl 2,3,4-tri-O-acetyl-β-D-galactopyranoside **5d** (470 mg, 0.815 mmol) K_2CO_3 (93 mg), and 4.0 mL of methanol were mixed in a round bottom flask. The reaction was allowed to stir at room temperature for 24 h and was monitored via TLC eluting with MeOH/CH_2Cl_2 (1/9) as the eluent. Upon consumption of the starting material, the reaction was filtered and rinsed with 3 × 5 mL MeOH. The solvent was removed under reduced pressure. The crude mixture was purified by column chromatography with a 75 × loading ratio and an eluent of MeOH/CH_2Cl_2 (1/8). The

alkyl-thiol terminated galactose derivative **6d** fractions were combined and the solvent removed under vacuum to provide galacto-thiol **6d** a white solid (134 mg, 45 %). ^{1}H NMR ($CDCl_3$): δ 4.79 (m, 2H), 3.88 (s, 1H), 3.75 (m, 7H), 2.65 (t, 2H), 1.98 (s, 1H), 1.61 (m, 8H), 1.32 (m, 16H).

*D-Mannopyranose pentaacetate (**2e**)*

To a mixture of D-mannose **1e** (1.00g, 5.55 mmol) and 20 mL acetic anhydride cooled to 0ºC, was added 4 drops of H_2SO_4. The reaction was allowed to stir for 20 h and allowed to warm to room temperature. The reaction was quenched with 100 mL aqueous $NaHCO_3$ and 25 mL AcOEt and allowed to stir until all unreacted acetic anhydride was removed. The organic phase was washed with 3 × 5 mL of aqueous $NaHCO_3$ and 5 mL H_2O. The organic phase was dried over sodium sulfate and concentrated under vacuum providing pentaacetate **2e** a yellow oil (1.41 g, 65 %). ^{1}H NMR ($CDCl_3$): δ 6.09 (d, 1H), 5.34 (m, 2H), 5.26 (t, 1H), 4.26 (dd, 1H), 4.12 (d, 1H), 4.08 (m, 1H), 2.18 (s, 3H), 2.17 (s, 3H), 2.09 (s, 3H), 2.06 (s, 3H), 2.01 (s, 3H).

*11-Bromoundecyl 2,3,4,6-tetra-O-acetyl-β-D-mannopyranoside (**4e**)*

To a solution of D-mannopyranose pentaacetate **2e** (1.39 g, 3.56 mmol) was added 11-bromo-undecanol (1.16 g, 4.63 mmol) in 35.6 mL of CH_2Cl_2. The reaction was cooled to 0ºC and stirred for 20 min. A solution of $SnCl_4$ (5.40 mL 1.0 M in heptane) was added dropwise and allowed to stir for 20 h and allowed to warm to room temperature. The reaction was monitored *via* TLC eluting with AcOEt/petroleum ether (1.5/3). The reaction was quenched with 250 mL aqueous $NaHCO_3$ and 250 mL AcOEt and allowed to stir for 2 h and then filtered through celite. The filtrate was washed with 3 × 50 mL of

AcOEt, and the organic phase was washed with 3 × 25 mL of H_2O and 25 mL of brine. The aqueous fractions were combined and then extracted with 3 × 25 mL of AcOEt. The organic fractions were dried over sodium sulfate, then concentrated under vacuum providing a crude product that was purified by column chromatography with a gradient eluent of AcOEt/petroleum ether (1/3 to1.5/3). The solvent was removed under vacuum providing the bromo derivative **4e** as a viscous orange oil (918 mg, 44 %). ^{1}H NMR ($CDCl_3$): δ 5.31 (m, 2H), 4.80 (d, 1H), 4.26 (dd, 1H), 4.08 (m, 1H), 3.96 (m, 1H), 3.66 (m, 1H), 3.39 (m, 3H), 2.16 (s, 3H), 2.11 (s, 3H), 2.05 (s, 3H), 1.99 (s, 3H), 1.86 (p, 2H), 1.60 (m, 2H), 1.29 (m, 14H).

*11-Acetylthioundecyl 2,3,4,6-tetra-O-acetyl-β-D-mannopyranoside (**5e**)*

For the addition of the thio-acetyl group to the alkyl linked mannopyranoside, 11-bromoundecyl 2,3,4,6-tetra-O-acetyl-β-D-mannopyranoside **4e** (918 mg, 1.58 mmol) and potassium thioacetate (541 mg, 4.74 mmol) were mixed in a round bottom flask with 12 mL of DMF. The reaction was stirred for 20 h and was monitored via TLC eluting with a mixture of AcOEt/petroleum ether (1/3) as the eluent. Upon consumption of the starting material, the reaction was quenched with 20 mL of H_2O and 20 mL of AcOEt/petroleum ether (1/1). The aqueous phase was extracted with 3 × 6 mL AcOEt/petroleum ether (1/1). The organic fractions were combined and washed with 3 × 6 mL of H_2O. The reaction was dried over Na_2SO_4 and concentrated under vacuum providing the manno-thiolacetyl derivative **5e** as a brown oil (852 mg, 94 %). ^{1}H NMR ($CDCl_3$): δ 5.33 (dd, 1H), 5.27 (d, 1H), 5.22 (dd, 1H), 4.79 (d, 1H), 4.25 (m, 1H), 4.08 (m, 1H), 3.95 (m, 1H),

3.63 (m, 1H), 3.41 (m, 1H), 2.84 (t, 2H), 2.32 (s, 3H), 2.12 (s, 3H), 2.10 (s, 3H), 2.04, (s, 3H), 1.99 (s, 3H), 1.54 (m, 5H), 1.28 (m, 15H).

*11-Mercaptoundecyl β-D-mannopyranoside (**6e**)*

For the synthesis of the alkyl-thiol terminated mannose derivative, 11-acetylthioundecyl 2,3,4-tri-O-acetyl-β-D-mannoopyranoside **5e** (803 mg, 1.40 mmol) K_2CO_3 (109 mg), and 7.0 mL of methanol were mixed in a round bottom flask. The reaction was allowed to stir at room temperature for 24 h and was monitored via TLC eluting with MeOH/CH_2Cl_2 (1/9) as the eluent. Upon consumption of the starting material, the reaction was filtered and rinsed with 3 × 5 mL of MeOH. The solvent was removed under reduced pressure. The crude mixture was purified by column chromatography with a 75 × loading ratio and an eluent of MeOH/CH_2Cl_2 (1/8). The alkyl-thiol terminated mannose derivative fractions were combined and the solvent removed under vacuum providing the alkyl-thiol mannose derivative **6e** as a white solid (160 mg, 31 %). ^{1}H NMR ($CDCl_3$): δ 4.79 (m, 2H), 3.88 (s, 1H), 3.75 (m, 7H), 2.65 (t, 2H), 1.98 (s, 1H), 1.61 (m, 8H), 1.32 (m, 16H).

Preparation of Gold Substrates

500 mm silicon wafers were purchased from WaferNet, Inc. (CA). These wafers were cleaned with piranha (3:1 = H_2SO_4: H_2O_2) for 1 hour, washed excessively with Milli-Q (18 MΩ) water and dried with nitrogen. For the evaporation, a base pressure of less than $1x10^{-6}$ torr was reached and 10 nm of Cr was used as an adhesion layer and 30 nm of Au was applied using an Edwards Auto 306 system.

Fabrication of Carbohydrate Microarrays

In order to remove any organic contaminant from the gold substrate before it was patterned, it was washed in a piranha solution at 40 ºC for 5 minutes. 11-Mercaptoundecyl β-L-rhamnopyranoside (**6a**) was patterned onto the gold surface via microcontact printing using poly(dimethylsiloxane) (PDMS) stamps. The PDMS stamps were fabricated by casting the PDMS polymer against photolithography-prepared silicon masters. The silicon masters used for this work consisted of 4.5 μm dots spacing distance of 4.5 μm, and 5 μm lines with a spacing distance of 4 μm. To coat the PDMS stamp with a thin layer of rhamnopyraniside **6a**, a 10 mM inking solution of **6a** in ethanol was dropped onto the PDMS stamp using a microliter pipette. The PDMS stamp was allowed to cure in air. The stamp was then applied to the gold surface for 5 seconds. The gold substrate was then rinsed with acetonitrile, ethanol, and then dried under a stream of N_2. Patterned substrates were then soaked in a 1 mM solution of MOU in ethanol for ~30 min to passivate the unpatterned areas.

Bacteria Cell Preparation

P. aeruginosa cells were grown from single colonies in Luria-Bertani (LB) broth in a rotary shaker incubator at 37 ºC and 225 rpm for 7-8 hours. When the culture reached an optical density (OD_{600}) of 0.5-0.8 (Shimadzu 2450 UV-vis), the bacterial cells were centrifuged at 4000 rpm for 20 min. The cells were then resuspended in M9 media that was prepared from commercially available M9 salts.

Imaging and Surface Characterization

Fabricated microarrays were characterized by AFM. A NanoInk, Inc. Nscriptor™ was employed to acquire topography images. A beam shaped, silicon tapping mode tip with a spring constant of 40 N/m, from Pacific Nanotechnology, was used for Tapping Mode AFM (TMAFM) imaging. All the AFM images were acquired with resolutions of 512 × 512 pixels.

Results and Discussion

Carbohydrate microarrays have been shown to be powerful tools to study carbohydrate-cell interactions for the detection of bacterial pathogens.[98] Several general methods have been utilized to prepare carbohydrate microarrays, many of which involve the non-covalent immobilization of sugars to surfaces such as nitrocellulose-coated glass slides.[81] Covalent attachment methods have also been reported in which chemically modified carbohydrates were attached to derivatized surfaces.[7, 81, 98, 99] These bottom-up, layer-by-layer approaches often result in cross-contamination as well as non-productive sugar orientation,[62] resulting in lost bacterial cell binding sensitivity. Therefore, in order to prepare pre-designed, spatially controlled high density arrays of carbohydrates using a bottom-up approach, it is imperative that the carbohydrate derivative is synthesized such that the sugar head group is accessible and presented in a regular and homogenous manner, so that bacterial cells access the immobilized ligand. To accomplish this goal, two different synthetic methodologies were developed to prepare a library of mono- and/or oligosaccharides with a thiol-containing tail that can form a covalent bond to gold surfaces.

In the first method, the carbohydrate was initially per-*O*-acetylated in 63-88% yield (Scheme 3). Per-*O*-acetylation allows for the functionalization of the glycoside at the α-carbon without the risk of side-product reactions at the other alcohol groups. Typical per-*O*-acetylation requires the use of acetic anhydride as both the acetylating reactant and the solvent of the reaction, along with a catalyst. A variety of catalysts for per-*O*-acetylation of glycosides can include bases such as pyridine[100] and imidazole;[101] acids such as $HClO_4$,[102] $ZnCl_2$,[103] TMSCl,[104] and $FeCl_3$,[105] and enzyme catalysts such as lipases.[106]

Scheme 3. Synthetic scheme for the synthesis of the alkyl-thiol terminated rhamnose derivative **6a** via Koenig-Knorr gycosidation.

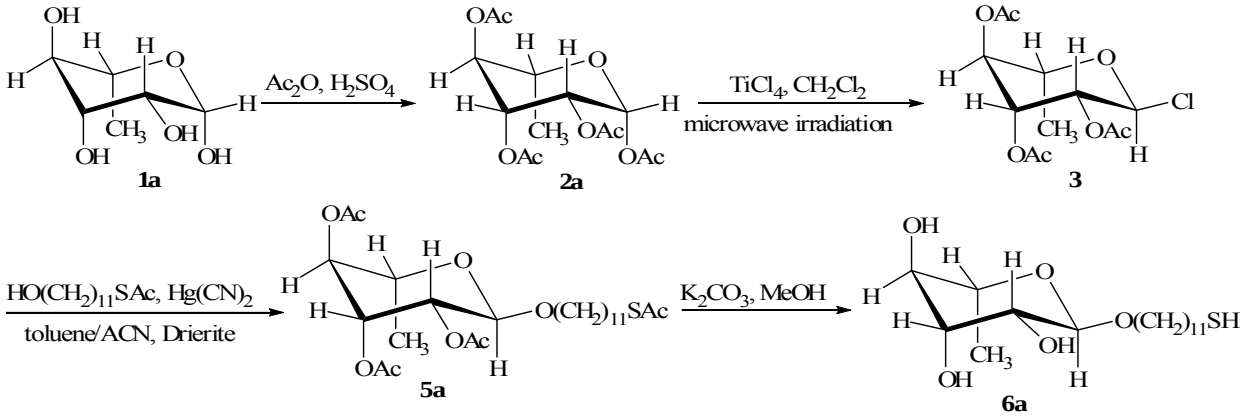

Tai and co-workers[107] were able to efficiently per-*O*-acetylate hexapyranoses in yields between 90 – 99% using stoichiometric amounts of acetic anhydride and catalytic amounts of $Cu(OTf)_2$. An effective method for the per-*O*-acetylization of glycosides is through the use of acetic anhydride as the acetylating reagent and solvent along with a catalytic amount of H_2SO_4 (Scheme 3).[108] This method offers a one pot synthesis to the per-*O*-acetylation glycosides in 63 – 88% yield (Table 3). This reaction was chosen as the first step in synthesizing an alkyl-thiol terminated carbohydrate derivative as it

offered the protected derivatives of the desired glycoside products, and can be readily characterized by ^{1}H NMR spectroscopy.

Table 3. Percent conversion to the desired per-*O*-acetylayed glycoside

Sugar	Product	yield (%)
L-rhamnose monohydrate	L-rhamnopyranose tetraacetate **2a**	88
L-fucose	L-fucopyranose tetraacetate **2b**	63
D-glucose	D-glucopyranose pentaacetate **2c**	75
D-galactose	D-galactopyranose pentaacetate **2d**	69
D-mannose	D-mannopyranose pentaacetate **2e**	65

The second step selectively chlorinates the glycoside at the α-carbon employing microwave radiation (Scheme 3).[109] The use of microwave irradiation with the per-*O*-acetylated sugar in the presence of a Lewis acid offers a rapid and operationally simple route to selectively chlorinate the α-carbon in high yields (< **75%**) with no further purification needed. The α-chloro-rhamnose (**3**) compound was then coupled to (11-hydroxyundecyl) ethanethioate *via* a Koenig-Knorr gycosidation, which involves the formation of a β-glycosidic bond from an α-halocarbohydrate, affording the desired alkyl-thiol linked rhamnose derivative (**5a**) (Scheme 3).[95, 110] Rhamnose derivative **5a** was then deacetylated resulting in thiol-terminated rhamnose derivative (**6a**). The addition of a thiol-containing linker to the α-position of rhamnose provides a molecule that can adhere to a gold surface with carbohydrate directed *away* from the surface thereby providing a surface-bound rhamnose group that can be used for the directed assembly of biological molecules that recognize rhamnose. This synthetic method is applicable to any glycoside head group as shown in Table 3.

While Scheme 3 provides the desired alkyl-thiol terminated carbohydrate derivative, a highly toxic mercuric cyanide reagent was used in the Koenig-Knorr gycosidation step. In order to eliminate the use of mercuric cyanide, an alternative method was developed for β-anomeric thiol-linked glycosides (Scheme 4). Consistent with the literature precedent, the unprotected sugar (**1a-e**) was diluted in acetic anhydride (38 eq) followed by the addition of an acid catalyst, H_2SO_4, at 0 to 5 ºC. This reaction was allowed to proceed for 24 h allowing the reaction to warm to room temperature. The reaction gave the desired per-*O*-acetylated products **2a-e** in 63 – 88 % yield, respectively, with no detectable side products. The excess unreacted acetic anhydride was removed during the separation of the desired product from the solvent. It was discovered that increasing the catalytic amount of H_2SO_4 or the reaction time did not improve the overall yields of the reaction.

Scheme 4. Alternative synthetic method for the synthesis of an alkyl-thiol linked carbohydrate library

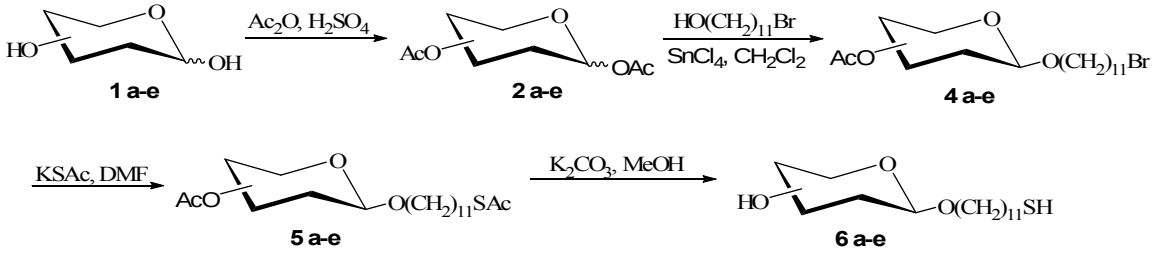

The most important step of the synthesis of glycoside derivatives for the formation of SAMs is the glycoslation of the α-carbon with an alkyl chain. In this glycosylation step, it is essential to control the ratio of the α/β glycosidic linkage products. Traditional conversion to a β-*n*-alkanol glycosidic linkage requires the intermediate step of conversion to an *O*-acetyl-protected glycosyl-β-halide.[111] Following

the conversion to the mono-halide, the *n*-alkanol is attached *via* the Koenigs-Knorr reaction with either mercury salts such as: $Hg(CN)_2$,[95] $HgBr_2$,[11] and $Hg(CN)_2$-$HgBr_2$[12]; or with silver salts: Ag_2CO_3,[112] $AgClO_4$,[113] and AgOTf[114] as the promoter. However, another efficient method for the glycosylation of glycosides is Schmidt's trichloroacetimidate method.[115, 116] This glycosylation method has been shown to be selective with reversible formation of *O*-glycosyl-tricholoracetimidate with control over the α/β anomers in high yields.[117, 118] Therefore, a method was developed that utilizes 11-bromo undecanol with $SnCl_4$ as the catalyst for the direct glycosylation of per-*O*-acetylated glycosides.[118] The per-*O*-acetylated glycoside **2a-e** was mixed with 11-bromo undecanol (1.3 eq) followed by the dropwise addition of $SnCl_4$ (1.5 eq) at 0-5 ºC and allowed to warm to room temperature for 5-24 hours (Scheme 4). The reaction was monitored via TLC and quenched when the per-*O*-acetate **2a-e** was consumed.

This $SnCl_4$ catalyzed direct glycosylation of per-*O*-acetylated glycosides gave the desired glycosylated products **4a-e** in 17-48 % yield (Table 4). Column chromatography was used to purify each of these products from the remaining starting material and by-products. Chromatographic elution revealed $Br(CH_2)_{11}OAc$, $Br(CH_2)_{11}OH$ as a by-product, along with the $Br(CH_2)_{11}OH$-glycosylation product **4a-e**, and pure **4a-e,** respectively. Since the mobility between the 11-bromo undecanol starting material and the desired glycosylated product were similar on TLC, the presence of glycosylated product was confirmed *via* ^1H NMR. Upon glycosylation, the C-11 protons resolve from a triplet into two separate doublets of triplets, each integrating to one proton. The two resonances appear at 3.66 and 3.42 ppm. This split from a triplet into two separate

doublet of triplets is due to the C-11 proton's loss of symmetry giving rise to geminal coupling, whereas the C-1 proton's are still resolved into a triplet without a field shift.

Table 4. Percent conversion to the desired glycosylated product.

Sugar	Product	yield (%)
L-rhamnopyranose tetraacetate	11-Bromoundecyl 2,3,4-tri-*O*-acetyl-β-L-rhamnopyranoside **4a**	48
L-fucopyranose tetraacetate	11-Bromoundecyl 2,3,4-tri-*O*-acetyl-β-L-fucopyranoside **4b**	42
D-glucopyranose pentaacetate	11-Bromoundecyl 2,3,4,6-tetra-*O*-acetyl-β-D-glucopyranoside **4c**	17
D-galactopyranose pentaacetate	11-Bromoundecyl 2,3,4,6-tetra-*O*-acetyl-β-D-galactopyranoside **4d**	35
D-mannopyranose pentaacetate	11-Bromoundecyl 2,3,4,6-tetra-*O*-acetyl-β-D-mannopyranoside **4e**	44

Product identity was also confirmed by noting the shift of the α-^{1}H of the glycoside from the acetylated starting material to the glycosylate bearing an alkyl chain via ^{1}H NMR. For example, the α-H of L-rhamnopyranose tetraacetate shifted upfield from 6.02 to 4.71 ppm, whereas the α-H proton of D-galactopyranose pentaacetate shifted from 6.39 to 5.46 ppm upon glycosylation.

Finally, the synthesis of the ω-mercaptoalkyl glycosides from the preceding ω-bromoalkyl glycosides **4a-e** was accomplished in a simple two step process. Initially, the ω-bromoalkyl glycoside was reacted with potassium thioacetate (KSAc, 3 eq) in DMF and allowed to stir at room temperature for ~20 hours (Scheme 4). TLC was used to monitor the consumption of starting material with 1.5/3 AcOEt/petroleum ether as the mobile phase. This reaction gave the desired thioacetates **5a-e** in high yields (Table 5).

Table 5. Percent conversion from the ω-bromoalkyl glycosides to the thio-acetate glycoside

Sugar	Product	Yield (%)
11-Bromoundecyl 2,3,4-tri-*O*-acetyl-β-L-rhamnopyranoside	11-Acetylthioundecyl 2,3,4-tri-*O*-acetyl-β-L-rhamnopyranoside **5a**	81
11-Bromoundecyl 2,3,4-tri-*O*-acetyl-β-L-fucopyranoside	11-Acetylthioundecyl 2,3,4-tri-*O*-acetyl-β-L-fucopyranoside **5b**	79
11-Bromoundecyl 2,3,4,6-tetra-*O*-acetyl-β-D-glucopyranoside	11-Acetylthioundecyl 2,3,4,6-tetra-*O*-acetyl-β-D-glucopyranoside **5c**	79
11-Bromoundecyl 2,3,4,6-tetra-*O*-acetyl-β-D-galactopyranoside	11-Acetylthioundecyl 2,3,4,6-tetra-*O*-acetyl-β-D-galactopyranoside **5d**	83
11-Bromoundecyl 2,3,4,6-tetra-*O*-acetyl-β-D-mannopyranoside	11-Acetylthioundecyl 2,3,4,6-tetra-*O*-acetyl-β-D-mannopyranoside **5e**	94

The reaction was purified through quenching with equal amounts of a 1:1 mixture of AcOEt/petroleum ether and H_2O. The aqueous phase was extracted with a 1/1 mixture of AcOEt/petroleum ether to remove the desired product from the remaining KSAc and DMF solvent. The conversion to the desired thioacetate derivative was confirmed with ^{1}H NMR. ^{1}H NMR showed the upfield shifted triplet of the C-1 protons from 3.41 to 2.86 ppm. The deactylation step of the thioacetate derivative utilized catalytic amounts of potassium carbonate (K_2CO_3) in freshly distilled methanol providing the final ω-mercaptoalkyl glycoside products (Table 6).[97] This reaction was monitored *via* TLC using 1/8 MeOH/CH_2Cl_2. Upon consumption of the starting material the solution was filtered and the MeOH was removed under vacuum.

Table 6. Percent conversion to the desired thio-alkyl glycoside

Sugar	Product	Yield (%)
11-Acetylthioundecyl 2,3,4-tri-*O*-acetyl-β-L-rhamnopyranoside	11-Mercaptoundecyl β-L-rhamnopyranoside **6a**	20
11-Acetylthioundecyl 2,3,4-tri-*O*-acetyl-β-L-fucopyranoside	11-Mercaptoundecyl β-L-fucopyranoside **6b**	23
11-Acetylthioundecyl 2,3,4,6-tetra-*O*-acetyl-β-D-glucopyranoside	11-Mercaptoundecyl β-D-glucopyranoside **6c**	-
11-Acetylthioundecyl 2,3,4,6-tetra-*O*-acetyl-β-D-galactopyranoside	11-Mercatoundecyl β-D-galactopyranoside **6d**	45
11-Acetylthioundecyl 2,3,4,6-tetra-*O*-acetyl-β-D-mannopyranoside	11-Mercaptoundecyl β-D-mannopyranoside **6e**	31

The successful synthesis of the target molecule with a rhamnose head group on the hundred-milligram scale allowed for testing the hypothesis that placing the alkylthiol tether in the anomeric beta-orientation of the glycoside will preserve the biological recognition and binding properties of the carbohydrate head group to be tested.[119] Therefore, the uniqueness of this rhamnose ink resides in the alkylthiol attachment method and specific position of the linker to the carbohydrate head group. The L-rhamnopyranose ink has good solubility in methanol or ethanol and fair solubility in methanol(ethanol):water (50:50%) mixtures which is required for patterning on gold.

Now that a tailored carbohydrate ink has been successfully designed and synthesized, presenting carbohydrate head groups in a homogeneous fashion on a surface was accomplished via PDMS stamping. PDMS generated patterns of **6a** were prepared by wetting the stamp with a 10 mM solution of rhamnose derivative **6a** in acetonitrile and bringing the stamp into contact with a gold surface for 5 s at 20ºC.[11] The sample was allowed to cure at room temperature in air for ~10 min, followed by rinsing the sample with acetonitrile, ethanol, and drying under a steady stream of nitrogen. In order to assess

the adsorption of **6a** onto the surface, frictional and topography changes were monitored by tapping-mode atomic force microscopy (TMAFM) and lateral force microscopy (LFM). Figure 6 shows typical LFM images of PDMS stamped patterns of **6a**. Surface-bound **6a** in Figure 6a are shown as vertical lines, ~5.3 μm in width. Due to the difference in the frictional force, the patterned **6a** lines are a lighter contrast to the unpatterned gold surface. Figure 6b shows **6a** patterned onto a bare gold surface in ~4.5 μm dots that are lighter in contrast to the bare gold surface due to the difference in frictional force between patterned **6a** and the bare gold surface.

Typical TMAFM images of PDMS stamped patterns of **6a** are shown in Figure 7. Surface-bound **6a** in Figure 7a are shown as vertical lines, ~5.3 μm in width, that are lighter contrast compared to the unpatterned bare gold. The estimated height of the PDMS generated line from Figure 7a was determined by TMAFM to be 1.4 ± 0.2 nm. The theoretical height of **6a**, calculated using an energy minimized structure with Spartan Pro, was estimated to be 1.3 nm. Thus the experimentally determined height-values obtained for **6a** are consistent with the theoretical height, consistent with the formation of SAMs of **6a** on the gold substrate. The thiol tethered β-rhamnose derivatives were also

Figure 6. AFM generated image of line or dot patterns of rhamnose derivative **6a** patterned onto the bare gold surface *via* PDMS stamping a) LFM image showing a lighter contrast of line patterns of **6a** compared to the bare gold surface b) LFM image showing a lighter contrast of dot patterns of **6a** compared to the bare gold surface.

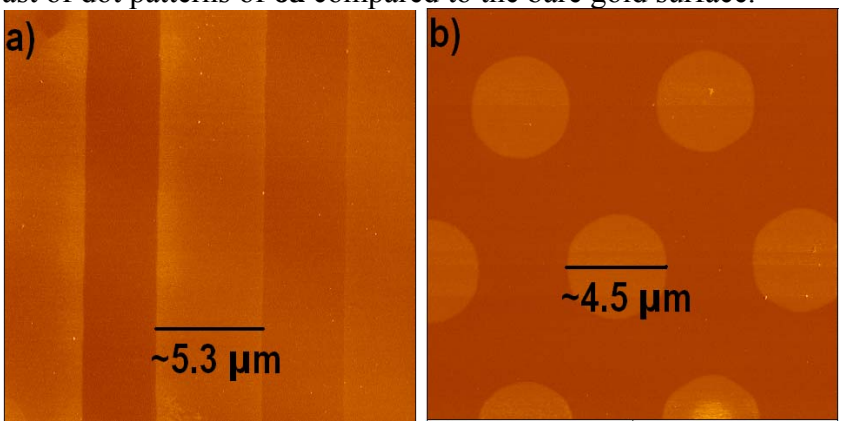

patterned into ~4.5 µm dots as shown in Figure 7c. TMAFM height profiles of the thiol tethered β-rhamnose derivative of **6a** from Figure 7d also confirm the height of the patterned images to be 1.4 ± 0.2 nm.

The unpatterned bare gold surfaces on the substrate were passivated by immersing the gold substrates containing SAMs of **6a** in a 1 mM solution of mercapto-1-undecanol (MOU) in ethanol for ~30 min. The substrate was rinsed with ethanol and dried under a stream of nitrogen. MOU was chosen to passivate the remaining bare gold due to its ability to significantly reduce bacterial adhesion compared to bare gold.[51] Typical heights of generated MOU SAMs are reported to be 1.3 nm, creating a binding area with potential for biological activity.[120] In Figure 8, the PDMS-generated rhamnose line patterns are shown as the lighter contrast in comparison to the backfilled MOU passivation SAMs. This is in good agreement with the height of the rhamnose being slightly greater than the height of the MOU backfilled layer.

Figure 7. AFM generated image of line or dot patterns of rhamnose derivative **6a** patterned onto the bare gold surface *via* PDMS stamping a) TMAFM image showing height increase of line patterns of **6a** b) Step height profile from TMAFM of the sample c) TMAFM image showing height increase of dot patterns of **6a** d) Step height profile from TMAFM of the sample.

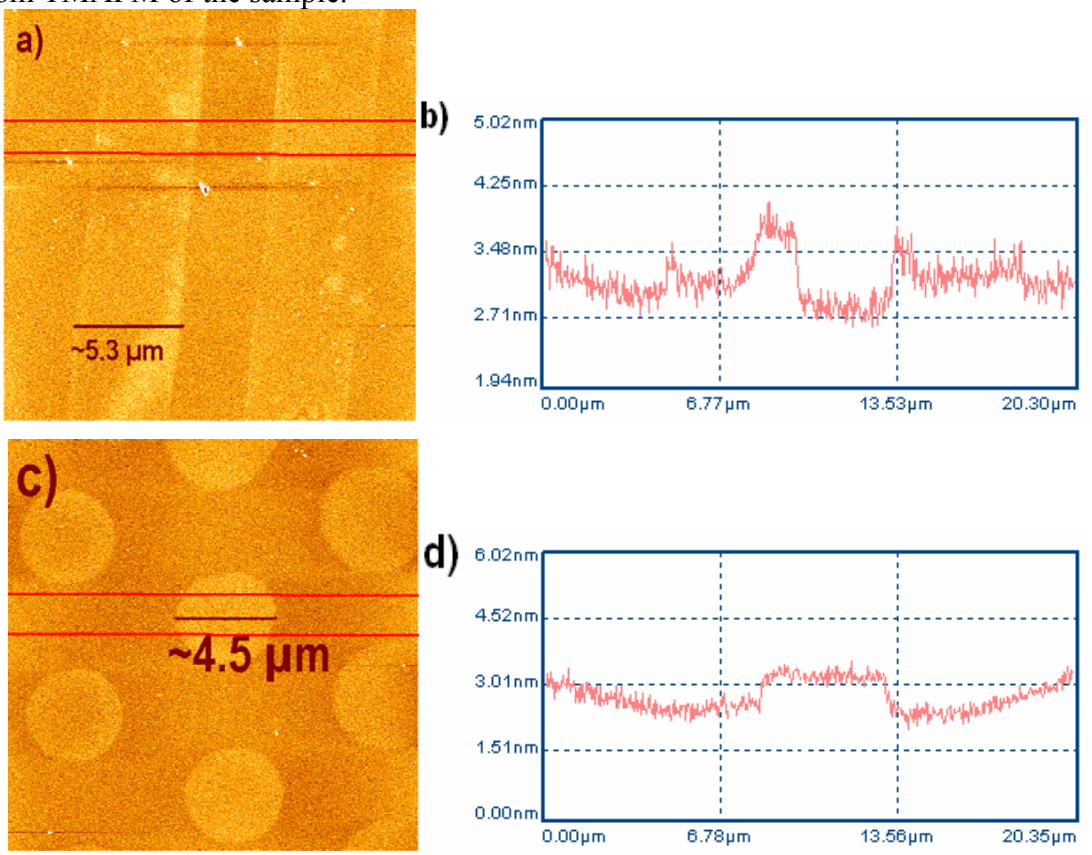

Figure 8. AFM generated image of line or dot patterns of rhamnose derivative **6a** patterned onto the bare gold surface *via* PDMS stamping and backfilled with MOU a) LFM image showing line patterns of **6a** as a lighter contrast compared to the MOU backfilled layer b) LFM image showing dot patterns of **6a** as a lighter contrast compared to the MOU backfilled layer.

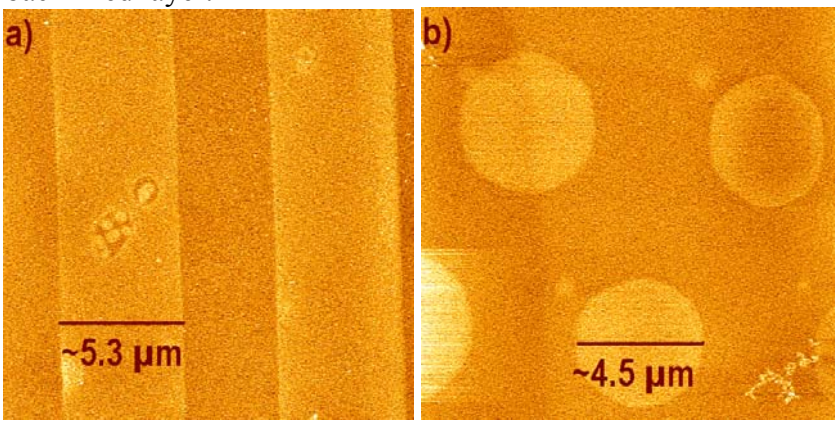

In order to determine if the PDMS generated rhamnose-template microarrays retained their bacterial binding activity, microarrays of **6a** were exposed to *Pseudomonas aeurginosa*. *P. aeruginosa* was initially tested as it is a significant contributor to nosocomial and/or food-borne infections. Microarrays of **6a** backfilled with MOU were immersed in a solution of M9 media containing *P. aeruginosa* cells for ~30 min. The substrate was then washed with fresh M9 media followed by rinsing with Milli-Q (18 MΩ) water. An optical microscope was used to monitor the adhesion of the bacteria to the patterned surface (Figure 9). As can be seen in Figure 9a, *P. aeruginosa* cells preferentially bind to rhamnose patterned lines with very little non-specific binding to MOU passivated gold. Interestingly, the cell density on carbohydrate microarrays are significantly higher than what we have observed on MHA-PLL features. TMAFM was used to further characterize the biological recognition of the PDMS-generated patterns of **6a**. A typical TMAFM image shows the biological recognition capabilities of the

patterned rhamnose ink **6a** to *P. aeruginosa*. The *P. aeruginosa* cells appear to order themselves in a head-to-tail fashion on lines of rhamnose (Figure 9c). These data provide "proof-of-concept" that carbohydrate-based nanopatterned inks provide excellent adhesion characteristics for bacterial cell surface binding.

Figure 9. Images of the patterned samples of **6a** after exposure to *P. aeruginosa* a) Optical microscope image showing the linear patterns of *P. aeruginosa* bound to the line patterns of **6a** b) TMAFM image showing the bacteria bound to the line patterns of **6a** c) TMAFM image showing the bacteria bound to the line patterned SAMs of **6a**.

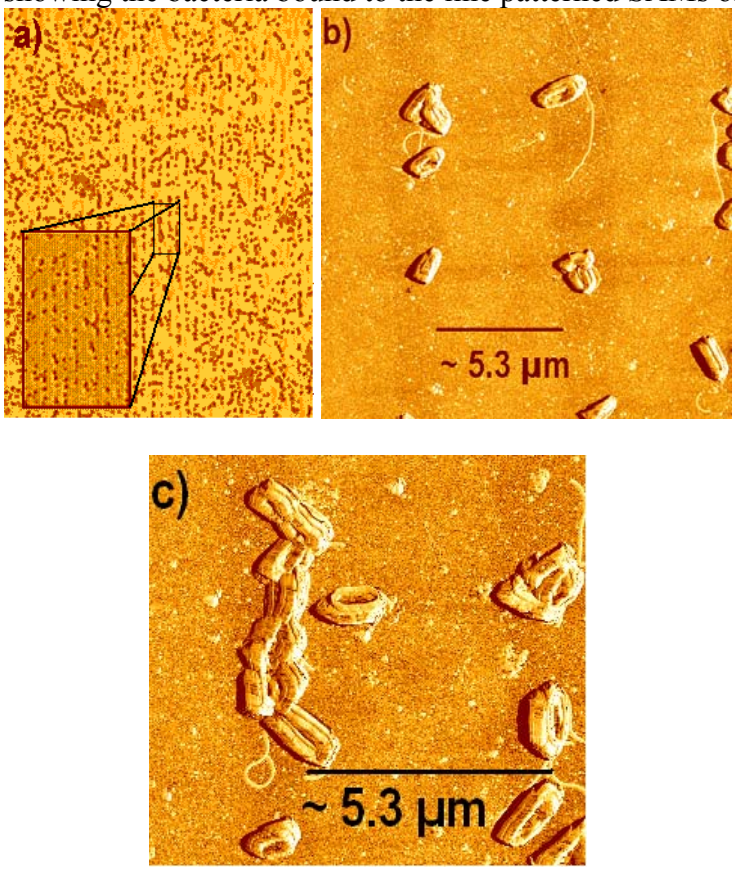

Conclusion

Carbohydrate-based inks were designed and synthesized, which provide the foundation to examine bacterial cell surface recognition and capture. The synthetic

methods using the classic Koenigs-Knorr glycosylation as well as the direct glycosylation of the per-*O*-acetylated carbohydrates described herein are generic so a library of carbohydrate based inks can be easily synthesized in order to take advantage of the specificity of bacterial cell-sugar interactions. Individual carbohydrate nanoarrays or mixed carbohydrate nanoarrays can potentially provide a fingerprint for specific pathogenic bacterial cells resulting in a "chip-based" method for the accurate and fast detection of multiple pathogenic bacterial cell types in parallel. Carbohydrate nanoarrays that can simultaneously recognize and capture bacterial cell pathogens lie at the interface between biological carbohydrate-cell binding and the chemistries associated with preparing nanoarrays of carbohydrate inks. Understanding the adhesion chemistries of carbohydrate functionalized surfaces will open new research avenues for building complex, multi-functional biological arrays.

CHAPTER THREE

DIRECT PATTERNING OF A CYCLOTRIVERATRYLENE (CTV) DERIVATIVE FOR DIRECTED SELF-ASSEMBLY OF C_{60}

Introduction

With its unique structure, physical and electronic properties, C_{60} (Buckminsterfullerene) has been shown to possess great potential for the development of organic electrical and optical devices.[121-124] The ability of C_{60} to be a potent electron acceptor has led to its utilization in donor-chromophore-acceptor based molecular triads that are capable of intramolecular photoinduced electron transfer (PET).[125] While C_{60} thin-films on metal surfaces have been widely studied,[123, 126-131] many challenges remain for the directed self-assembly of organic optoelectronic materials such as C_{60} into two-dimensional surface structures. Therefore, developing methods to pattern and immobilize organic electronic or optoelectronic materials with nanometer-scale control will provide a simple, robust, and flexible approach for the preparation of predetermined two-dimensional organic materials. By controlling the spatial distribution of organic molecules on a surface by directed molecular binding, these materials will potentially enable for the development of new nanooptical, nanoelectronic, and/or nanoelectrochemical systems (NEMS).[3, 8-12]

One way to pattern and immobilize organic electronic or optoelectronic materials with nanometer scale control is to utilize a bottom-up, layer-by-layer approach based on host-guest chemistry.[123] Host-guest chemistry involves complementary binding between two different molecules that can involve electrostatic, hydrogen bonding, π-π stacking interactions, inductive and dispersion forces, as well as hydrophobic or solvatophobic effects.[132] Over the past decade, host-guest chemistry involving synthetic receptor molecules has received increasing interest partly due to the ever-advancing ability to synthesize complex molecular scaffolds to serve as host structures. One such receptor molecule, CTV,[3, 70, 71] has been extensively employed in host-guest chemistry as a supramolecular scaffold.[2, 133, 134] Enabled by its rigid bowl-shaped structure, CTV has been shown to act as a host molecule for a variety of small molecules including neutral or ionic polyhedral C_{60} and *o*-carborane derivatives.[4, 69] In 1994, Atwood *et al*.[135] showed that the bowl-shaped crown conformer of CTV forms inclusion complexes with C_{60} in the ratio of $(C_{60})_{1.5}$(CTV)$(toluene)_{0.5}$ referred to as a "ball and socket" structure. Zhang *et al*.[136-139] utilized this ball and socket structure to prepare C_{60} self-assembled monolayers on gold utilizing CTV, however the CTV was derivatized on its perimeter resulting in the concave shape of the CTV molecule facing *toward* the gold surface, thus irreversibly trapping C_{60} against the surface and isolating it from neighboring CTV guests. This orientation of CTV prohibits its ability to function as a template for a layer-by-layer approach to building organic electronic or optoelectronic materials.

Herein describes a robust and reliable method to produce predesigned, spatially controlled, high-density microarrays of C_{60}. We have designed and synthesized an apex-

modified CTV derivative providing a surface bound CTV template with its bowl shaped cavity directed *away* from the surface. By utilizing a layer-by-layer approach and Dip-Pen Nanolithography, which provides a flexible nanolithographic method capable of positioning molecules on a substrate with 10 nm resolution,[58, 140] predesigned, spatially controlled microarrays of this modified CTV derivative were prepared on gold surfaces. The molecular recognition capabilities of this CTV-template toward C_{60} described herein provides proof-of-concept that supramolecular CTV scaffolds can be directly patterned on surfaces and through host-guest interactions provide a template for the development of organic electronic or optoelectronic materials.

Experimental Section

All solvents and reagents were used without further purification unless otherwise noted. All solvents were distilled prior to use. All reactions were conducted under a nitrogen atmosphere. Sorbent Technologies silica gel 60 A, 40 – 75 μm (200 x 400 mesh) was used for column chromatography unless otherwise noted. Sorbent Technologies aluminum-backed Silica gel 200 μm plates were used for TLC. ^{1}H NMR spectra were obtained utilizing either a Varian INOVA 300 or Varian GEMINI 2000 300 MHz spectrometer with trimethylsilane (TMS) as the internal standard.

*10,15-Dihydro-2,3,7,8,12,13-hexamethoxy-5H-tribenzo[a,d,g]-cyclononene (**7**)*

According to the method of Robinson, veratryl alcohol (18 mL, 120 mmol) was mixed with formic acid (325 mL) in a round bottom flask and the reaction was stirred at 60ºC for 3 h. The reaction was cooled to room temperature and filtered. The crude mixture was purified *via* recrystallization from toluene and filtered to afford **7** as a white

crystalline solid (9.36 g, 52 %). ^{1}H NMR (300 MHz, $CDCl_3$) δ 6.83 (s, 6H), 4.76 (d, 3H), 3.83 (s, 18 H), 3.54 (d, 3H).

*10,15-Dihydro-2,3,7,8,12,13-hexamethoxy-5H-tribenzo[a,d,g]- cyclononen-5-one (**8**)*

For the synthesis of the CTV-ketone derivative according to the method of Lutz *et al*.,[141] CTV **7** (2.0 g, 4.4 mmol), $Na_2CrO_7 \cdot 2H_2O$ (2.1 g, 7.0 mmol), and 22 mL of HOAc were mixed in a round bottom flask. The reaction was refluxed at 120 ºC for ~ 20 h and the reaction was monitored via TLC using AcOEt/CH_2Cl_2 (5/95) as the eluent. Upon consumption of the starting material, the reaction was quenched with 25 mL of H_2O. The reaction was extracted 3 x 25 mL of CH_2Cl_2. The organic fractions were collected and were washed with 3 x 15 mL H_2O, and the organic fraction was dried over Na_2SO_4. Concentration afforded **8** as an off white solid (1.9 g, 92%). ^{1}H NMR (300 MHz, $CDCl_3$) δ 7.43 (s, 2H), 6.76 (s, 2H) 6.49 (s, 2H), 3.96 (s, 6H), 3.92 (s, 6H), 3.81 (s, 6H), 3.77 (br s, 4H).

*10,15-Dihydro-2,3,7,8,12,13-hexamethoxy-5H-tribenzo[a,d,g]- cyclononen-5-oxime (**9a/b**)*

For the synthesis of the crown and saddle CTV-oxime derivatives , CTV-monoketone **8** (500 mg, 1.08 mmol), hydroxylamine hydrochloride ($H_2NOH \cdot HCl$) (750 mg, 10.8 mmol), and 6 mL of pyridine were mixed in a round bottom flask and was brought to reflux. The reaction was allowed to reflux for ~23 hours and was monitored via TLC using AcOEt/CH_2Cl_2 (5/95). Upon consumption of the starting material, the reaction was cooled to room temperature and diluted with 20 mL of CH_2Cl_2. The reaction was washed 4 x 10 mL 10 % HCl, 2 x 10 mL H_2O, and 10 mL of brine. The organic

fractions were filtered over Na_2SO_4. The solvent was removed under reduced pressure. The crude reaction mixture was purified using column chromatography with a 75× loading ratio and an eluent gradient of AcOEt/CH_2Cl_2 (1/4 to 1/1). The crown/saddle (**9a/b**) fractions were combined and removal of solvent afforded a light brown solid was recovered (375 mg, 73 %). ^{1}H NMR (300 MHz, $CDCl_3$) δ 9.41(br s, 1H), 6.96 (s, 1H), 6.90 (s, 1H), 6.86 (s, 1H), 6.81 (s, 1H), 6.71 (s, 1H), 4.77 (d, 1H), 4.38 (d, 1H), 3.89 (s, 3H), 3.87 (s, 3H), 3.83 (s, 12H), 3.58 (d, 1H), 3.50 (d, 1H).

*10,15-Dihydro-2,3,7,8,12,13-hexamethoxy-5H-tribenzo[a,d,g]- cyclononen-O-[5-(1,2-dithiolan-3-yl)pentanoyl]-5-oxime (**10a/b**)*

For the synthesis of the crown and saddle CTV oxime-lipoic acid derivatives, lipoic acid (283 mg, 1.37 mmol), hydroxybenzotriazole (HOBT) (200 mg, 1.48 mmol), N,N'-dicyclohexylcarbodiimide (DCC) (330 mg, 1.60 mmol), and 3.0 mL of dry tetrahydrofuran (THF) were mixed in a round bottom flask and was allowed to stir at room temperature for 1 hour. A mixture of crown and saddle conformers of CTV oxime **9a/b** (545 mg, 1.14 mmol) in 2.7 mL of dry THF was then added to the round bottom flask dropwise. The reaction was allowed to stir for ~24 hours and was monitored via TLC using AcOEt/CH_2Cl_2 (1/9) as the eluent. Upon consumption of the starting material, the reaction was filtered over celite to remove the insoluble urea and washed with ~30 mL of CH_2Cl_2. The solvent was then removed under reduced pressure. The crude mixture was purified using flash chromatography with an RS-40 cartridge and an eluent gradient of AcOEt/hexane (1/2 to 2/1, v/v). The crown/saddle **10a/b** fractions were combined and removal of solvent afforded a light brown solid (434 mg, 57%). This

product was characterized by ^{1}H NMR. ^{1}H NMR (300 MHz, $CDCl_3$) δ 7.33 (s, 1H), 6.94 (s, 1H), 6.93 (s, 1H), 6.91 (s, 1H), 6.83 (s, 1H), 6.80 (s, 1H), 6.78 (s, 1H), 6.68 (s, 1H), 6.65 (s, 1H), 6.64 (s, 1H), 6.58 (s, 1H), 6.54 (s, 1H).

Preparation of Gold Substrates

500 mm silicon wafers were purchased from WaferNet, Inc. (CA). These wafers were cleaned with piranha (3:1 = H_2SO_4: H_2O_2) for 1 hour, washed excessively with Milli-Q (18 MΩ) water and dried with nitrogen. For the evaporation, a base pressure of less than $1x10^{-6}$ torr was reached and 10 nm of Cr was used as an adhesion layer and 30 nm of Au was applied using an Edwards Auto 306 system.

Fabrication of CTV Microarrays

A NanoInk, Inc. Nscriptor™ was used to prepare DPN arrays under ambient conditions with temperatures ranging from 20 to 22˚C and humidity levels within the enclosed chamber between 25 and 35%. V-shaped, silicon nitride contact mode tips (NanoInk, Inc.) with a spring constant of 0.5 N/m were used for DPN patterning. A 10 mM solution of **10a/b** was prepared in acetonitrile containing 1% polysorbate 20 for wettability. For DPN patterning, atomic force microscopy (AFM) tips were first dipped into inkwells filled with **10a/b**. The stationary diffusion constants were calculated based on the model developed by J. Jang *et al.*[142] prior to each patterning process. Dot shaped patterns were made by holding the tip stationary in contact with the surface according to calculated stationary diffusion constants. The samples with DPN arrays were allowed to stand at room temperature for ~10 minutes and rinsed with acetonitrile then ethanol and dried under a stream of nitrogen.

Modification of the DPN-patterned templates

Substrates with DPN-generated patterns were incubated in a 1 mM solution of octadecanethiol (ODT) in ethanol for ~30 min to block any exposed gold surface from further unwanted contaminations or modifications. The samples were then rinsed with ethanol and dried under a stream of nitrogen. Regions coated with **10a/b** were then functionalized by exposure to a 1 mM solution of C_{60} in toluene with deposition times ranging from 20 minutes to 1 hour. Functionalized samples were rinsed with toluene and dried under a stream of nitrogen.

Imaging and Surface Characterization

Fabricated microarrays were characterized by AFM. A NanoInk, Inc. Nscriptor™ was employed to acquire topography images. A beam shaped, silicon tapping mode tip with a spring constant of 40 N/m, from Pacific Nanotechnology, was used for Tapping Mode AFM (TMAFM) imaging. All the AFM images were acquired with resolutions of 512 x 512 pixels.

Results and Discussion

It was hypothesized that derivatizing the apex of the CTV bowl would provide a supramolecular scaffold with the concave bowl receptor pointed *away* from the surface, enabling CTV to function as a surface-bound host molecule. To accomplish this, CTV was oxidized to the monoketone and converted to the oxime in high yield as an equilibrium mixture of the crown **9a** and the saddle **9b** conformers (Scheme 5).[16] The CTV oxime was coupled to (±)-α-lipoic acid affording a mixture of the coupled crown **10a** and saddle **10b** conformers in 52% yield (Scheme 5). The resulting CTV-lipoic acid

derivatives **10a/b** contain a dithiolane-terminated linker for coordination to gold, thus enabling the bowl of CTV to face away from the surface.

Scheme 5. Synthetic scheme for the synthesis of the apex-modified dithiol CTV-oxime (**10a/b**).

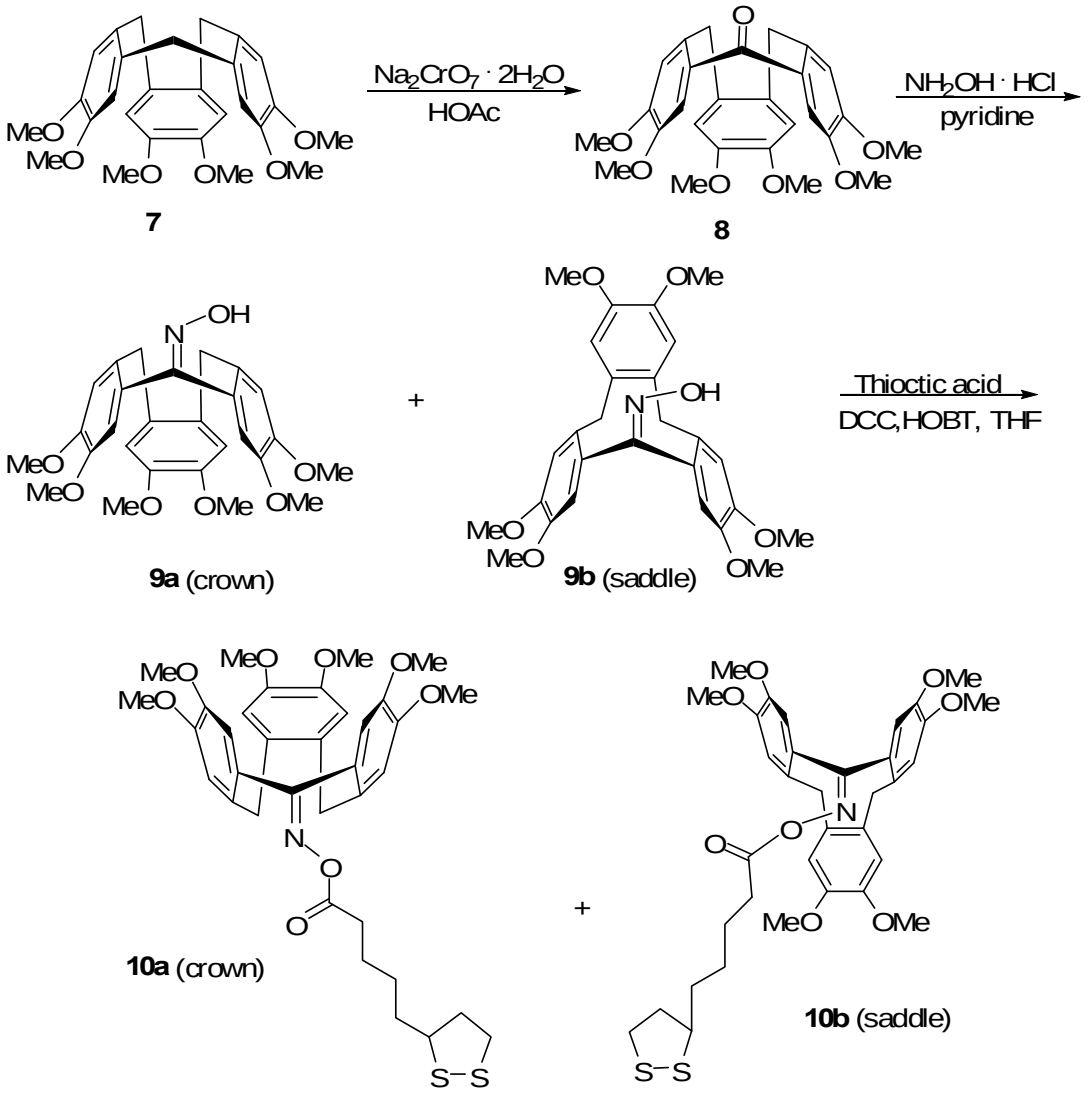

With the successful design and synthesis of an apex modified CTV supramolecular scaffold head group with a dithiolane tail, microarrays of **10a/b** were prepared via DPN by direct patterning using a NanoInk, Inc. Nscriptor^{TM} system.[58, 140]

DPN is a particularly important nanolithographic method for patterning molecular inks since DPN is capable of positioning molecules on a substrate with 10 nm resolution in pre-designed, spatially controlled arrays.[58] As previously reported, the addition of 1% polysorbate 20 to a 10 mM solution of **10a/b** in acetonitrile enhanced the diffusion of **10a/b** during the DPN process by making the solvent more wettable.[143] DPN generated patterns of **10a/b** were prepared at 20^{o}C with humidity levels between 25 and 35%.[144] To assess the adsorption of the **10a/b** molecular ink, surface topography changes were measured by AFM (LFM and TMAFM) after curing in air at room temperature for ~10 minutes, followed by rinsing with acetonitrile and ethanol and drying under a stream of nitrogen. LFM is a method of imaging a surface by detecting the change in the torsion of the cantilever as the cantilever tip encounters a change in friction on the surface as the tip moves in the forward and reverse directions. Typical AFM images of DPN-generated **10a/b** patterns are shown in Figure 10. Surface-bound **10a/b**, which is more hydrophilic than gold, is observed as the light contrast areas in the TMAFM image (Figure 10a) and a darker contrast in the LFM image (Figures 10b).

Figure 10. AFM generated images of **10a/b** dot patterns patterned onto the bare gold surface a) TMAFM image showing height increase of **10a/b** patterned onto the bare gold surface via DPN b) LFM images of **10a/b** patterned on a base gold substrate utilizing DPN c) Step height profile from AFM of the sample represented in image **a**.

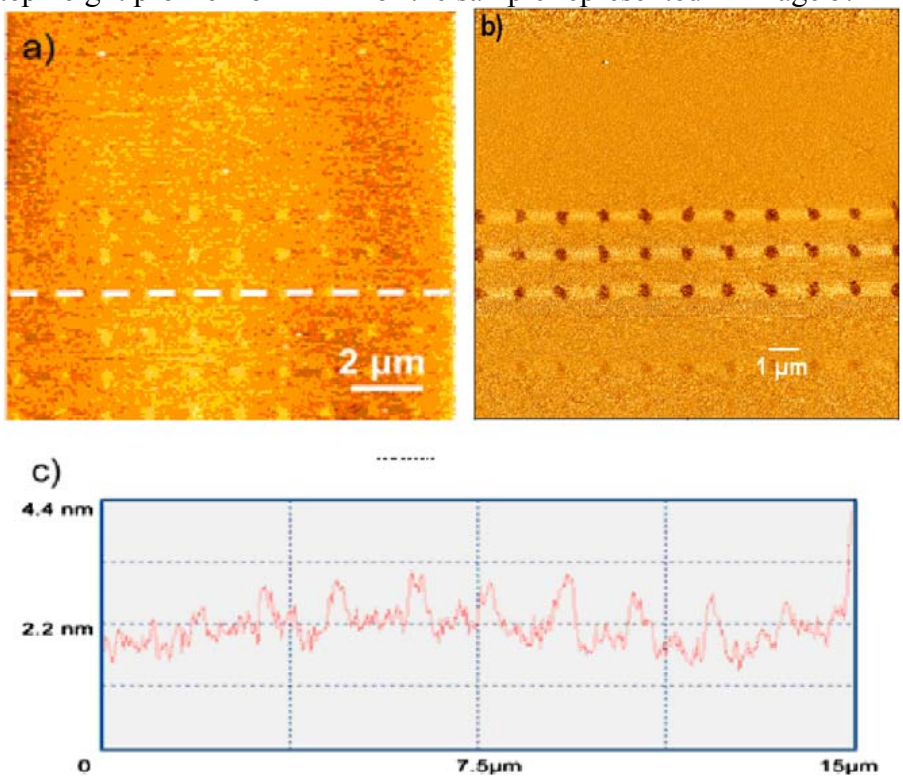

The estimated height of DPN generated patterns of **10a/b**, measured from randomly placed height profiles using tapping-mode AFM revealed a height of 1.2 ± 0.3 nm every 1.5 µm with a width of 0.5 µm (Figure 10c). The calculated height of a **10a/b** monolayer is 1.5 nm, consistent with the experimentally observed height values obtained for **10a/b**, indicating the formation of a **10a/b** SAM. Gold substrates containing **10a/b** SAMs were immersed in a 1 mM solution of ODT in ethanol for ~30 min, rinsed with ethanol, and dried under a stream of nitrogen. A tapping-mode AFM topography image after passivation with ODT and a corresponding height profile are shown in Figure 11a. Tapping-mode AFM images demonstrate the comparable heights of spots containing the

10a/b SAM and the surrounding ODT back-filled resist layers due to the similar heights of their SAMs (ca. 1.5 nm vs. 1.8 nm, respectively).[145] However, microarrays of **10a/b** backfilled with ODT can be clearly differentiated by LFM due to the greater frictional force and darker contrast in comparison to the ODT resist layer between the AFM tip and the **10a/b** SAM (Figure 11b). The graininess of the images shown in Figures 11a and 10b reveal the granularity of the gold surface, which was not investigated further.

Figure 11. AFM generated images of **10a/b** dot patterns after backfilling the bare gold substrates with ODT a) TMAFM and b) LFM images of **10a/b** dot patterns.

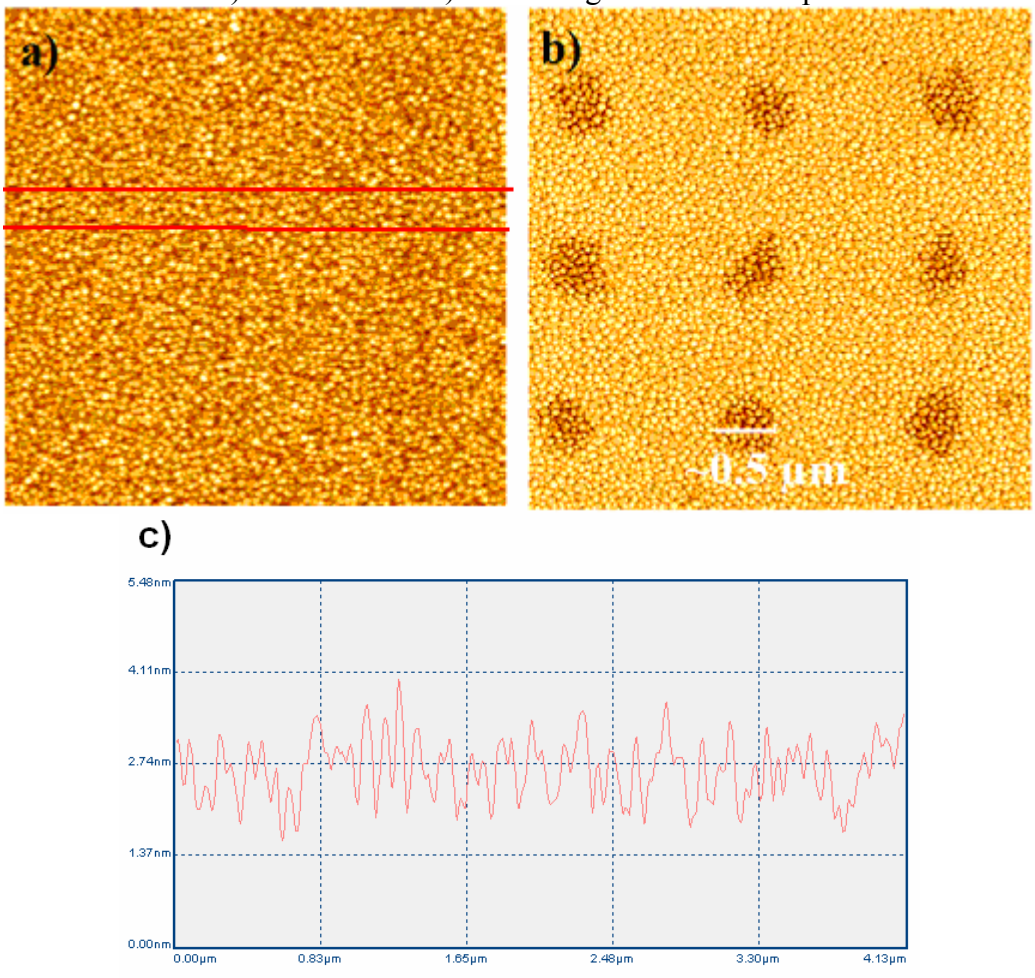

The molecular recognition capabilities of the DPN generated CTV-template microarrays towards C_{60} were examined. Arrays of **10a/b**–ODT were immersed in a 1 mM solution of C_{60} in toluene for ~40 min and after extensive rinsing with toluene they were dried with nitrogen and characterized via AFM. A typical AFM image showing C_{60} attached to the CTV-template is presented in Figure 11a. The binding interaction of the **10a/b**–ODT SAMs with C_{60} results in a light TMAFM contrast (Figure 12a) and a clearly visible contrast in the LFM image (Figure 12b). This is in good agreement with the frictional behavior of C_{60}, which is somewhat more hydrophilic than ODT. C_{60} was observed bound to individual dots with little or no binding to the resist ODT monolayer. Additional confirmation of C_{60} binding to DPN generated **10a/b** templates was obtained from SAMDI-TOF mass spectroscopy. Mrksich and co-workers have shown that SAMDI-TOF MS is an excellent tool to directly detect organic molecules, such as synthetic intermediates, at surfaces.[93] Therefore, SAMDI-TOF MS spectra were collected on DPN generated SAMS of **10a/b** before and after exposure to C_{60}. For SAMs of **10a/b**, a significant (74%) *m/z* peak at 462.27 was observed, which I assign to the cleavage product of **10a/b** at the N-O bond (Scheme 5). No parent peak was observed for **10a/b** and no peaks at larger masses were detected indicating that the lipoic acid tail of **10a/b** was lost in the laser desorption process. Exposure of DPN generated SAMS of **10a/b** to C_{60} resulted in the observation of an *m/z* peak at 720.05 (the mass of C_{60}) in the SAMDI-TOF mass spectrum indicating the presence of C_{60} bound to the **10a/b** monolayer. These data, taken together, provide proof-of-concept that supramolecular

CTV scaffolds can be directly patterned on surfaces and retain their ability to bind host molecules such as C_{60}.

Figure 12. AFM images of the sample after C_{60} deposition a) TMAFM image showing that a height increase of ~1.0 nm is observed where the CTV-disulfide ink was patterned, but not on the surrounding ODT surface b) The frictional contrast between CTV-C_{60} is apparent relative to the backfilled ODT surface in the LFM image c) Cross-sectional step height profile from tapping-mode AFM shows the periodic height increase of ~1.0 nm on the sample.

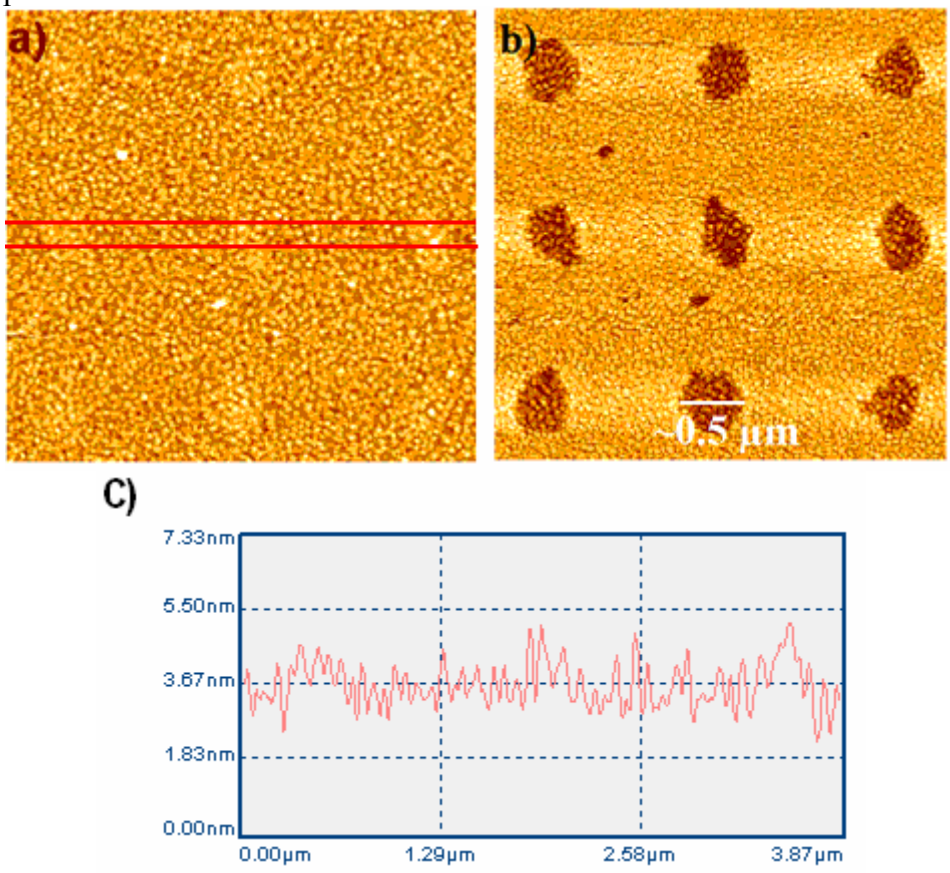

Given that the diameter of C_{60} is ~1 nm, a height increase for a SAM of **10a/b** after the addition of C_{60} is expected if C_{60} binds to the CTV macrocycle in a ball and socket fashion as observed by Atwood *et al.*[135] in the solid state. AFM height profiles of the **10a/b**-C_{60} SAM after the addition of the ODT resist was found to be 1.0 ± 0.3 nm

(Figure 12c). Since **10a/b** and ODT have approximately the same height, the 1 nm height increase is consistent with C_{60} binding through π-π interactions (Figure 13) similar to the binding mode reported for the solid state.[135] Previously it had been shown that apex-modified CTV derivatives interconvert between two different conformers, crown **9a** and saddle **9b**.[141] The interconversion equilibrium between the two conformers was shown to be solvent dependent with the crown conformer being favored in non-polar solvents.[146] Given the nearly complete coverage with C_{60} of the CTV-surface bound template, the equilibrium between the crown conformer **10a** and the saddle conformer **10b** must be shifted towards **10a** (Figure 13) enabling a ball-and-socket interaction between the host CTV molecules and the C_{60} guest.[146] Therefore, the apex-bound lipoic acid-CTV linked molecule **10a** must reside on the surface with its bowl shaped cavity directed *away* from the surface. The proposed conformation of the CTV bowl is consistent with other cyclophane SAMs, such as calix[n]arenes (n = 4, 6, 8).[137, 147]

Figure 13. Proposed C_{60} binding to the apex-modified, surface-bound CTV

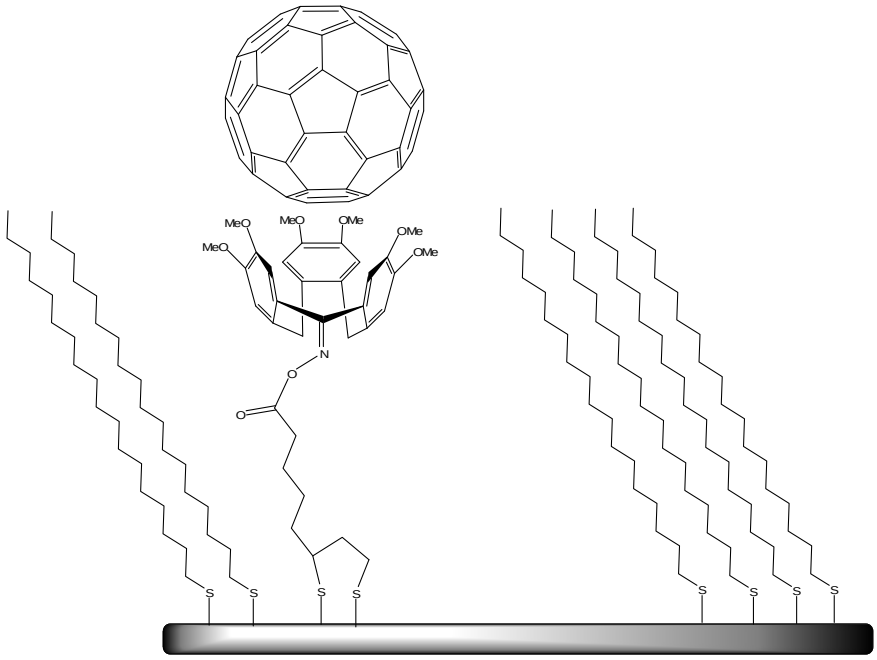

Conclusion

It has been shown that an apex-modified CTV supramolecular scaffold can be patterned into pre-defined microarrays via DPN. Through host-guest interactions, these microarrays have been shown to form bottom-up, layer-by-layer complexes with C_{60} with potential toward advancing nanoelectronics and optoelectronics. Having the ability to directly pattern molecular host active surfaces via DPN opens the door to preparing a wide range of host-guest materials with reproducible, homogeneous features with high edge resolution, which will facilitate the fabrication of microcircuitry and opticalelectronics based on host-guest chemistry.

CHAPTER FOUR

AN ANALYTICALLY QUANTITATIVE METHOD FOR DETERMINIG METHOXYARYL-TRANSITION METAL BINDING AFFINITY USING CYCLOTRIVERATRYLENE FUNCTIONALIZED GOLD NANOPARTICLES

Introduction

Cyclotriveratrylene (CTV) is a common supramolecular scaffold that has been previously employed in self-assembled binding motifs.[1] The most common CTV derivative employed in host-guest chemistry is designated C_3 due to its C_3 point group symmetry. This C_3 derivative consists of alternating methoxy and phenol groups on the aromatic rings and enabled by its rigid shaped -bowl structure, CTV can form host-guest complexes. For example, the CTV host forms "ball-and-socket" complexes with guests, including $[Na[2.2.2]cryptate]^+$, fullerene-C_{60}, *closo*-1,2-dicarbadodecaborane, and $[CpFe^{II}(arene)]^+$.[4, 135, 148-152] C_3 CTV can also be utilized as a tripodal scaffold for the attachment of other binding elements. Liskamp, *et al.*[5] *O*-alkylated the CTV-triol, which was then coupled with one or two amino acids, and solution phase combinational chemistry methods were used to catalog a 40-member library of tripodal molecules using CTV as a scaffold. On the other hand, Zhang *et al*.[136] utilized CTV derivatives to noncovalently but irreversibly bind fullerene-C_{60} to self-assembled monolayers on gold surfaces while Collet *et al*.[153] synthesized C_3 CTV derivatives with ligands capable of iron(II) and iron(III) octahedral coordination.

CTV derivatives that bind both divalent and trivalent metal ions with their methoxy ether groups are an interesting aspect of host-guest chemistry. Metal binding can occur via empty metal valence orbitals and electron loan pairs residing on the methoxy groups on the outer rim of the CTV bowl. Metal ion binding to these methoxy moieties has been shown to form coordination polymers as well as clatharate crystalline materials.[4,5, 69, 154] In a study conducted by Raston *et al*.[155] X-ray crystal structures was obtained of CTV binding to alkali-earth metal cations (Na^+, K^+, Rb^+, and Cs^+) forming large crystalline coordinate polymers by binding the methoxy group of CTV. Hardie *et al*.[156] revealed that lanthanide metal ions can also bind to CTV-methoxy groups. X-ray crystallographic data on CTV-lanthanide complexes indicated that the water molecules of the capped triangular dodecahedral $[Eu(H_2O)_9]^{3+}$ cations are at distances favorable for hydrogen bond formation with the CTV perimeter methoxy lone-pairs.

In order to examine solution host-guest interactions between colorless di- and trivalent metal ions and CTV molecules, a colorimetric analytical device for the detection of di- and trivalent metal ions was developed based on gold nanoparticles (AuNP). An apex-modified CTV supramolecular scaffold head group with a dithiolane tail for binding to a gold surface with the CTV bowl shaped cavity directed *away* from the surface was synthesized and bound to AuNPs. Unlike traditional organic fluorescent dyes, AuNPs have much stronger molar absorptivities that are 3 -5 orders of magnitude higher than organic fluorescent dyes.[157, 158] The optical properties of AuNPs are due to their unique surface plasmon resonance (SPR) where electrons on the surface of an AuNP are in collective oscillation and become in resonance with incident electro-magnetic

radiation.[159, 160] Modified AuNPs make excellent colorimetric analytical platforms because NP aggregation due to analyte detection results in a color change from red to blue.[41, 161-169] CTV-functionalized AuNPs provide the basis for the design of an analytical tool that can be used to examine the affinity of methoxy groups towards di- and trivalent transition metal ions in solution. This analytical spectroscopic method provides a new method for the use of host-guest interactions as a detection method for environmentally toxic metal ions.

Experimental Section

All solvents and reagents were used without further purification unless otherwise noted. All solvents were distilled prior to use. All reactions were conducted under a nitrogen atmosphere. Sorbent Technologies silica gel 60 A, 40 – 75 μm (200 x 400 mesh) was used for column chromatography unless otherwise noted. Sorbent Technologies aluminum-backed Silica gel 200 μm plates were used for TLC. ^{1}H NMR spectra were obtained on either a Varian INOVA 300 or Varian GEMINI 2000 300 MHz spectrometer with trimethylsilane (TMS) as the internal standard.

*10,15-Dihydro-2,3,7,8,12,13-hexamethoxy-5H-tribenzo[a,d,g]-cyclononene (**7**)*

Veratryl alcohol (18 mL, 120 mmol) was mixed with formic acid (325 mL) in a round bottom flask. The reaction was stirred at 60 ºC for 3 h. The reaction was cooled to room temperature and filtered. The crude mixture was purified *via* recrystallization in toluene and filtered to afford **7** as a white crystalline solid (9.36 g, 52 % yield). ^{1}H NMR (300 MHz, $CDCl_3$) δ 6.83 (s, 6H), 4.76 (d, 3H), 3.83 (s, 18 H), 3.54 (d, 3H).

*10,15-Dihydro-2,3,7,8,12,13-hexamethoxy-5H-tribenzo[a,d,g]- cyclononen-5-one (**8**)*

For the synthesis of the CTV-ketone derivative according to the method of Lutz *et al*.,[141] CTV **7** (2.0 g, 4.4 mmol), $Na_2CrO_7 \cdot 2H_2O$ (2.1 g, 7.0 mmol), and 22 mL of HOAc were mixed in a round bottom flask. The reaction was refluxed at 120 ºC for ~20 h and the reaction was monitored via TLC using AcOEt/CH_2Cl_2 (5/95) as the eluent. Upon consumption of the starting material, the reaction was quenched with 25 mL of H_2O. The reaction was extracted in 3 x 25 mL lots using CH_2Cl_2. The organic fractions were collected and washed with 3 x 15 mL of H_2O, and the organic fraction was dried over Na_2SO_4. Concentration afforded **8** as an off white solid (1.9 g, 92%). ^{1}H NMR (300 MHz, $CDCl_3$) δ 7.43 (2H, s), 6.76 (2H, s) 6.49 (2H, s), 3.96 (6H, s), 3.92 (6H, s), 3.81 (6H, s), 3.77 (4H, br s).

*10,15-Dihydro-2,3,7,8,12,13-hexamethoxy-5H-tribenzo[a,d,g]- cyclononen-5-oxime(**9a/b**)*

For the synthesis of the crown and saddle CTV-oxime derivatives, CTV-monoketone **8** (500 mg, 1.08 mmol), hydroxylamine hydrochloride ($H_2NOH \cdot HCl$) (750 mg, 10.8 mmol), and 6 mL of pyridine were mixed in a round bottom flask and refluxed for ~23 hours. The reaction was monitored via TLC using AcOEt/CH_2Cl_2. Upon consumption of the starting material, the reaction was cooled to room temperature and diluted with 20 mL of CH_2Cl_2. The reaction was washed with 4 x 10 mL of 10 % HCl, 2 x 10 mL of H_2O, and 10 mL of brine. The organic fractions were dried over Na_2SO_4 and the solvent removed under vacuum. The crude reaction mixture was purified using column chromatography with a 75× loading ratio and an eluent gradient of

AcOEt/CH_2Cl_2 (1/4 to 1/1). The crown/saddle (**9a/b**) fractions were combined and the solvent removed affording a light brown solid (375 mg, 73 %). ^{1}H NMR (300 MHz, $CDCl_3$) δ 9.41(br s, 1H), 6.96 (s, 1H), 6.90 (s, 1H), 6.86 (s, 1H), 6.81 (s, 1H), 6.71 (s, 1H), 4.77 (d, 1H), 4.38 (d, 1H), 3.89 (s, 3H), 3.87 (s, 3H), 3.83 (s, 12H), 3.58 (d, 1H), 3.50 (d, 1H).

*10,15-Dihydro-2,3,7,8,12,13-hexamethoxy-5H-tribenzo[a,d,g]- cyclononen-O-[5-(1,2-dithiolan-3-yl)pentanoyl]-5-oxime (**10a/b**)*

For the synthesis of the crown and saddle CTV oxime-lipoic acid derivatives, lipoic acid (283 mg, 1.37 mmol), hydroxybenzotriazole (HOBT) (200 mg, 1.48 mmol), N,N'-dicyclohexylcarbodiimide (DCC) (330 mg, 1.60 mmol), and 3.0 mL of dry tetrahydrofuran (THF) were mixed in a round bottom flask and allowed to stir at room temperature for 1 hour. A mixture of crown and saddle conformers of CTV oxime **9a/b** (545 mg, 1.14 mmol) in 2.7 mL of dry THF was then added dropwise. The reaction was allowed to stir for ~24 hours and monitored via TLC using AcOEt/CH_2Cl_2 (1/9) as the eluent. Upon consumption of the starting material, the reaction was filtered over celite to remove the insoluble urea and washed with ~30 mL of CH_2Cl_2. The solvent was then removed under vacuum. The crude mixture was purified using flash chromatography with an RS-40 cartridge and an eluent gradient of AcOEt/hexane (1/2 to 2/1). The crown/saddle (**10a/b**) fractions were combined and removal of the solvent afforded a light brown solid (434 mg, 57%). This product was characterized by ^{1}H NMR. ^{1}H NMR (300 MHz, $CDCl_3$) δ 7.33 (s, 1H), 6.94 (s, 1H), 6.93 (s, 1H), 6.91 (s, 1H), 6.83 (s, 1H),

6.80 (s, 1H), 6.78 (s, 1H), 6.68 (s, 1H), 6.65 (s, 1H), 6.64 (s, 1H), 6.58 (s, 1H), 6.54 (s, 1H).

Preparation of CTV -lipoate conjugated 15 nm AuNPs

In order to modify the surface of AuNPs (Figure 1) with the CTV-lipoate conjugate derivatives (**10a/b**), 7.4 µL of a 2.7 mM 1% polysorbate 20/MeCN solution of **10a/b** was pipetted into 992.6 µL of tannic acid stabilized 15 nm AuNPs. The microcuvettes were vortexed for 20 s and allowed to rest at room temperature for ~24 h. The microcuvettes were then centrifuged at 14,000 rpm for 30 min. and the supernatant removed. The conjugated particles were then resuspended in a 1% polysorbate 20/ACN solution. In order to remove any excess unbound CTV-lipoate conjugate **10a/b** from the AuNP solution, the microcuvettes were centrifuged at 14,000 rpms for 30 min. The supernatant was removed and the AuNPs were resuspended in a 1% polysorbate 20/ACN solution. This centrifugation and resuspension procedure was repeated three times.

Titration of M^{2+} into AuNPs

To 247 µL of CTV-lipoate conjugated to 15 nm AuNP in 1% polysorbate 20/MeCN in each of six different microcuvettes was added 2.5 µL of 1, 2, 5, 6, 9, and 10 mM solution of Pb^{2+}, Cd^{2+}, Zn^{2+}, Cu^{2+}, Hg^{2+}, and Eu^{3+} in milli-Q nanopure water. The microcuvettes were then vortexed for 10 s and were allowed to sit at room temperature for 20 h.

UV/vis detection

A Shimadzu UV-3101PC spectrophotometer was used for all UV-Vis experiments. A 100 µL sample of each metal titration into the CTV modified AuNP's in

1% polysorbate 20/ACN was pipetted into a quartz cell with a 1 mm path length. Spectra were recorded from 200 – 900 nm with a sample interval of 2 nm. In between each sample, the UV-Vis cell was rinsed with aqua regia (3:1 $HCl:HNO_3$) followed by nanopure water and dried under a stream of N_2 gas. It was then rinsed with 200 μL of 1% tween 20/ACN solution and finally dried under a stream of N_2 gas.

Results and Discussion

Cyclotriveratrylene (CTV) is a supramolecular scaffold that is known to bind mono and trivalent metal ions.[4, 69, 154, 156, 170] CTV has been used to generate self-assembled monolayers on gold surfaces through modifications of the outer perimeter of the CTV bowl, resulting in the concave shape of the CTV molecule facing *toward* the surface.[136] Although SAMs of these outer perimeter modified CTV derivatives afford densely packed monolayers that were shown to bind host molecules such as C_{60}, the non-covalently bound host molecules were trapped against the surface.[125] This configuration of the CTV bowl adhered to a gold surface limits its ability to bind di and trivalent metal ions and function as a template for a layer-by-layer approach to build novel nanostructures. Therefore, we hypothesized that derivatizing the apex of the CTV bowl would provide a supramolecular scaffold with the concave bowl receptor pointed *away* from the surface, enabling CTV to function as a AuNP-bound host molecule.[171] To accomplish this, CTV was oxidized to the monoketone and converted to the oxime in high yield as an equilibrium mixture of the crown **9a** and the saddle **9b** conformers (Scheme 6).[16] The CTV oxime was coupled to (±)-α-lipoic acid affording a mixture of the coupled crown **10a** and saddle **10b** conformers in 52% yield. The resulting CTV-lipoic

acid derivatives **10a/b** contain a dithiolane-terminated linker for coordination to gold, thus enabling the bowl of CTV to face away from the surface of an AuNP.

With the successful design and synthesis of an apex modified CTV supramolecular scaffold head group with a dithiolane tail, 15 nm AuNPs were functionalized by the addition of a 2.7 mM solution of **10a/b** in a 1% polysorbate 20 acetonitrile (ACN) solutiion (Scheme 7).[163] These samples were then vortexed for 20s to

Scheme 6. Synthetic method for the preparation of an apex-modified dithiol CTV-oxime (**10a/b**) for the modification of 15 nm AuNPs.

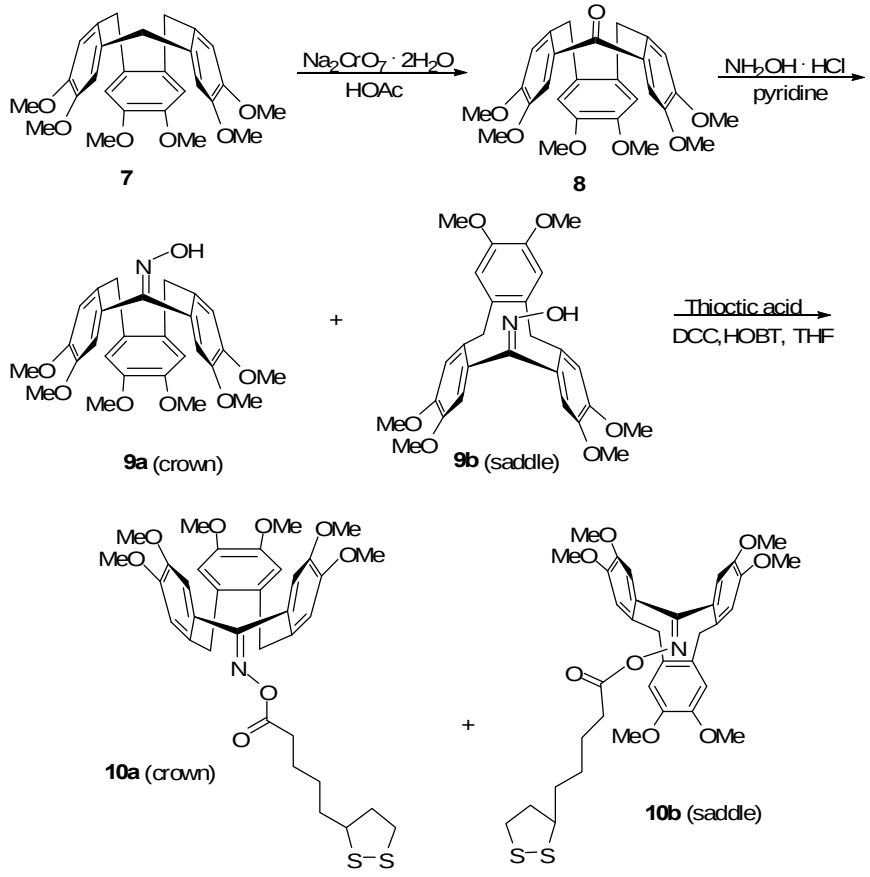

ensure homogeneity throughout the solution. The AuNP/CTV-dithiolane solution was allowed to sit at room temperature for ~24 h to allow full functionalization of the AuNPs.

In order to remove the excess CTV-dithiolane, the AuNPs were centrifuged at 14,000 rpm for ~30 min. The denser CTV-dithiolane functionalized AuNPs precipitated while the excess CTV-dithiolane remained in solution. The supernatant was carefully removed and the functionalized AuNPs were resuspended in a 1 % polysorbate 20/MeCN solution. This process was repeated three times to ensure complete removal of any excess CTV-dithiolane from the AuNP solution. Transmission electron microscopy (TEM) was used to confirm that the AuNPs were intact after

Scheme 7. Route to functionalizing the AuNPs with the CTV-dithiolate ligand.

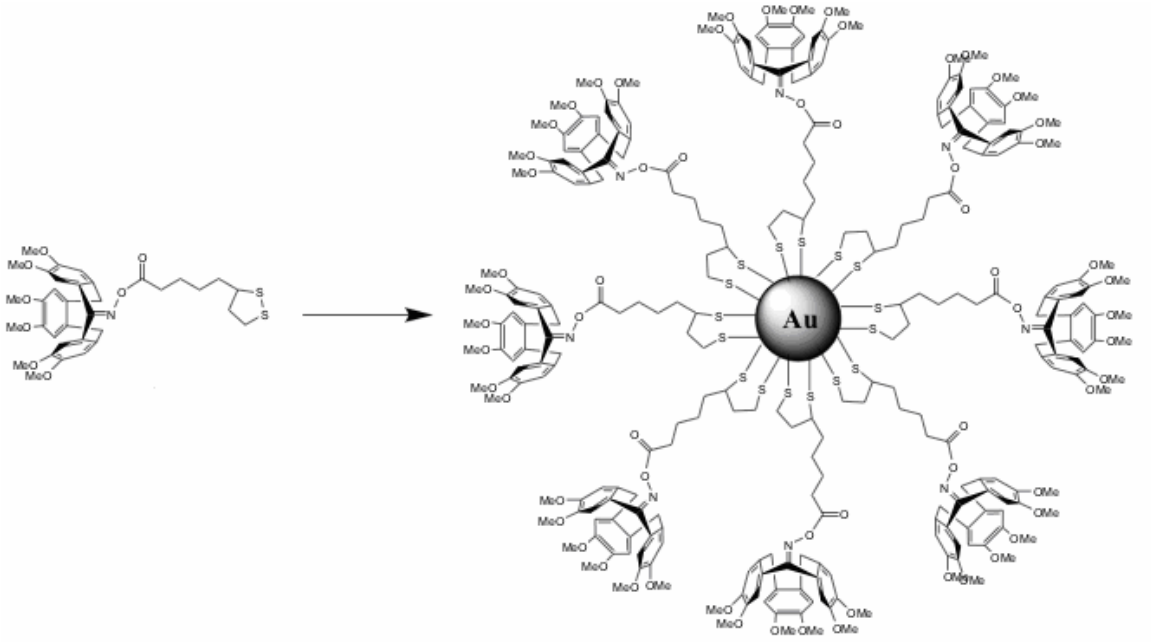

functionalization with the CTV-dithiolate ligand (Figure 14). TEM images reveal that the CTV-functionalized AuNPs retain their roughly spherical structure. Due to the differences in the refractive indices between the water and acetonitrile solvents, the UV-

vis spectra shifted to the right upon modification CTV-AuNPs in MeCN. The expected shift in the SPR of the AuNP solution had shifted from 522 nm in water to 550 nm in MeCN solution (Figure 15).[172] The decrease in absorbance is due to the loss of nanoparticles from the washing and extracting of solvent to remove excess CTV after modification.

With the successful functionalization of stable CTV-dithiolate 15nm AuNPs, a series of colorless di- and trivalent metal ions (Cu^{2+}, Pb^{2+}, Hg^{2+}, Zn^{2+}, Cd^{2+}, and Eu^{3+}) were titrated into a solution of CTV-lipoate modified AuNPs in tween 20/MeCN. Various concentrations of each metal ion (10 μM, 20 μM, 50 μM, 60 μM, 90 μM, and 100 μM) in nanopure water were pipetted into the CTV-dithiolate AuNP solution. The solution was incubated at room temperature (~21 ^{o}C) for ~24 h in order to allow for complexation

Figure 14. TEM images a) and b) of the CTV-dithiolate functionalized AuNPs show that after modification, the AuNPs retain their spherical shape and show that the CTV-lipoate AuNPs do not polymerize without the addition of metal cataions.

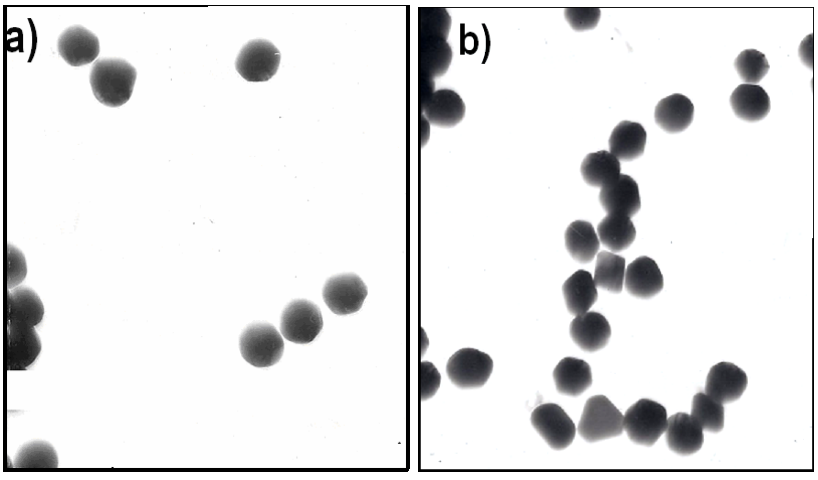

Figure 15. UV-vis spectra of the unmodified nanoparticles purchased from Ted Pella (black) versus the CTV-lipoate modified AuNPs in 1% Tween 20/MeCN (red) showing that modification of the AuNPs with the CTV-lipoate moiety and the subsequent solvent change results in a decrease and shift in absorbance from 515 nm to 550 nm.

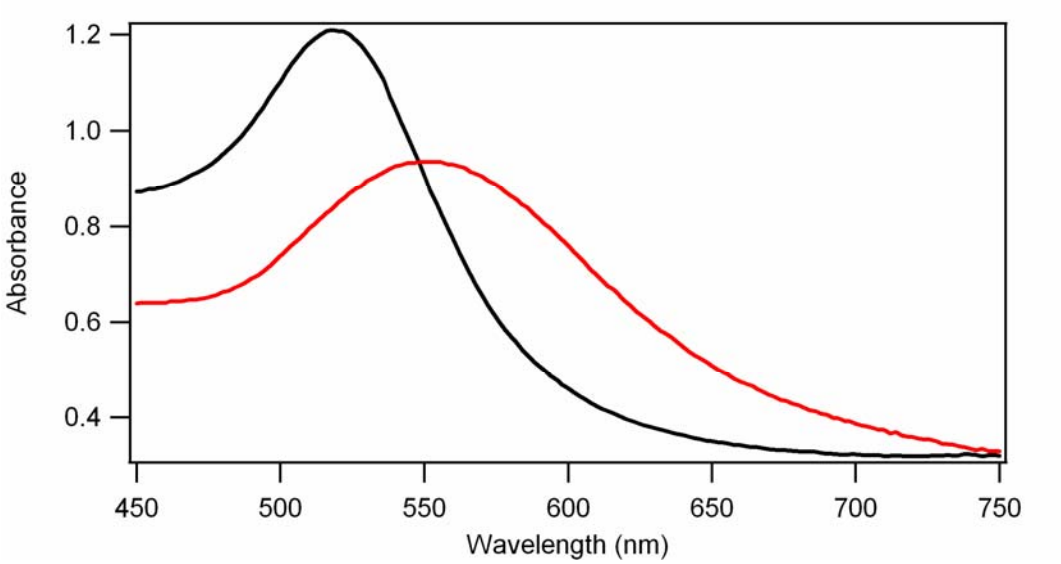

between CTV-methoxy moieties and the divalent metal cations, which resulted in the formation of a purple precipitate. Binding interactions between the methoxy moieties of the CTV ligands and the metal cation in solution were examined by recording the UV-Vis spectrum of the supernatant between 450 – 750 nm. Typical UV-Vis spectra are shown in Figures 16a-c. The initial absorbance of the CTV-thiolate functionalized 15 nm AuNPs monitored at 550 nm decreases accompanied by broadening as the metal ion concentration is increased from 10 to 100 μM. A decrease in absorbance at 550 nm and the observed precipitate are consistent with metal cation binding to CTV methoxy groups in and intra-NP fashion resulting in the formation of a metal ion assisted polymerization of the CTV-lipoate modified AuNPs. Evidence of the formation of a metal ion-CTV-AuNP polymerization was obtained from TEM images (Figure 17).

Figure 16. Typical spectroscopic metal binding titrations of increasing a) [Cu^{2+}], b) [Pb^{2+}], and c) [Eu^{3+}] binding to 15 nm CTV-dithiolate functionalized AuNPs resulting in a decrease in absorbance after 24 hours.

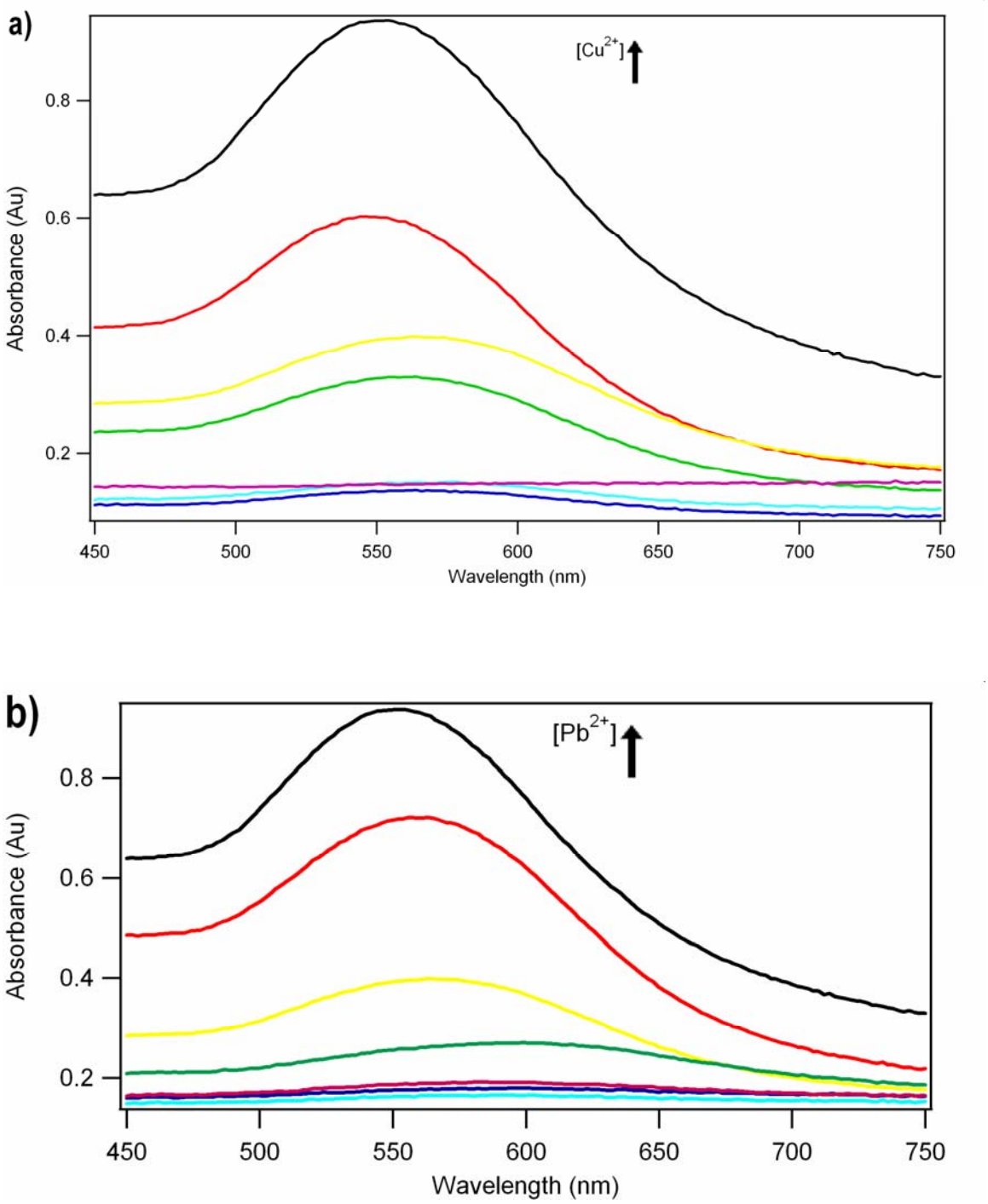

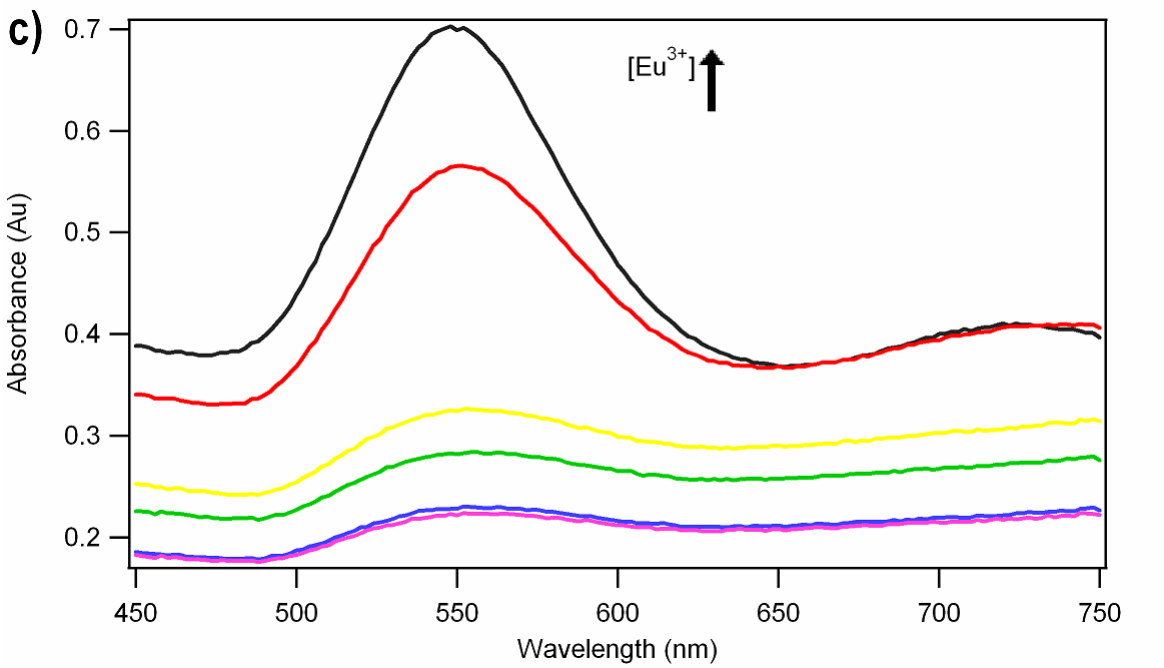

Figure 17. TEM image of the observed CTV-lipoate AuNP precipitate upon metal complexation.

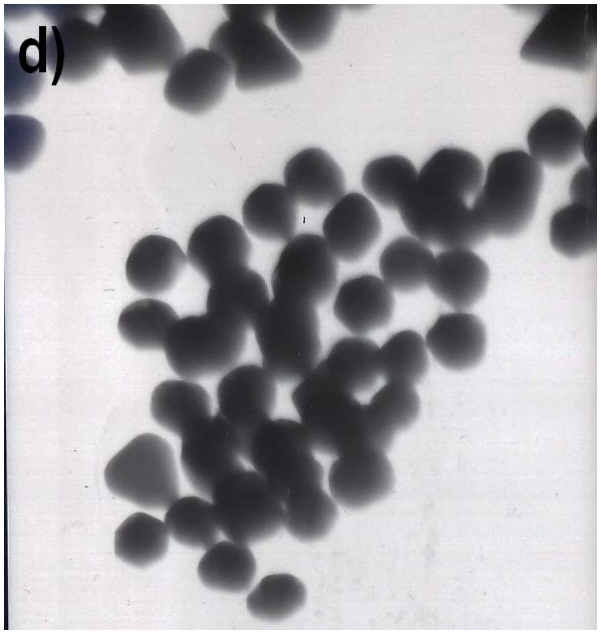

Metal cation affinities to the methoxy moieties of the CTV-dithiolate functionalized AuNPs were determined by titrating metal ions into a CTV-dithiolate functionalized AuNP solution and monitoring the decrease in absorbance at 550 nm (Figure 17a-c). Dissociation constants (K_d) for a single metal binding event were determined by fitting plots of absorbance vs. metal ion concentration to eq 1[173]

$$r = pC_m /(K_d + C_m) \quad (1)$$

where p is the number of sites for which the interaction with the metal cation is governed by the intrinsic dissociation constant, K_d, and r is the binding function calculated by subtracting the metal titration absorbance, Ab_m, at 550 nm from the initial absorbance, Ab_i using eq 2. C_m is the concentration of the metal ion that was titrated into the AuNP solution.

$$r = Ab_i - Ab_M \quad (2)$$

A value for K_d was obtained by fitting the data via an iterative process that allowed both K_d and p values to vary (Figure 18a-c). The best fits obtained provided p values that ranged from 0.3 - 1.4 and K_d values that range from 13 μM ± 1 for Cd^{2+} to 60 μM ± 1 for Cu^{2+} (Table 7). Based on these K_d values, a binding affinity series was created represented by the following order: Cu^{2+}>Zn^{2+}>Pb^{2+}>Hg^{2+}>Eu^{3+}>Cd^{2+}.

Figure 18. Plot of binding function *r* vs C_m (the concentration of the metal ions in the solution) for a) Cu^{2+}, b) Pb^{2+}, and c) Eu^{3+} titrated into CTV-lipoate AuNPs.

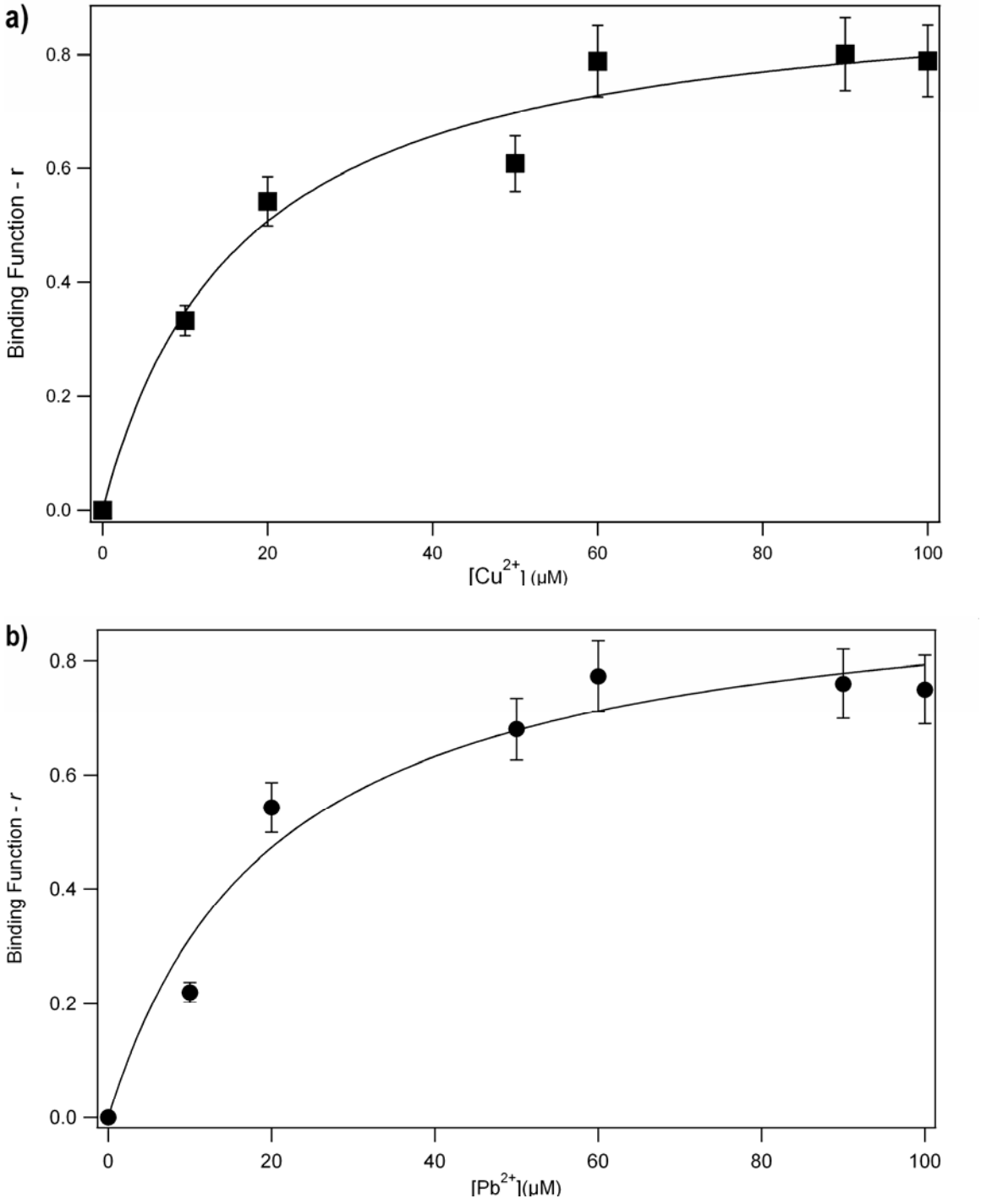

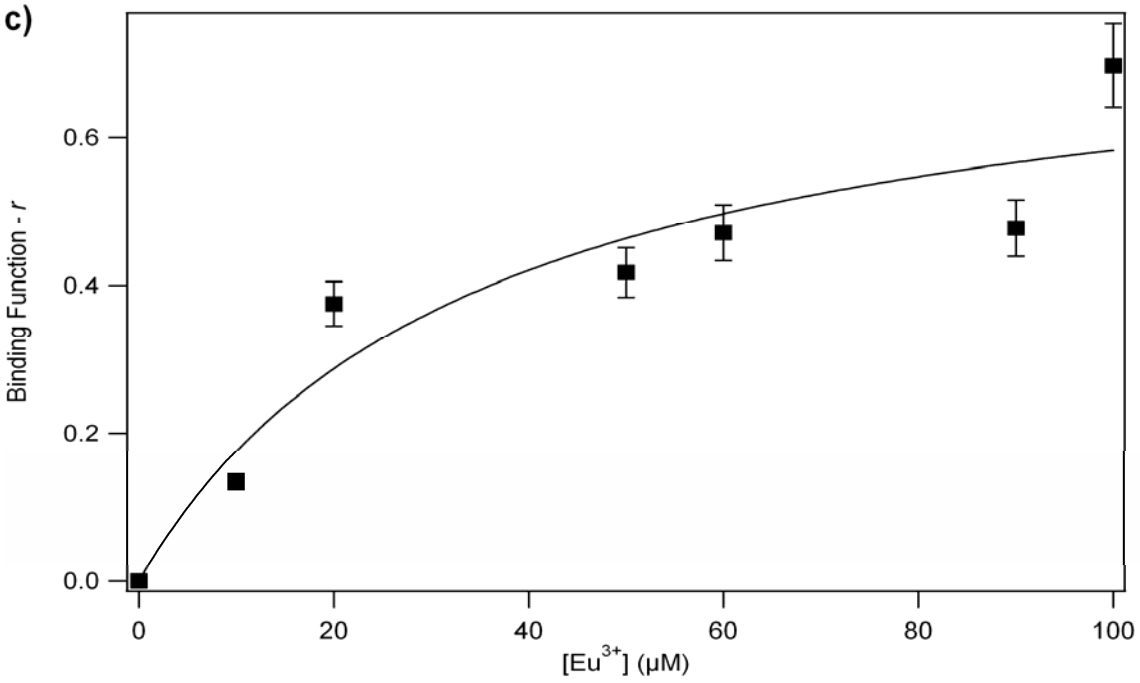

Table 7. Metal binding affinity data for varying metals titrated into CTV-lipoate AuNPs.

Metal	p	K_d (μM)	σ (±)	χ^2
Pb^{2+}	1.0	49	2	0.020
Cd^{2+}	1.4	13	1	0.069
Zn^{2+}	0.5	51	3	0.014
Cu^{2+}	0.9	60	1	0.013
Hg^{2+}	0.3	34	1	0.011
Eu^{3+}	0.8	29	2	0.033

Since the divalent metal ions used can adopt four, five, or six coordinate geometries in solution whereas Eu^{3+} can exhibit coordination geometries of 8 or higher, we hypothesized that the metal ion's coordination sphere is made up of CTV-methoxy oxygens and water molecules. Evidence for the existence of such a structure can be gleaned from X-ray crystallographic data of a Na^+ bound CTV complex.[170] In this structure, each Na^+ ion coordinates to symmetry-equivalent CTV molecules resulting in the Na^+ cation residing in a highly distorted octahedral geometry where each CTV

molecule chelates edge-bound to Na^+ through one dimethoxy moiety and *cis* water/hydroxy ligands (Figure 19). Likewise, the X-ray crystal structures of the Cs^+ and Rb^+ CTV complexes revealed that both of the larger monovalent cations bind to the dimethoxy moieties of CTV and two *cis* water/hydroxyl ligands forming a highly distorted six-coordinate complex in a similar fashion to Na^+ (Figure 20).[155] Interestingly, the X-ray structure of the Eu^{3+} CTV complex indicates that the methoxy moieties act as hydrogen bond acceptors with the aquo ligands of the $[Eu(H_2O)_9]^{3+}$ cations forming hydrogen-bonded superstructures (Figure 21).[156] The $[Eu(H_2O)_9]^{3+}$ cations reside in two distinct environments but both retain their water ligands and do not form direct bonding interactions with the methoxy moieties of CTV.

Figure 19. Section of the two-tiered, infinite two-dimensional sheet structure formed through hydrogen bonding and coordination of the CTV-methoxy ligands to the Na^+ ions. Darkened CTV molecules represent those that are concave down, whereas the lighter CTV molecules represent those that are concave up. Na^+ ions are represented as shaded black dots.[170]

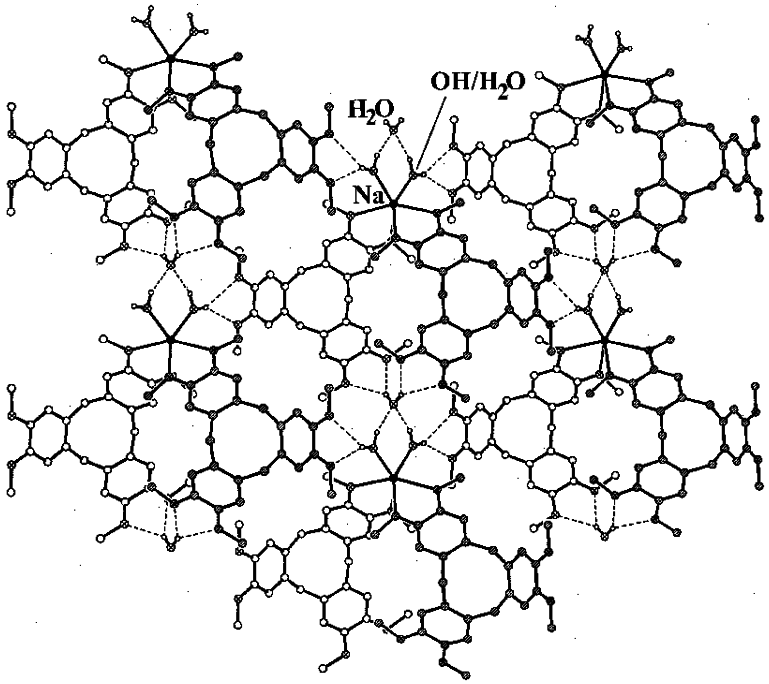

Figure 20. Crystal structure of Cs^+ bound to CTV through direct coordination of the methoxy groups and hydroxide/water bridges.[155]

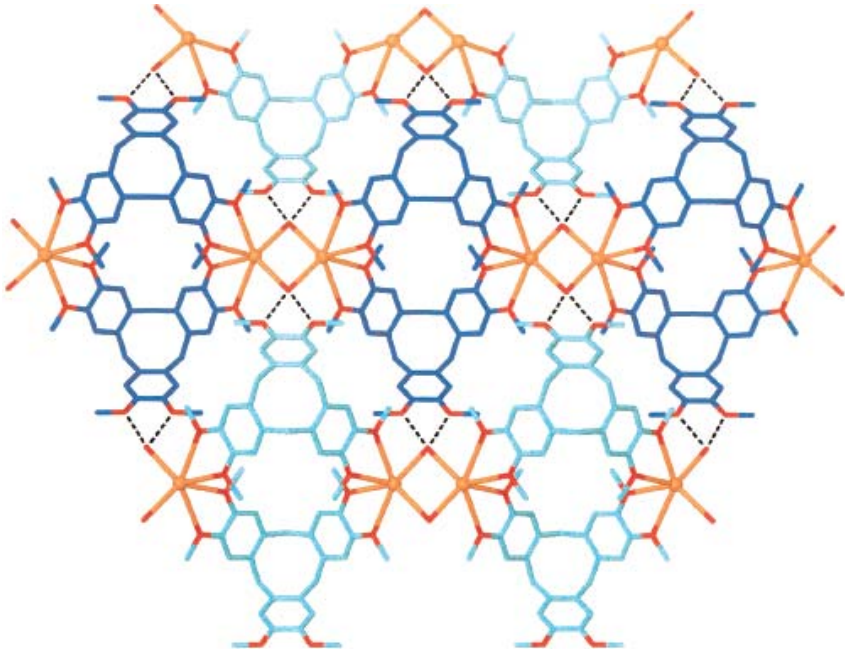

Figure 21. CTV molecules stacked back-to-back and hydrogen bonded to two distinct $[Eu(H_2O)_9]^{3+}$ complexes denoted as Eu(1) yellow, Eu(2) pink, MeCN in green, and unbound water in orange. a) Type 1, regular CTV assembly and b) type 2, splayed CTV assembly.[156]

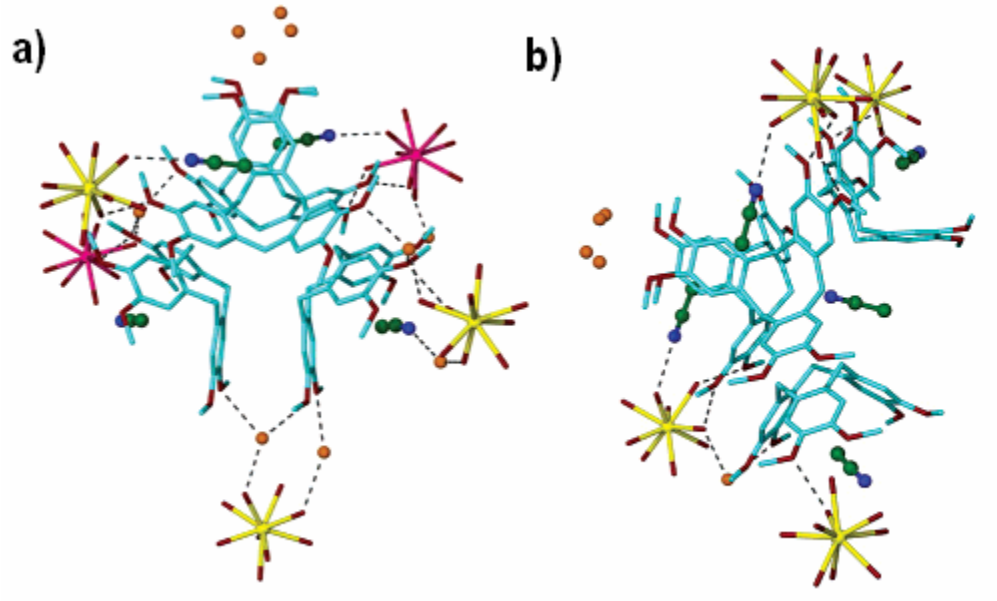

The binding mode observed for Eu^{3+}, while different from that observed for the alkali metal ions, is likely the result of the more Lewis acidic Eu^{3+} ion vs. the M^{2+} cations examined. Since methoxy moieties are not as strong a Lewis base as water molecules, the highly Lewis acidic Eu^{3+} cation will preferentially bind to water over CTV methoxy groups. Therefore, one would expect the K_d value of 29 ± 2 nM observed for Eu^{3+} results from $[Eu(H_2O)_9]^{3+}$ cations hydrogen-bonding with the methoxy moieties of CTV, similar to the reported CTV-Eu^{3+} X-ray crystal structure. For the remaining divalent transition metal complexes capable of forming octahedral complexes in solution (Cd^{2+}, Pb^{2+}, Cu^{2+}), all three are soft metal acids and exhibit p values of ~1. The K_d values for these three complexes increase with increasing hardness of these soft metal acids, suggesting that the softer the metal ion the better affinity for a methoxy ligand. Therefore, we hypothesize that these three metal ions will be chelated by some combination of CTV-methoxy groups and water molecules (Figure 22), similar to the alkali metal cations. Likewise, the soft metal acids Hg^{2+} and Zn^{2+} likely bind to the CTV-methoxy groups and water molecules in some combination, similar to the alkali metal cations, since the softer Hg^{2+} ion binds more tightly (34 ± 1nM) than Zn^{2+} (51 ± 3 nM). However, the observed p values for these two divalent metal ions are 0.3 and 0.5, respectively, indicating a difference in the type of polymeric structure formed upon binding. Given Hg^{2+} and Zn^{2+} preference for tetrahedral geometries, an altered superstructure is not unexpected.

Figure 22. Proposed binding interaction between a metal cation and the CTV-methoxy ligand in solution, forming insoluble AuNP based polymer aggregates.

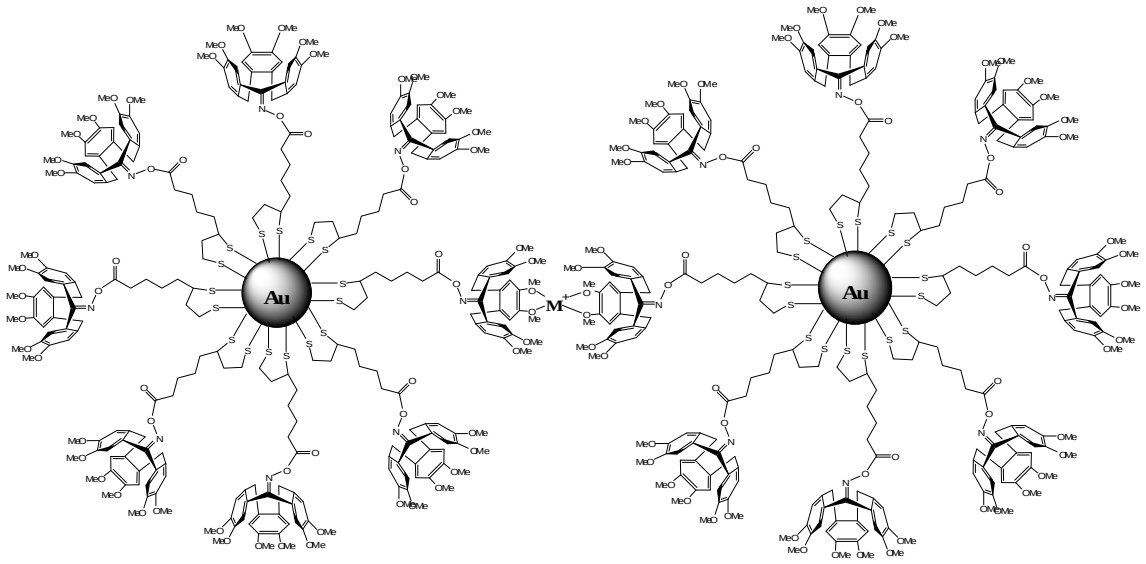

A variety of selective colorimetric metal ion detection devices, such as chemosensors,[174-181] metal ion induced colour change (MICC),[182] and Förster resonance energy transfer systems[183] have previously been reported for the detection of cations in solution. Nanoparticle based colorimetric copper (II) sensors such as those reported by Larpent *et al*.[184] utilized an aqueous 15 nm fluorescent metal-chelating polymer nanoparticle with a 1,4,8,11-tetraazacyclotetradecane (Cyclam) selective ligand on the surface and 9,10-diphenylanthracene (DPA) as the fluorophore that was encapsulated in the core. These functional nanoparticles showed quenching of the observed fluorescence upon binding to Cu^{2+} in solution. While these different devices allow for the detection of metal ions in solution, no determination of metal ion binding constants was reported. The CTV-AuNP method that was developed offers an advantage as being able to both detect and analytically quantify metal ion concentrations in the solution.

Conclusion

An apex-modified CTV derivative containing a dithiolane tail was used to functionalize 15 nm AuNPs. Taking advantage of the optical properties of AuNPs, a colorimetric analytical method was developed to determine the metal binding properties of a series of di- and trivalent metal ions in solution. This spectroscopic method provides a new method for the use of host-guest interactions as a method for studying metal-ligand binding interactions. It is of importance to develop spectroscopic detection methods to determine the binding properties of toxic colorless metal ions such as Hg^{2+} and Pb^{2+}, as well as other potentially harmful metal ions such as Cd^{2+}. The environmental and biological impact of metal ion contamination is of great importance and the toxicity of lead and mercury ions are well documented. Moreover, the toxicity of Cu^{2+} at high concentrations to algae, fungi, bacteria and viruses as well as the fact that high copper concentrations in children leads to cirrhosis of the liver and potentially plays a role in neurodegenerative diseases such as Alzheimers suggests that a sensitive, optical detection method for the detection of Cu^{2+} would be advantagious.[1,2]

CHAPTER FIVE

CONCLUSION

The overall goal of this thesis, as outlined in Chapter 1, was to examine host – guest interactions for the fabrication of pre-designed, spatially controlled arrays of immobilized supramolecular and biological molecules utilizing a bottom-up, layer-by-layer approach. This research was accomplished through the use of modern synthetic organic methodologies to produce novel biological and supramolecular scaffolds that were attached to gold surfaces *via* a gold – sulfur bond. Lithographic techniques including microcontact printing (μCP) and dip-pen nanolithography (DPN) were used to fabricate pre-designed, spatially controlled arrays of immobilized biological and supramolecular scaffolds.

In Chapter 1, evidence was presented that carbohydrates could be synthesized and patterned onto gold surfaces. Two different synthetic methods were developed to create an alkyl thiol-linked carbohydrate derivative where the sugar head group was accessible for bacterial attachment at a surface. The first synthetic method utilized the classic Koeing-Knorr glycosylation reaction for the attachment of the alkyl-linkage while a second more simplified method was developed to facilitate the creation a library of different alkyl thiol-linked carbohydrate derivatives. An L-rhamnose derivative that was developed from the first synthetic method was patterned onto a gold surface *via*

microcontact printing. TMAFM data confirmed that the L-rhamnose derivative had been patterned into pre-designed, spatially controlled (5.3 μm) biological arrays. To provide "proof-of-concept" that the biological activity of the carbohydrate arrays were retained, *Pseudomonas aeruginosa* bacterial cells in M9 media solution were applied to the L-rhamnose array. TMAFM images confirmed that *P. aeruginosa* selectively binds to the patterned L-rhamnose arrays.

In Chapter 2, the research involved the synthesis and patterning of a supramolecular scaffold, CTV. This synthetic method was devised to produce an apex-modified CTV derivative where the bowl-shaped cavity faced *away* from the surface. This apex-modified CTV molecule was patterned onto a gold surface into pre-defined, spatially controlled 0.5 μm dots *via* DPN. These DPN patterned CTV substrates were then exposed to a solution of fullerene C_{60}. LFM, TMAFM, and SAMDI-TOF MS data confirmed the specific host-guest interaction between the patterned CTV scaffold and the C_{60}. This research establishes that host-guest interactions on the surface can be utilized at the nanometer scale using a bottom-up, layer-by-layer approach for the assembly of potential optical or electrical devices.

In Chapter 3, the apex-modified CTV molecule was used as a supramolecular scaffold for the development of an analytical, spectroscopic method to determine di- and trivalent metal ion binding affinities to the methoxy moieties of CTV. In order to accomplish this, the apex-modified CTV molecule was used to functionalize gold nanoparticles. These CTV-functionalized nanoparticles were then used to analytically

quantify the binding affinity between the CTV's methoxy groups and transition metals. This work will lead to future insight into how to quantify host – guest interactions.

The research detailed in this dissertation shows that host – guest interactions are integral to the future design and fabrication of nano-optical and nano-electrical systems. Future work from these projects will include the use of carbohydrate libraries to fabricate mixed carbohydrate-arrays that are capable of selectively binding specific, targeted bacterial cells. The host-guest interaction between CTV and C_{60} will be expanded to the fabrication of pre-designed, spatially controlled arrays of supramolecular scaffolds for the directed placement of carbon nanotubes.[185] Finally, the CTV-AuNP work will be expanded to include new dithiolate functionalized ligands and proteins with greater metal ion affinities.

REFERENCES

1. Beer, P. D.; Gale, P. A.; Smith, D. K., *Supramolecular Chemistry*. Oxford University Press: Oxford, England, 1999; p 4, 90.

2. Hardie, M. J., Recent advances in the chemistry of cyclotriveratrylene. *Chemical Society Reviews* **2010,** 39, 516-527.

3. Robinson, G. M., Reaction of Homopiperonyl and Homoveratryl Alcohols. *J. Chem. Soc.* **1915,** 107, 267-276.

4. Holman, K. T.; Halihan, M. M.; Steed, J. W.; Jurisson, S. S.; Atwood, J. L., Hosting a Radioactive Guest: Binding of $^{99}TcO_4^-$ by a Metalated Cyclotriveratrylene. *J. Am. Chem. Soc.* **1995,** 117, 7848-7849.

5. Steed, J. W.; Zhang, H.; Atwood, J. L., Inclusion Chemistry of Cyclotriveratrylene and Cyclotricatechylene. *Supramolecular Chemistry* **1996,** 7, 37-45.

6. Westcott, A.; Sumby, C. J.; Walshaw, R. D.; Hardie, M., Metallo-Gels and Organo-Gels with Tripodal Cyclotriveratrylene-Type and 1,3,5-Substituted Benzene-Type Ligands. *New J. Chem.* **2009,** 33, 902-912.

7. Houseman, B. T.; Mrksich, M., Carbohydrate Arrays for the Evolution of Protein Binding and Enzymatic Modification. *Chem. Biol.* **2002,** 9, 443-454.

8. Mrksich, M., What can surface chemistry do for cell biology? *Curr. Opin. Chem. Biol.* **2002,** 6, 794-797.

9. Hooper, L.; Gordon, J., Glycans As Legislators of Host–Microbial Interactions: Spanning the Spectrum From Symbiosis to Pathogenicity. *Glycobiol.* **2001,** 11, 1R-10R

10. Mammen, M.; Choi, S.-K.; Whitesides, G., Polyvalent Interactions in Biological Systems: Implications for Design and Use of Multivalent Ligands and Inhibitors. *Angew. Chem. Int. Ed. Engl.* **1998,** 37, 2754-2794.

11. Sperling, O.; Fuchs, A.; Lindhorst, T. K., Evaluation of the Carbohydrate Recognition Domain of the Bacterial Adhesion FimH: Design, Synthesis, and Binding Properties of Mannoside Ligands. *Org. Biomol. Chem.* **2006,** 4, 3913.

12. Karlsson, K., Microbial Recognition of Target-Cell Glycoconjugates. *Curr. Opin. Struct. Biol.* **1995,** 5, 622-635.

13. Imberty, A.; Chabre, Y.; Roy, R., Glycomimetics and Glycodendrimers as High Affinity Microbial Anti-adhesins. *Chem. Eur. J.* **2008,** 14, 7490.

14. Liang, P.-H.; Wu, C.-Y.; Greenberg, W.; Wong, C.-H., Glycan Arrays: Biological and Medical Applications. *Curr. Op. Chem. Biol.* **2008,** 12, 86–92.

15. Demerec, M., Origin of Bacterial Resistance to Antibiotics. *J. Bacteriol.* **1948,** 56, 63-74.

16. Dobrindt, U.; Agerer, F.; Michaelis, K.; Janka, A.; Buchrieser, C.; Samuelson, M.; Svanborg, C.; Gottschalk, G.; Karch, H.; Hacker, J., Analysis of Genome Plasticity in Pathogenic and Commensal *Escherichia coli* Isolates by Use of DNA Arrays. *J. Bacteriol.* **2003,** 185, 1831-1840.

17. Sokurenko, E. V.; Chesnokova, V.; Dykhuizen, D. E.; Ofek, I.; Wu, X. R.; Krogfelt, K. A.; Struve, C.; Schembri, M. A.; Hasty, D., Pathogenic adaptation of Escherichia coli by natural variation of the FimH adhesin. *Proc. Natl. Acad. Sci. USA* **1998,** 95, 8922–8926.

18. Sokurenko, E.; Chesnokova, V.; Doyle, R.; Hasty, D., Diversity of the *Escherichia coli* Type 1 Fimbrial Lectin. Differential Binding to Mannosides and Uroepithelial Cells. *J. Biol. Chem.* **1997,** 272, 17880–17886.

19. Klevens, R.; Edwards, J.; Richards, C., Estimating Healthcare-Associated Infections and Deaths In U.S. hospitals. *Public Health Rep* **2007,** 122, 160-166.

20. Love, J. C.; Estroff, L. A.; Kriebel, J. K.; Nuzzo, R. G.; Whitesides, G. M., Self-Assembled Monolayers of Thiolates on Metals as a Form of Nanotechnology. *Chem. Rev.* **2005,** 105, 1103-1169.

21. Korobov, M. V.; Mirakyan, A. L.; Avramneko, N. V.; Olofsson, G.; Smith, A. L.; Ruoff, R. S., Calorimetric Studies of Solvates of C_{60} and C_{70} with Aromatic Solvents. *J. Phys. Chem. B.* **1999,** 103, 1339-1346.

22. Wang, L.; Liu, B.; Liu, D.; Yao, M.; Hou, Y.; Yu, S.; Cui, T.; Li, D.; Zou, G.; Iwasiewicz, A.; Sundqvist, B., Synthesis of Thin, Rectangular C_{60} Nanorods Using *m*-Xylene as a Shape Controller. *Adv. Mater.* **2006,** 18, 1883-1888.

23. Geng, J.; Zhou, W.; Skelton, P.; Yue, W.; Kinloch, I. A.; Windle, A. H.; Johnson, B. F. G., Crystal Structure and Growth Mechanism of Unusually Long Fullerene (C_{60}) Nanowires. *J. Am. Chem. Soc.* **2008,** 130, 2527-2534.

24. El-Sayed, M. A., Some Interesting Properties of Metals Confined in Time and Nanometer Space of Different Shapes. *Acc. Chem. Res.* **2001,** 34, 257-330.

25. Ariga, K.; Hill, J. P.; Ji, Q., Layer-By-Layer Assembly As A Versatile Bottom-Up Nanofabrication Technique for Exploratory Research and Realistic Application. *Phys. Chem. Chem. Phys.* **2007,** 9, 2319-2340.

26. Shin, H. S.; Yoon, S. M.; Tang, Q.; Chon, B.; Joo, T.; Choi, H. C., Highly Selective Synthesis of C_{60} Disks on Graphite Substrate by a Vapor-Solid Process. *Angew. Chem. Int. Ed.* **2008,** 47, 693-696.

27. Liu, H.; Li, Y.; Jiang, L.; Luo, H.; Xiao, S.; Fang, H.; Li, H.; Zhu, D.; Yu, D.; Xu, J.; Xiang, B., Imaging As-Grown [60]Fullerene Nanotubes by Template Techniques. *J. Am. Chem. Soc.* **2002,** 124, 13370-13371.

28. Miyazawa, K.; Kuwasaki, Y.; Obayashi, A.; Kuwabara, M., C_{60} Nanowhiskers Formed by the Liquid-Liquid Interfacial Precipitation Method. *J. Mater. Res* **2002,** 17, 83-88.

29. Howell, S. W.; Inerowicz, H. D.; Regnier, F. E.; Reifenberger, R., Patterned Protein Microarrays for Bacterial Detection. *Langmuir* **2003,** 19, 436-439.

30. Inerowicz, H. D.; Howell, S.; Regnier, F. E.; Reifenberger, R., Multiprotein Immunoassay Arrays Fabricated by Microcontact Printing. *Langmuir* **2002,** 18, 5263-5268.

31. Premkumar, J. R.; Lev, O.; Marks, R. S.; Polyak, B.; Rosen, R.; Belkin, S., Antibody-Based Immobilization of Bioluminescent Bacterial Sensor Cells. *Talanta* **2001,** 55, 1029-1038.

32. Groves J. T.; Mahal, L. K.; Bertozzi C. R., Control of Cell Adhesion and Growth with Micropatterned Supported Lipid Membranes. *Langmuir* **2001,** 17, 5129-5133.

33. Rowan, B.; Wheeler, M. A.; Crooks, R. M., Patterning Bacteria within Hyperbranched Polymer Film Templates. *Langmuir* **2002,** 18, 9914-9917.

34. Razatos, A.; Ong, Y. L.; Boulay, F.; Elbert, D. L.; Hubbell, J. A.; Sharma, M. M.; Georgiou, G., Force Measurements between Bacteria and Poly(ethylene glycol)-Coated Surfaces. *Langmuir* **2000,** 16, 9155-9158.

35. Qian, X.; Metallo, S. J.; Choi, I. S.; Wu, H.; Liang, M. N.; Whitesides, G. M., Arrays of Self-Assembled Monolayers for studying Inhibition of Bacterial Adhesion. *Anal. Chem.* **2002,** 74, 1805-1810.

36. Chapman, R. G.; Ostuni, E.; Liang, M. N.; Meluleni, G.; Kim, E.; Yan, L.; Peir, G.; Warren, H. S.; Whitesides, G. M., Polymeric Thin Films that Resist the Adsorption of Proteins and the Adhesion of Bacteria. *Langmuir* **2001,** 17, 1225-1233.

37. Ostuni, E.; Chapman, R. G.; Holmlin, R. E.; Takayama, S.; Whitesides, G. M., A Survey of Structure-Property Relationships of Surfaces that Resist the Adsorption of Protein. *Langmuir* **2001,** 17, 5605-5620.

38. Razatos, A.; Ong, Y.-L.; Sharma, M. M.; Georgiou, G., Molecular Determinants of Bacterial Adhesion Monitored by Atomic Force Microscopy. *PNAS* **1998,** 95, 11059-11064.

39. Rozhok, S.; Piner, R. D.; Mirkin, C. A., Dip-Pen Lithography: What Controls Ink Transport? *J. Phys. Chem. B.* **2003,** 107, 751-757.

40. St. John, R. M.; Davis, R.; N., C.; Czajka, J.; Batt, C. A.; Craighead, H. G., Diffraction-Based Cell Detection Using a Microcontact Printed Antibody. *Anal. Chem.* **1998,** 70, 1108-1111.

41. Rosi, N. L.; Mirkin, C. A., Nanostructures in Biodiagnostics. *Chem. Rev.* **2005,** 105, 1547-1562.

42. Sarikaya, M.; Tamerler, C.; Schwartz, D. T.; Baneyx, F., Materials Assembly and Formation Using Engineered Polypeptides. *Ann. Rev. Mater. Res.* **2004,** 34, 373-408.

43. Medintz, I., Universal Tools for Biomolecular Attachment to Surfaces *Nat. Mater.* **2006,** 5, 842.

44. Mershin, A.; Cook, B.; Kaiser, L.; Zhang, S., A Classic Assembly of Nanobiomaterials. *Nat. Biotech.* **2005,** 23, 1379 - 1380.

45. Wilson, D. L.; Martin, R.; Hong, S.; Cronin-Golomb, M.; Mirkin, C. A.; Kaplan, D. L., Surface Organization and Nanopatterning of Collagen by Dip-Pen Nanolithography *PNAS* **2001,** 98, 13660-13664.

46. Ginger, D. S.; Zhang, H.; Mirkin, C. A., The Evolution of Dip-Pen Nanolithography. *Angew. Chem. Int. Ed.* **2004,** 43, 30 – 45.

47. Chovan T; Guttman, A., Microfabricated Devices in Biotechnology and Biochemical Processing. *Trends Biotechnol* **2002,** 20, 116-122.

48. Kikuchi, J.-I.; Murakami, Y., Steroid Cyclophanes as Artificial Cell-Surface Receptors. Molecular Recognition and it Consequence in Signal Transduction Behavior. *J. Incl. Phenom. Mol. Rec. Chem.* **1998,** 32, 209-221.

49. Michaud, F.; Barrio, M.; López, D. O.; Tamarit, J. L.; Agafonov, S. T.; Szwarc, H.; Céolin, R., Solid-State Studies on a C_{60} Solvate Grown from 1,1,2-Trichloroethane. *Chem. Mater.* **2000,** 12, 3595-3602.

50. Rozhok, S.; Clifton, K. F.; Shen, F.; Littler, P. H.; Fan, Z.; Liu, C.; Mirkin, C. A.; Holz, R. C., Methods for Fabricating Microarrays of Motile Bacteria. *Small* **2005,** 1, 445-451.

51. Rozhok, S.; Clifton K. F.; Shen, F.; Littler, P. L.; Fan, Z.; Liu, C.; Mirkin, C. A.; Holz, R. C., Methods for Fabricating Microarrays of Motile Bacteria. *Small* **2005,** 1, 445-451.

52. Verschoor, J. A.; Meiring, M. J.; Van Wyngraardt, S.; Weyer, K., Polystyrene, Poly-Lysine, and Nylon As Absorptive Surfaces for the Binding of Whole Cells of *Mycobacterium terburculosis* H37 RV to ELISA Plates. *J. Immunoassay* **1990,** 11, 413-28.

53. Eisenbach, M.; Wolf, A.; Welch, M.; Caplin, S. R.; Lapidus, I. R.; Macnab, R. M.; Aloni, H.; Asher, O., Pausing, Switching, and Speed Flucuation of the Bacterial Flagellar Motor and Their Relation to Motillity and Chemotaxis. *J. Mol. Bio.* **1990,** 211, 551-563.

54. Berg, H. C., Constraints On Models for the Flagellar Rotary Motor. *Philos. Trans. R. Soc. London, Ser. B.* **2000,** 355, 491-501.

55. Liang, M. N.; Smith, S. P.; Metallo, S. J.; Choi, I. S.; Prentiss, M.; Whitesides, G. M., *Proc. Natl. Acad. Sci. USA* **2000,** 97, 13092-13096.

56. Rozhok, S.; Holz, R. C., Electrochemical Adhesion of Motile Bacteria to Gold. *Talanta* **2005,** 67, 538-542.

57. Abu-Lail, N. I.; Camesano, T. A., Specific and Nonspecific Interaction Forces Between *Eschericia coli* and Silicon Nitride, Determined by Poisson Statistical Analysis. *Langmuir* **2006,** 22, 7296-7301.

58. Piner, R. D.; Zhu, J.; Xu, F.; Hong, S.; Mirkin, C. A., "Dip-Pen" Nanolithography. *Science* **1999,** 283, 661-663.

59. Ginger, D. S.; Zhang, H.; Mirkin, C. A., The Evolution of Dip-Pen Nanolithography. *Angew. Chem. Int. Ed.* **2004,** 43.

60. Bellido, E.; de Miguel, R.; Ruiz-Molina, D.; Lostao, A.; Maspoch, D., Controlling the Number of Proteins with Dip-Pen Nanolithography. *Adv. Mater.* **2010,** 22, 352-355.

61. Vega, R. A.; Maspoch, D.; Salaita, K.; Mirkin, C. A., Nanoarrays of Single Virus Particles. *Angew. Chem. Int. Ed.* **2005,** 44, 6013-6015.

62. Demers, L. M.; Ginger, D. S.; Park, S.-J.; Li, Z.; Chung, S.-W.; Mirkin, C. A., Direct Patterning of Modified Oligonucleotides on Metals and Insulators via Dip-Pen Nanolithography. *Science* **2002,** 296, 1836-1838.

63. Rozhok, S.; Fan, Z.; Nyamjav, D.; Liu, C.; Mirkin, C. A.; Holz, R. C., Attachment of Motile Bacterial Cells to Prealigned Holed Microarrays. *Langmuir* **2006,** 22, 11251-11254.

64. Walter, N.; Selhuber, C.; Kessler, H.; Spatz, J. P., Cellular Unbinding Forces of Initial Adhesion Processes on Nanopatterned Surface Probed with Magnetic Tweezers. *Nano Lett.* **2006,** 6, 398-402.

65. Wang, W. M.; LeMieux, M. C.; Selvarasah, S.; Dokmeci, M. R.; Bao, Z., Dip-Pen Nanolithography of Electrical Contacts to Single-Walled Carbon Nanotubes. *ACSNano* **2009,** 3, 3543-3551.

66. Turkevitch, J.; Stevenson, P. C.; Hillier, J., A Study of the Nucleation and Growth Process in the Synthesis of Colloidal Gold. *Discuss. Faraday Soc.* **1951,** 11, 55-75.

67. Frens, G., Controlled Nucleation for the Regulation of the Particle Size in Monodisperse Gold Suspensions. *Nature: Phys. Sci.* **1973,** 241, 20-22.

68. Brust, M.; Walker, M.; Bethell, D.; Schiffrin, D. J.; Whyman, R., Synthesis of Thiol-derivatised Gold Nanoparticles in a Two-phase Liquid-Liquid System. *J. Chem. Soc., Chem. Commun.* **1994**, 801-802.

69. Brust, M.; Fink, J.; Bethell, D.; Schiffrin, D. J.; Kiely. C. J., Synthesis and Reactions of Functionalised Gold Nanoparticles. *J. Chem. Soc., Chem. Commun.* **1995**, 1655-1656.

70. Ghosh, P.; Han, G.; De, M.; Kim, C. K.; Rotello, V. M., Gold Nanoparticles in Delivery Applications. *Advanced Drug Delivery Reviews* **2008,** 60, 1307-1315.

71. Lee, J.-S.; Han, M. S.; Mirkin C. A., Colorimetric Detection of Mercuric Ion (Hg^{2+}) in Aqueous Media using DNA-Functionalized Gold Nanoaprticles. *Angew. Chem. Int. Ed.* **2007,** 46, 4093-4096.

72. Adams, E. W.; Ratner, D. M.; Bokesch, H. R.; McMahon, J. B.; O'Keefe, B. R.; Seeberger, P. H., Oligosaccharide and Glycoprotein Microarrays as Tools in HIV Glycobiology: Glycan-Dependent gp120/Protein Interactions. *Chem. Biol.* **2004,** 11, 875-881.

73. Seo, J. H.; Kim, C. S.; Hwang, B. H.; Cha, H. J., A Functional Carbohydrate Chip Platform for Analysis of Carbohydrate-Protein Interaction. *Nanotechnology* **2010,** 21, 215101-215109.

74. Zhi, Z.-L.; Laurent, N.; Powell, A. K.; Karamanska, R.; Fais, M.; Voglmeir, J.; Wright, A.; Blackburn, J. M.; Crocker, P. R.; Russell, D. A.; Flitsch, S.; Field, R. A.; Turnbull, J. E., A Versatile Gold Surface Approach for Fabrication and Interrogation of Glycoarrays. *ChemBioChem* **2008,** 9, 1568-1575.

75. Ahmad, R.; Hardie, M. J. Building Cyclotriveratrylene Host Molecules into Network Structures. *Cryst. Eng. Comm.* **2002,** 42, 227-231.

76. Sperling, O.; Fuchs, A.; Lindgorst, T. K. , Evaluation of the Carbohydrate Recognition Domain of the Bacterial Adhesion FimH: Design, Synthesis, and Binding Properties of Mannoside Ligands. *Org. Biomol. Chem.* **2006,** 4.

77. Karlsson, K., Microbial Recognition of Target-Cell Glycoconjugates. *Curr. Opin. Struct. Biol.* **1995,** 5, 622-635.

78. Imberty, A.; Chabre, Y. M.; Roy, R. , Glycomimetics and Glycodendrimers as High Affinity Microbial Anti-Adhesins. *Chem. Eur. J.* **2008,** 14.

79. Liang, P. H.; Wu, C. Y.; Greenberg, W.; Wong, C. H., Glycan Arrays: Biological and Medical Applications. *Curr. Opin. Chem. Biol.* **2008,** 12, 86-92.

80. Gentry, T.; Wickham, G.; Schadt, C.; He, Z.; Zhou, J., Microarray Applications in Microbial Ecology Research. *Microb. Ecol.* **2006,** 52, 159-175.

81. Feizi, T.; Fazio, F.; Chai, W.; Wong, C.-H., Carbohydrate Microarrays-A New Set of Technologies at the Frontiers of Glycomics. *Cur. Opin. Chem. Biol.* **2003,** 13, 637-645.

82. Disney, M.; Seeberger, P., The Use of Carbohydrate Microarrays to Study Carbohydrate-Cell Interactions and to Detect Pathogens. *Chem. Biol.* **2004,** 11, 1701-1707.

83. Walz, A.; Odenbreit, S.; Mahdavi, J.; Borén, T.; Ruhl, S., Identification and Characterization of Binding Properties of *Helicobacter pylori* by Glycoconjugate Arrays. *Glycobiology* **2005,** 15, 700–708.

84. Graeter, S. V.; Huang, J.; Perschmann, N.; López-García, M.; Kessler, H.; Ding, J.; Spatz, J. P., Mimicking Cellular Environments by Nanostructured Soft Interfaces. *Nano Lett.* **2007,** 7, 1413-1418.

85. Raghavan, S.; Desai, R. A.; Kwon, Y.; Mrksich, M.; Chen, C. S., Micropatterned Dynamically Adhesive Substrates for Cell Migration. *Langmuir* **2010,** 26, 17733-17738.

86. Deeg, J. A.; Louban, I.; Aydin, Daniel; Selhuber-Unkel; Christine; Kessler, Horst; Spatz, Joachim P., Impact of Local versus Global Ligand Density on Cellular Adhesion. *Nano Lett.* **2011,** 11, 1469-1476.

87. Eisenberg, J. L.; Piper, J. L.; Mrksich, M., Using Self-Assembled Monolyaers to Model Cell Adhesion to the 9th and 10th Type III Domains of Fibronectin. *Langmuir* **2009,** 25, 13942-13951.

88. Fritz, M. C.; Hähner, G.; Spencer, N. D., Self-Assembled Hexasaccharides: Surface Characterization of Thiol-Terminated Sugars Adsorbed on a Gold Surface. *Langmuir* **1996,** 12, 6074-6082.

89. Revell, D. J.; Knight, J. R.; Blyth, D. J.; Haines, A. H.; Russell, D. A., Self-Assembled Carbohydrate Monolayers: Formation and Surface Selective Molecular Recognition. *Langmuir* **1998,** 14, 4517-4524.

90. Nimrichter, L.; Gargir, A.; Gortler, M.; Altstock, R. T.; Shtevi, A.; Weisshaus, O.; Fire, E.; Dotan, N.; Schnaar, R. L., Intact Cell Adhesion to Glycan Microarrays. *Glycobiology* **2004,** 14, 197-203.

91. Seo, J. H.; Adachi, K.; Lee, B. K.; Kang, D. G.; Kim, Y. K.; Kim, K. R.; Lee, H. Y.; Kawai, T.; Cha, H. J., Facile and Rapid Direct Gold Surface Immobilization with Controlled Orientation for Carbohydrates. *Bioconjugate Chem.* **2007,** 18, 2197-2201.

92. Disney, M. D.; Seeberger, P. H., The Use of Carbohydrate Microarrays to Study Carbohydrate-Cell Interactions and to Detect Pathogens. *Chem. Biol.* **2004,** 11, 1701-1707.

93. Ban, L.; Mrksich, M., On-Chip Synthesis and Label-Free Assays of Oligosaccharide Arrays. *Angew. Chem. Int. Ed.* **2008,** 47.

94. Hatch, D. M.; Weiss, A. A.; Kale, R. R.; Iyer, S. S., Biotinylated Bi- and Tetra-antennary Glycoconjugates for *Escherichia coli* Detection. *ChemBioChem* **2008,** 9, 2433-2442.

95. Lin, C. C.; Yeh, Y. C.; Yang, C. Y.; Chen, C. L.; Chen, G. F.; Chen, C. C.; Wu, Y. C., Selective Binding of Mannose-Encapsulated Gold Nanoparticles to Type 1 Pili in *Escherichia coli*. *J. Am. Chem. Soc.* **2002,** 124, 3508-3509.

96. Chen, Y. J.; Chen, S. H.; Chien, Y. Y.; Chang, Y. W.; Liao, H. K.; Chang, C. Y.; Jan, M. D.; Wang, K. T.; Lin, C. C., Carbohydrate-Encapsulated Gold Nanoparticles for Rapid Target-Protein Indentification and Binding-Epitope Mapping. *ChemBioChem* **2005,** 6, 1169-1173.

97. Robinson, A.; Fang, J. M.; Chou, P. T.; Liao, K. W.; Chu, R. M.; Lee, S. J., Probing Lectin and Sperm with Carbohydrate-Modified Quantum Dots. *ChemBioChem* **2005,** 6, 1899-1905.

98. De Paz, J.; Seeberger, P., Recent Advances in Carbohydrate Microarrays. *QSAR Comb. Sci.* **2006,** 25, 1027 – 1032.

99. Yonzon, C. R.; Jeoung, E.; Zou, S.; Schatz, G. C.; Mrksich, M.; Van Duyne, R. P., A Comparative Analysis of Localized and Propagating Surface Plasmon Resonance

Sensors: The Binding of Concanavalin A to a Monosaccharide Functionalized Self-Assembled Monolayer *J. Am. Chem. Soc.* **2004,** 126, 12669-12676.

100. Rodríguez-Pérez, T.; Lavandera, I.; Fernández, S.; Sanghvi, Y. S.; Ferrero, M.; Gotor, V., Novel and Efficient Chemoenzymatic Synthesis of D-Glucose 6-Phosphate and Molecular Modeling Studies on Selective Biocatalysis. *Eur. J. Inorg. Chem.* **2007,** 2007, 2769-2778.

101. Tiwari, P.; Kumar, R.; Maulik, P. R.; Misra, A. K., Efficient Acetylation of Carbohydrates Promoted by Imidazole *Eur. J. Inorg. Chem.* **2005,** 2005, 4265-4270.

102. Dorokhin, D.; Hsu, S. H.; Tomczak, N.; Reinhoudt, D. N.; Huskens, J.; Velders, A. H.; Vancso, G. J., Fabrication and Luminescence of Designer Surface Patterns with β-Cyclodextrin Functionalized Quantum Dots *via* Multivalent Supramolecular Coupling. *ACSNano* **2010,** 4, 137-142.

103. Limousin, C.; Oleskar, A.; Cleophax, J.; Petit, A.; Loupy, A.; Lukacs, G., Halogenation of Carbohydrates by Triphenylphosphine Complex Reagents in Highly Concentrated Solution Under Microwave Activation or Conventional Heating. *Carbohydrate Research* **1998,** 312, 23-31.

104. Chuang, C. L.; dos. Santos, O.; Xu, X.; Canary, J. W., Synthesis and Cyclic Voltammetry Studies of Copper Complexes of Bromo- and Alkoxyphenyl-Substituted Derivatives of Tris(2-pyridylmethyl)amine: Influence of Cation-Alkoxy Interactions on Copper Redox Potentials. *Inorg. Chem.* **1997,** 36, 1967-1972.

105. Odom, T. W.; Love, J. C.; Wolfe, D. B.; Paul, K. E.; Whitesides, G. M., Improved Pattern Transfer in Soft Lithography Using Composite Stamps *Langmuir* **2002,** 18, 5314-5320.

106. Bonifazi, D.; Enger, O.; Diederich, F., Supramolecular [60]Fullerene Chemistry on Surfaces. *Chem. Soc. Rev.* **2007,** 36, 390-414.

107. Deguise, I.; Lagnoux, D.; Roy, R., Synthesis of Glycodendrimers Containing Both Fucoside and Galactoside Residues and Their Binding Properties to PA-IL and PA-IIL Lectins from *Pseudomonas aeruginosa*. *New J. Chem.* **2007,** 31, 1321-1331.

108. Hyatt, J. A.; Tindall, G. W., The Intermediacy of Sulfate Esters in Sulfuric Acid Catalyzed Acetylation of Carbohydrates. *Heterocycles* **1993,** 35, 227-234.

109. Steinmann, A.; Thimm, J.; Thiem, J., First Direct Glycosylation of Unprotected Nonreducing Mono- and Disaccharides. *Eur. J. Inorg. Chem.* **2007,** 2007, 5506-5513.

110. Lin, C. C.; Yeh, Y. C.; Yang, C. Y.; Chen, G. F.; Chen, Y. C.; Wu, Y. C.; Chen, C. C., Quantitative Analysis of Multivalent Interactions of Carbohydrate-Encapsulated Gold Nanoparticles with Concanavalin A. *Chem. Commun.* **2003**, 2920-2921.

111. Giguère, D.; Sato, S.; St-Pierre, C.; Sirois, S.; Roy, R., Aryl *O*- and *S*-galactosides and Lactosides as Specific Inhibitors of Human Galectins-1 and -3: Role of Elecrostatic Potential at O-3. *Bioorg. Med. Chem. Lett.* **2006,** 16, 1668-1672.

112. Kubo, S.; Diaz, A.; Tang, Y.; Mayer, T. S.; Khoo, I. C.; Mallouk, T. E., Tunability of the Refractive Index of Gold Nanoparticle Disersions. *Nano Lett.* **2007,** 7, 3418-3423.

113. Turnbull, W. B.; Harrison, J. A.; Kartha, K. P. R.; Schenman, S.; Field, R. A., Observations on Chemical and Enzymatic Approaches to α-2,3-Sialylated Octyl β-Lactoside. *Tetrahedron* **2002,** 58, 3207-3216.

114. Hanessian, S.; Banoub, J., Chemistry of the Glycosidic Linkage. An Efficient Synthesis of 1,2-*trans*-Saccharides. *Carbohydr. Res.* **1977,** 53, C13-C16.

115. Schmidt, R. R., Recent Developments in the Synthesis of Glycoconjugates. *Pure & Appl. Chem.* **1989,** 61, 1257-1270.

116. Schmidt, R. R.; Kinzy, W., Anomeric-Oxygen Activation for Glycoside Synthesis: The Trichloroacetimidate Method. *Adv. Carbohydr. Chem. Biochem.* **1994,** 50, 21-123.

117. Urban, F. J.; Moore, B. S.; Breitenbach, R., Synthesis of Tigogenyl β-O-Cellobioside Heptaacetate and Glycoside Tetraacetate via Schmidt's Trichloroacetimidate Method; Some New Observations. *Tetrahedron Lett.* **1990,** 31, 4421-4424.

118. Sinnott, M. L., *Carbohydrate Chemistry and Biochemistry*. RSC Publishing: Cambridge, UK, 2007.

119. Mateo-Alonso, A.; Guldi, D. M.; Paolucci, F.; Prato, M., Fullerenes: Multitask Components in Molecular Machinery. *Angew. Chem. Int. Ed.* **2007,** 46, 8120-8126.

120. Schwendel, D.; Hayashi, T.; Dahint, R.; Pertsin, A.; Grunze, M.; Steitz, R.; Schreiber, F., Interaction of Water with Self-Assembled Monolayers; Neutron Reflectivity Measurements of the Water Density in the Interface Region. *Langmuir* **2003,** 19, 2284-2293.

121. Mateo-Alonso, A.; Guldi, D. M.; Paolucci, F.; Prato, M., Fullerenes: Multitask Components in Molecular Machinery. *Angewandte Chemie International Edition* **2007,** 46, 8120-8126.

122. Shirai, Y.; Guerrero, J. M.; Sasaki, T.; He, T.; Ding, H.; Vives, G.; Yu, B.; Cheng, L.; Flatt, A. K.; Taylor, P.; Gao, Y.; Tour, J. M. , Fullerene/Thiol-Terminated Molecules. *J. Org. Chem.* **2009,** 74.

123. Bonifazi, D.; Enger, O.; Diederich, F., Supramolecular [60]Fullerene Chemistry on Surfaces. *Chemical Society Reviews* **2007,** 36, 390-414.

124. Song, J.; Aratani, N.; Shinokubo, H.; Osuka, A., A Porphyrin Nanobarrel That Encapsulates C60. *Journal of the American Chemical Society* **2010,** 132, 16356-16357.

125. Saha, S. J., E.; Flood, A. H.; Tseng, H.; Zink, J. I.; Stoddart, J. F. , A Photoactive Molecular Triad as a Nanoscale Power Supply for a Supramolecular Machine. *Chem. Eur. J.* **2005,** 11.

126. Chen, W.; Zhang, H.; Huang, H.; Chen, L.; Wee, A. T. S., Orientationally Ordered C60 on p-Sexiphenyl Nanostripes on Ag(111). *ACS Nano* **2008,** 2, 693-698.

127. Sedona, F.; Di Marino, M.; Sambi, M.; Carofiglio, T.; Lubian, E.; Casarin, M.; Tondello, E., Fullerene/Porphyrin Multicomponent Nanostructures on Ag(110): From Supramolecular Self-Assembly to Extended Copolymers. *ACS Nano* **2010,** 4, 5147-5154.

128. Tait, S. L., Function Follows Form: Exploring Two-Dimensional Supramolecular Assembly at Surfaces. *ACS Nano* **2008,** 2, 617-621.

129. Zhao, J.; Feng, M.; Yang, J.; Petek, H., The Superatom States of Fullerenes and Their Hybridization into the Nearly Free Electron Bands of Fullerites. *ACS Nano* **2009,** 3, 853-864.

130. Zhong, D.; Wedeking, K.; Blömker, T.; Erker, G.; Fuchs, H.; Chi, L., Multilevel Supramolecular Architectures Self-Assembled on Metal Surfaces. *ACS Nano* **2010,** 4, 1997-2002.

131. Marois, J. S.; Morin, J. F., Synthesis and Surface Self-Assembly of [3]Rotaxane-Porphyrin Conjugates: Toward the Development of a Supramolecular Surface Tweezer for C_{60}. *Langmuir* **2008,** 24, 10865-10873.

132. Beer, P. D.; Gale, P. A.; Smith, D. K. , *Supramolecular Chemistry*. Oxford University Press: Oxford, England, 1999.

133. Huerta, E.; Isla, H.; Perez, E. M.; Bo, C.; Martin, N.; de Mendoza, J., Tripodal exTTF-CTV Hosts for Fullerenes. *Journal of the American Chemical Society* **2010,** 132, 5351-5353.

134. Carruthers, C.; Fisher, J.; Harding, L. P.; Hardie, M. J., Host-Guest Influence on Metallo-Supramolecular Assemblies with a Cyclotriveratrylene-Type Ligand. *Dalton Transactions* **2010,** 39, 355-357.

135. Steed, J. W.; Junk, P. C.; Atwood, J. L.; Barnes, M. J.; Raston, C. L.; Burkhalter, R. S, Ball and Socket Nanostructures: New Supramolecular Chemistry Based on Cyclotriveratrylene. *J. Am. Chem. Soc.* **1994,** 116, 10346-10347.

136. Zhang, S.; Palkar, A.; Fragoso, A.; Prados, P.; de Mendoza, J.; Echegoyen, L., Noncovalent Immobilization of C60 on Gold Surfaces by SAMs of Cyclotriveratrylene Derivatives. *Chem. Mater.* **2005,** 17, 2063-2068.

137. Zhang, S.; Echegoyen, L. , Supramolecular Immobilization of Fullerenes on Gold Surfaces: Receptors Based on Calix[n]Arenes, Cyclotriveratrylene (CTV) and Porphyrins. *Comptes Rendus Chimie* **2006,** 9.

138. Nierengarten, J. F.; Oswald, L.; Eckert, J.; Nicoud, J.; Armaroli, N. , Complexation of Fullerenes with Dendritic Cyclotriveratrylene Derivatives. *Tetrahedron Lett.* **1999,** 40.

139. Nierengarten, J., Supramolecular Encapsulation of [60]Fullerene with Dendritic Cyclotriveratrylene Derivatives. *Fullerenes, Nanotubes, and Carbon Nanostructures* **2005,** 13.

140. Salaita, K.; Wang, Y. H.; Fragala, J.; Vega, R. A.; Liu, C.; Mirkin, C. A., Massively parallel dip-pen nanolithography with 55000-pen two-dimensional arrays. *Angewandte Chemie-International Edition* **2006,** 45, 7220-7223.

141. Lutz Jr., M. R.; Frecnh, D. C.; Rehage, P.; Becker, D. P. , Isolation of the Saddle and Crown Conformers of Cyclotriveratrylene (CTV) Oxime. *Tetrahedron Lett.* **2007,** 48.

142. Jang, J.; Hong, S.; Schatz, G. C.; Ratner, M. A., Self-Assembly of Ink Molecules in Dip-Pen Nanolithography: A Diffusion Model. *J. Chem. Phys.* **2001,** 115, 2711.

143. Nyamjav, D.; Holz, R. C., Direct Patterning of Silanized-Biomolecules on Semiconductor Surfaces. *Langmuir* **2010**, 26, 18300-18302.

144. Jung, H.; Dalal, C. K.; Kuntz, S.; Shah, R.; Collier, C. P., Surfactant Activated Dip-Pen Nanolithography. *Nano Lett.* **2004,** 4, 2171-2177.

145. Barczewski, M.; Walheim, S.; Heiler, T.; Błaszczyk, A.; Mayor, M.; Schimmel, T., High Aspect Ratio Constructive Nanolithography with a Photo-Dimerizable Molecule. *Langmuir* **2009,** 26, 3623-3628.

146. French, D. C.; Lutz, M. R., Jr.; Lu, C.; Zeller, M.; Becker, D. P. , A Thermodynamic and Kinetic Characterization of the Solvent Dependence of the Saddle-Crown Equilibrium of Cyclotriveratrylene Oxime. *J. Phys. Chem. A* **2009,** 113.

147. Zhang, S.; Echegoyen, L. , Supramolecular Incorporation of Fullerenes on Gold Surfaces: Comparison of C60 Incorporation by Self-Assembled Monolayers of Different Calix[n]Arenes (n = 4, 6, 8) Derivatives. *J. Org. Chem.* **2005,** 70.

148. Hardie, M. J.; Raston, C. L., Solid State Supramolecular Assemblies of Charged Supermolecules (Na[2.2.2]cryptate)$^{+}$ and Anionic Carboranes with Host Cyclotriveratrylene. *Chem. Commun.* **2001**, 905-906.

149. Atwood, J. L.; Barnes, M. J.; Gardiner, M. G.; Raston, C. L., Cyclotriveratrylene Polarisation Assisted Aggregation of C_{60}. *Chem. Commun.* **1996**, 1449-1450.

150. Blanch, R. J.; Williams, M.; Fallon, G. D.; Gardiner, M. G.; Kaddour, R.; Raston, C. L., Supramolecular Complexation of 1,2-Dicarbadodeccarborane(12). *Angew. Chem. Int. Ed.* **1997,** 36, 504-506.

151. Hardie, M. J.; Raston, C. L.; Wells, B., Altering the Inclusion Properties of CTV through Crystal Engineering: CTV, Carborane, and DMF Supramolecular Assemblies. *Chem. Eur. J.* **2000,** 6, 3293-3298.

152. Holman, K. T.; Atwood, J. L.; Steed, J. W., Intra-Cavity Inclusion of $[CpFe^{II}(arene)]^{+}$ Guests by Cyclotriveratrylene *Angew. Chem. Int. Ed.* **1997,** 36, 1736-1738.

153. Collet, A.; Dutasta, J.P.; Vériot, G.; Matouzenko, G., Synthesis of C_3-Cyclotriveratrylene Ligands for Iron(II) and Iron(III) Coordination. *Tetrahedron* **1995,** 51, 389-400.

154. Hardie, M. J.; Raston, C. L., Alkali-Metal-Cyclotriveratrylene Coordination Polymers: Inclusion of Neutral $C_2B_{10}H_{12}$ or Anionic $[CB_{11}H_{12}]^{-}$ and DMF. *Crystal Growth & Design* **2001,** 1, 53-58.

155. Salaita, K.; Wang, Y.; Mirkin, C. A., Applications of Dip-Pen Nanolithography. *Nature Nanotech.* **2007,** 2, 145-155.

156. Ahmad, R.; Dix, I.; Hardie, M., Hydrogen-Bonded Superstructures of a Small Host Molecule and Lanthanide Aquo Ions. *Inorg. Chem.* **2003,** 42, 2182-2184.

157. Lim, S. Y.; Kim, J. H.; Lee, J. S.; Park, C. B., Gold Nanoparticle Enlargement Coupled with Fluorescence Quenching for Highly Sensitive Detection of Analytes. *Langmuir* **2009,** 25, 13302-13305.

158. Huang, C. C.; Chiang, C. K.; Lin, Z. H.; Lee, K. H.; Chang, H. T., Bioconjugated Gold Nanodots and Nanoparticles for Protein Arrays Based on Photoluminescence Quenching *Anal. Chem.* **2008,** 80, 1497-1504.

159. Myroshnychenko, V.; Rodríguez-Fernández, J.; Pastoriza-Santos, I.; Funston, A. M.; Novo, C.; Mulvaney, P.; Liz-Marzán, L. M.; García de Abajo, F. Javier, Modelling the Optical Response of Gold Nanoparticles. *Chem. Soc. Rev.* **2008,** 37, 1792-1805.

160. Gosh, S. K.; Pal, T., Interparticle Couping Effects on the Surface Plasmon Resonance of Gold Nanoparticles: From Theory to Applications. *Chem. Rev.* **2007,** 107, 4797-4862.

161. Grzelczak, M.; Vermant, J.; Furst, E. M.; Liz-Marzan, L. M., Directed Self-Assembly of Nanoparticles. *ACSNano* **2010,** 4, 3591-3605.

162. Lee, J. S.; Han, M. S.; Mirkin, C. A., Colorimetric Detection of Mercuric Ion (Hg^{2+}) in Aqueous Media using DNA-Functionalized Gold Nanoparticles. *Angew. Chem. Int. Ed.* **2007,** 46, 4093-4096.

163. Lee, J. S.; Ulmann, P. A.; Han, M. S.; Mirkin, C. A., A DNA-Gold Nanoparticle-Based Colorimetric Competition Assay for the Detection of Cysteine. *Nano Lett.* **2008,** 8, 529-533.

164. Liu, R.; Liew, R.; Zhou, J.; Xing, Bengang, A Simple and Specific Assay for Real-Time Colorimetric Visualization of β-Lactamase Activity by Using Gold-Nanoparticles. *Angew. Chem. Int. Ed.* **2007,** 46, 8799-8803.

165. Medley, C. D.; Smith, J. E.; Tang, Z.; Wu, Y.; Bamrungsap, S.; Tan, W., Gold Nanoparticle-Based Colorimetric Assay for the Direct Detection of Cancerous Cells. *Anal. Chem.* **2008,** 80, 1067-1072.

166. Kim, S. K.; Kim, S.; Hong, E. J.; Han, M. S., Alkyl Phosphate Functionalized Gold Nanoparticles-Based Colorimetric Probe for Pb^{2+} Ions. *Bull. Korean Chem. Soc.* **2010,** 31, 3806-3808.

167. Velu, R.; Ramakrishnan, V. T.; Ramamurthy, P., Colorimetric and Fluorometric Chemosensors for Selective Signaling Toward Ca^{2+} and Mg^{2+} by Aza-Crown Ether

Acridinedione-Functionalized Gold Nanoparticles. *Tetrahedron Lett.* **2010,** 51, 4331-4335.

168. Hung, Y. L.; Hsiunng, T. M.; Chen, Y. Y.; Huang, Y. F.; Huang, C. C., Colorimetric Detection of Heavy Metal Ions Using Label-Free Gold Nanoparticles and Alkanethiols. *J. Phys. Chem. C* **2010,** 114, 16329-16334.

169. Kim, Y.; Johnson, R. C.; Hupp, J. T., Gold Nanoparticle-Based Sensing of "Spectroscopically Silent" Heavy Metal Ions. *Nano Lett.* **2001,** 1, 165-167.

170. Hardie, M. J.; Raston, C. L.; Wells, B., Altering the Inclusion Properties of CTV Through Crystal Engineering: CTV, Carborane, and DMF Supramolecular Assemblies. *Chem. Eur. J.* **2000,** 6, 3293-3298.

171. Osner, Z. R.; Nyamjav, D.; Holz, R. C.; Becker, D. P., Direct Patterning of a Cyclotriveratrylene (CTV) Derivative for Directed Self-Assembly of C_{60}. *Nanotechnology* **2011,** 22, 275611-275618.

172. Ghosh, S. K.; Nath, S.; Kundu, S.; Esumi, K.; Pal, T., Solvent and Ligand Effects on the Localized Surface Plasmon Resonance (LSPR) of Gold Colloids. *J. Phys. Chem. B* **2004,** 108, 13963-12971.

173. Winzor, D. J.; Sawyer, W. H., *Quantitative Characterization of Ligand Binding*. Wiley-Liss: New York, 1995.

174. Dujols, V.; Ford, F.; Czarnik, A. W., A Long-Wavelength Fluorescent Chemodosimeter Selective for Cu(II) Ion in Water. *J. Am. Chem. Soc.* **1997,** 119, 7386-7387.

175. Reynal, A.; Etxebarria, J.; Nieto, N.; Serres, S.; Palomares, E.; Vidal-Ferran, A., A Bipyridine-Based "Naked-Eye" Fluorimetric Cu^{2+} Chemosensor. *Eur. J. Inorg. Chem.* **2010**, 1360-1365.

176. Huang, J.; Xu, Y., Qian, X., A Colorimetric Sensor for Cu^{2+} in Aqueous Solution Based on Metal Ion-Induced Deprotonation: Deprotonation/Protonation Mediated by Cu^{2+}-Ligand Interactions. *Dalton Trans.* **2008**, 1761-1766.

177. Arunkumar, E.; Chithra, P.; Ajayaghosh, A., A Controlled Supramolecular Approach toward Cation-Specific Chemosensors: Alkaline Earth Metal Ion-Driven Exciton Signaling in Squaraine Tethered Podands. *J. Am. Chem. Soc.* **2004,** 126, 6590-6598.

178. Cao, Y. D.; Zheng, Q. Y.; Chen, C. F.; Huang, Z. T., A New Fluorescent Chemosensor for Transition Metal Cations and On/Off Molecular Switch Controlled by pH. *Tetrahedron Letters* **2003,** 44, 4751-4755.

179. Cheng, Y. F.; Zhao, D. T.; Zhang, M.; Liu, Z. Q. ; Zhou, Y. F.; Shu, T. M.; Li, F. Y.; Yi, T.; Huang, C. H., Azo 8-hydroxyquinoline benzoate as selective chromogenic chemosensor for Hg^{2+} and Cu^{2+}. *Tetrahedron Letters* **2006,** 47, 6413-6416.

180. Xia, W. S.; Schmehl, R. H.; Li, C. J.; Mague, J. T.; Luo, C. P.; Guldi, D. M., Chemosensors for Lead(II) and Alkali Metal Ions Based on Self-Assembling Fluorescence Enhancement (SAFE). *J. Phys. Chem. B* **2002,** 106, 833-843.

181. Lin, W.; Cao, X.; Ding, Y.; Yuan, L.; Yu, Q., A Reversible Fluorescent Hg^{2+} Chemosensor Based on a Receptor Composed of a Thiol Atom and an Alkene Moiety for Living Cell Fluoresence Imaging. *Org. Biomol. Chem.* **2010,** 8, 3618-3620.

182. Rodriguez-Morgade, M. S.; Planells, M.; Torres, T.; Ballester, P.; Palomares, E., A Colorimetric Molecular Probe for Cu(II) Ions Based on the Redox Properties of Ru(II) Phthalocyanines. *J. Mater. Chem.* **2008,** 18, 176-181.

183. Frigoli, M.; Ouadahi, K.; Larpent, C., A Cascade FRET-Mediated Ratiometric Sensor for Cu^{2+} Ions Based on Dual Fluorescent Ligand-Coated Polymer Nanoparticles. *Chem. Eur. J.* **2009,** 15, 8319-8330.

184. Gouanvé, F.; Schuster, T.; Allard, E.; Méallet-Renault, R.; Larpent, C., Fluorescence Quenching Upon Binding of Copper Ions in Dye-Doped and Ligand-Capped Polymer Nanoparticles; A Simple Way to Probe the Dye Accessibility in Nano-Sized Templates. *Ad. Func. Mater.* **2007,** 17, 2746-2756.

185. Pradhan, B.; Kohl, R. R.; Chen, J. , Fabrication of in-Plane Aligned Carbon Nanotube-Polymer Composite Thin Films. *Carbon* **2010,** 48, 217-222.

VITA

Zachary Richard Osner was born in Des Plaines, IL, a suburb of Chicago. He grew up in Deerfield, IL and lived there until he was 11, when his family moved out east to Pennsylvania first and then Delaware. After graduating from high school in Newark, Delaware, he moved back to the Chicago-land area. As a young student, Zachary was interested in literature and music. It wasn't until after he graduated from high school that Zachary found his passion for chemistry. As an undergraduate student at DePaul University, Zachary had the opportunity to do research in a synthetic organic chemistry laboratory. It was in this laboratory where Zachary discovered his passion for research and decided his future was going to graduate school. Zachary hopes to continue his research and looks forward to expanding his knowledge of synthetic organic chemistry as it relates to nanotechnology.

In addition to his scientific studies, Zachary is married and live with his wife, dog, and cat. He also enjoys reading, riding his bike, great beer, the Chicago Cubs, talking politics, and his friends.